Modeling of Metal-Molecular Nanoelectronics Network: Analysis and Electrical Properties

by

Tabassum Perveen Ananna

B. Sc., Ahsanullah University of Science and Technology, 2015
M.Sc., University of Dhaka, 2018.

A Project Report Submitted in Partial Fulfillment
of the Requirements for the Degree of

MASTER OF ENGINEERING

in the Department of Electrical and Computer Engineering

Supervisory Committee

Modeling of Metal-Molecular Nanoelectronics Network: Analysis and Electrical Properties

by

Tabassum Perveen Ananna

B. Sc., Ahsanullah University of Science and Technology, 2015
M.Sc., University of Dhaka, 2018.

Supervisory Committee

Dr. Christo Papadopoulos (Department of Electrical and Computer Engineering)
Supervisor

Dr. Mihai Sima (Department of Electrical and Computer Engineering)
Departmental Member

Dr. Anusha Venkataraman (Department of Electrical and Computer Engineering)
Outside Member

Abstract

Supervisory Committee

Dr. Christo Papadopoulos (Department of Electrical and Computer Engineering)
Supervisor

Dr. Mihai Sima (Department of Electrical and Computer Engineering)
Departmental Member

Dr. Anusha Venkataraman (Department of Electrical and Computer Engineering)
Outside Member

Complementing electronic components with molecular counterparts offers a hopeful option for advancing beyond the current size limitations of traditional silicon electronic devices in the effort to create operational molecular nanoscale circuit components. Molecular modules have been extensively studied to evaluate their suitability for use in future nanoelectronic circuits. This study focuses on investigating the theoretical and experimental aspects of the electrical and electronic properties of metal-molecular networks bridged with dithiol molecules. The ratio of (di)thiol molecules and/or the type of molecules in the network can be adjusted to modify the electronic transport paths through the network. Furthermore, the electronic conductivity of small-scale networks made up of interconnected graphene clusters and thiolated molecules (benzene/alkanedithiol) in linear chains and extended networks is analyzed using simulations based on first-principles density functional theory. Geometry optimization and Energy Analysis using DMol^3 that determines the electronic characteristics of molecules, surfaces, clusters, and crystalline solid materials through DFT were performed. The ability to adjust simulations by changing the molecule-to-nanoparticle ratio yields results that align well with the findings of the

previously reported experiments. This offers valuable insights into manipulating network properties with various types of molecules. The analysis ended with VAMP Analysis on Carbon-based molecules such as benzene dithiol and graphene nanosheet. The outcome of experimental VAMP analysis presents a step-by-step process to work on carbon-based structures. The findings from these simulations are used to suggest molecular-level circuits for purposes like memory, switching, hardware security, and biosensors. The molecular electronic networks involving metal nanoparticles, as described in this study, offer a way to develop electronics at the molecular scale.

Table of Contents

List of Tables

List of Figures

List of Abbreviations

Abbreviation	Meaning
AFM	Atomic force microscope
BDMT	Benzenedimethanethiol
BDT	Benzenedithiol
CMOS	Complementary metal-oxide-semiconductor
CNT	Carbon nanotube
CNTFET	Carbon nanotube FET
DFT	Density-functional theory
DFT-NEGF	Density Functional Non-equilibrium Green's Function
DOS	Density of states
FET	Field effect transistor
GAA	Gate-all-around
GAA-NWFET	Gate-All-Around nanowire field effect transistor
GGA	Generalized gradient approximation
HOMO	Highest occupied molecular *orbital*
IC	Integrated circuit
IRDS	International Roadmap for Devices and Systems
ITRS	International Technology Roadmap for Semiconductors
LB	Langmuir-Blodgett
LDA	Local density approximation
LDOS	Local density of states
LUMO	Lowest unoccupied molecular *orbital*

MO	Molecular orbital
MOSFET	Metallic oxide semiconductor field effect transistor
MWCNT	Multi-walled carbon nanotube
NEGF	Non-equilibrium green's function
NW	Nanowire
NWFET	Nanowire field effect transistor
PDOS	Projected density of states
SAM	Self-assembled monolayer
SCE	Short channel effects
SCF	Self-consistent field method
SET	Single electron transistor
STM	Scanning tunneling microscope
SWCNT	Single-walled CNT
TEM	Transmission electron microscope
QM	Quantum mechanics

Acknowledgments

I want to sincerely thank Dr. Chris Papadopoulos, my supervisor, for all his help and support during my academic program. I could not have had such a satisfying and gratifying program without his unceasing oversight and hard work.

Additionally, I appreciate Dr. Mihai Sima and Dr. Anusha Venkataraman's time and effort in serving on my supervisory committee and their insightful recommendations.

A special thank you to Ebere, and Zhang my friends and fellow researchers at the Nanoscale Research Laboratory, for their assistance and encouragement in the lab. Lastly, I want to express my sincere gratitude to my family for their unwavering encouragement and support throughout my graduate program.

Chapter 1 - Introduction

1.1 Introduction to Nanotechnology and Nanoelectronics

Any technique that uses single atoms and molecules to create functional structures at the nanoscale and has applications in the real world is referred to as nanotechnology [1]. Nanotechnology includes the creation and use of chemical, physical, and biological systems with structural elements with dimensions as small as a single atom or molecule or even smaller. It also entails incorporating the generated nanostructures into bigger systems [2,3]. Nanotechnology means "technology on the nanoscale," a scale covering 1–100nm [4]. Nanotechnology is a specialized field of study that falls under the heading of colloidal science and encompasses several scientific fields, including chemistry, physics, biology, and others. Its focus is on examining events that happen at the nanoscale [5]. Exciting potential for the advancement of inventive nanostructured materials and nano systems is presented by the investigation of novel nanoscale materials, phenomena, and processes as well as the creation of unique theoretical and experimental processes [6,7]. The Greek prefix "nano" comes from the term "dwarf" and signifies a reduction in size or time by a factor of 10^{-9}, a thousand times smaller than a micron [8]. The nanometer (nm) scale is commonly defined as a dimension that is one billionth of a meter, approximately equivalent to the width of three or four atoms. This measurement is equal to 10 angstroms (10 Å) and is smaller than one-tenth of a micrometer in at least one dimension [9]. A comparison of nanomaterial with real-world objects is presented in Figure 1.1.

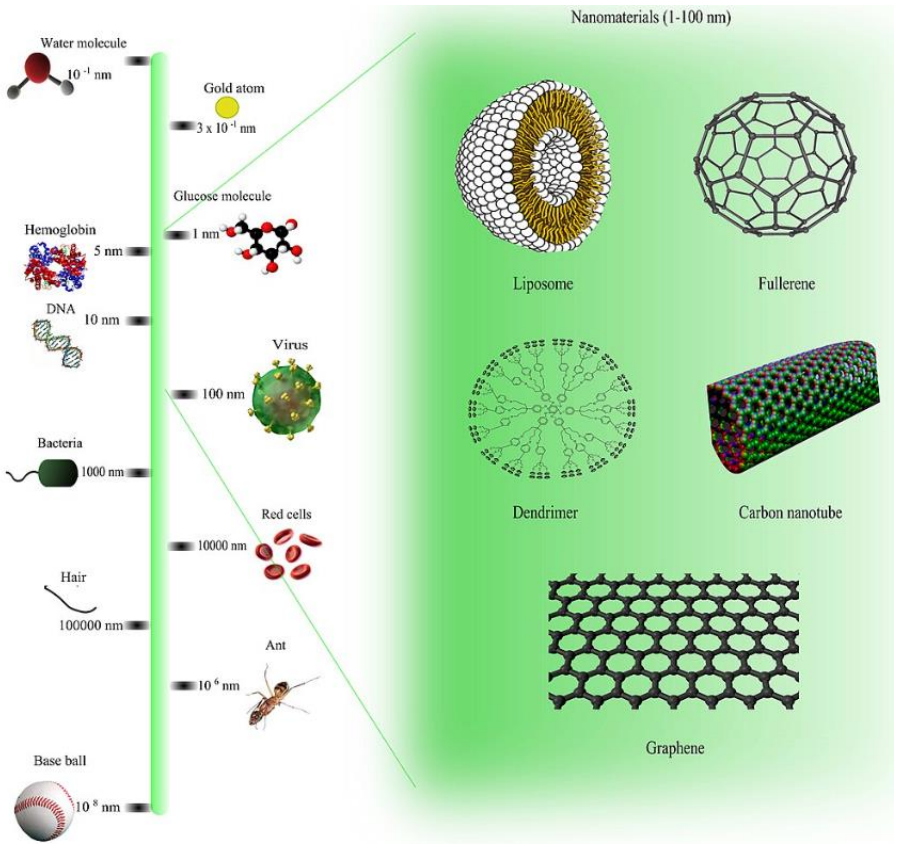

Figure 1.1: Comparison of nanomaterials [10]

The concept of nanotechnology is thought to come from the physicist and the famous Nobel Laureate Dr. Richard P. Feynman. The American Physical Society's annual meeting was being held at the California Institute of Technology on December 29, 1959, and Nobel Prize winner Richard P. Feynman gave a talk during it. Since then, this speech has emerged as one of the most iconic scientific talks of the 20th century entitled, “There’s Plenty of Room at the Bottom: An Invitation to Enter a New Field of Physics” [11]. Feynman brought up the fascinating idea of fitting the complete Encyclopedia Britannica on the tip of a needle during his lectures. He highlighted that such an accomplishment was not prohibited by any basic laws. Feynman also argued that our inability to control atoms and molecules was not what prevented us from manipulating the rules of nature; rather, it was our inadequate methods and tools. Additionally, he discussed the ideas of

"writing and reading in atoms," "information storage on a small scale," and "miniaturization of computers" [11].

Germanium (Ge) was used to make the first transistors, but starting in the 1960s, silicon (Si) became the favored raw material for making electronic devices due to its abundance, inexpensive cost, and advancements in silicon purification research. Due to the requirement for small, lightweight systems and computers with thousands of transistors, the integrated circuit (IC) was separately developed in 1958 by Jack Kilby and in 1959 by Robert Noyce [12].

The development of the microprocessor [13] and metallic oxide semiconductor field effect transistors (MOSFETs) [14] served as catalysts for advancements in integrated circuit technology. Moore's law was introduced in 1965 because of the desire to make gadgets smaller [15]. This law states that every two years, the total number of transistors in an integrated circuit double. As a result, over time, a growing number of transistors have been crammed into a smaller space and scaled down in size (Figure 1.2 (a-b)). Complementary metal-oxide-semiconductor (CMOS) integrated circuits' persistent two-dimensional and functional scaling is primarily linked to the sharp increase in the number of transistors per integrated circuit.

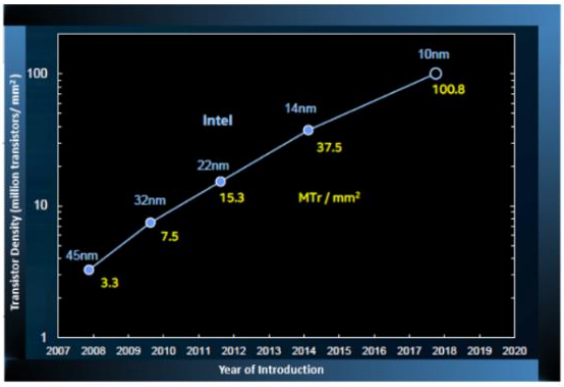

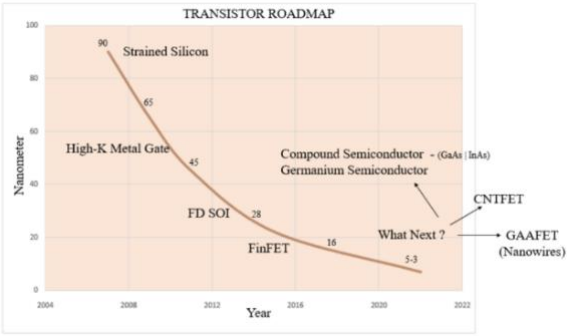

(a) (b)

Figure 1.2: (a-b) Transistor density and feature size of integrated circuits *vs.* year of introduction. (Adapted from Intel.com; solid state technology-semiconductor-digest.com:2020)

However, researchers are confronting difficulties that severely slow down or impede further scaling down of CMOS transistors due to multiple material, physical, power, and technological limits [16], [17]. Some of these problems include providing resolution below the wavelength of light and pushing the limits of optical lithography methods to generate photoresists and suitable mask materials [18].

The scanning tunneling microscope gave scientists and engineers the capacity to view and control individual atoms in 1981, marking the beginning of contemporary nanotechnology [19]. Numerous businesses and governments made significant investments in nanotechnology around the end of the 20th century. The 1990s saw significant advancements in nanotechnology, including the creation of carbon nanotubes [20]. As the new millennium began, nanomaterials started to appear in a variety of consumer goods, from digital cameras to sporting goods [21]. Fuel cells, molecular electronics, long-lasting substances, quantum devices, carbon nanotubes (CNTs), graphene, nano

biological devices, and other breakthroughs have all benefited from the development of nanotechnology [9].

Nanoelectronics involves researching and using electronic gadgets on a very small scale, presenting great opportunities for technological progress. Recent research emphasizes nanomaterials, quantum effects, and device architectures.

Duan et al. (2001) investigate the possibility of utilizing indium phosphide nanowires as foundational elements in nanoscale electronic and optoelectronic devices, demonstrating possibilities for creative device construction on a nanoscale level [22].

Li et al. (2004) explore bottom-up nanoelectronics, highlighting the construction of functional electronic devices with nanowires, leading to new methods in device manufacturing and nanotechnology progress [23].

In his study from 2007, Avouris investigates the field of carbon nanotube electronics and optoelectronics, pointing out their promise for cutting-edge electronic and optical tools. The analysis delves into the latest developments and uses of carbon nanotube-related technologies [24].

From 2008 to 2010, nanoelectronics experienced notable developments. Scientists made progress in using graphene for fast transistors and flexible devices [25]. Improvements were also seen in nanowire technology, including new synthesis methods and application integration. Quantum dot devices were identified as potential options for future optoelectronics and quantum computing advancements.

Cheng et al. (2012) introduce nanotubes assembled with graphene quantum dots for improved Raman spectroscopy. They examine a unique system that provides effective Raman enhancement, demonstrating possible uses in sensing and analytical chemistry [26].

Chen et al. (2020) spotlight advancements in nanoelectronics through their study on graphene-based transistors, emphasizing the potential of graphene for high-performance electronic devices and providing valuable insights into nanoscale transistor design and functionality [27].

Su et al. (2020) investigate small-scale tools at the molecular level, furthering nanoelectronics. The study examines the progress of molecular electronics, providing an understanding of designing and operating tiny electronic parts [28].

Rakshe et al. (2023) synthesize and characterize graphene-based nanomaterials for energy applications. Their study explores graphene's potential in various energy-related fields, offering insights into material synthesis and characterization techniques [29].

1.2 Carbon Nanostructures

One-of-a-kind element, carbon can generate a wide range of macroscopic and nanoscopic compounds and structures. Carbon-based molecules account for more than 95% of all known chemical substances. This is because of the four valence electrons (2s and 2p) that take part in the single, double, and triple bond formation. Stable compounds containing more electronegative and electropositive components can be created by carbon reactions [30-35].

Three distinct hybridization forms for carbon (sp, sp^2, and sp^3) enable the formation of a wide range of amorphous and crystalline structures as well as diverse forms and dimensions. For a variety of uses in the domains of electronics, optoelectronics, sensing, mechanical, construction, automotive, and aerospace, CNs are very appealing [36-39]. Figure 1.3 represents different forms of carbon nanostructures.

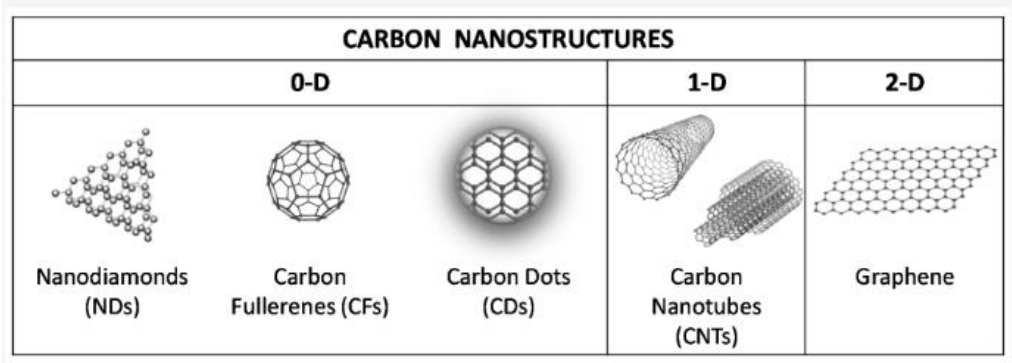

Figure 1.3: Different forms of Carbon Nanostructures (adapted from [40])

1.2.1 Diamond

A diamond is a structure made of sp3 hybridized carbon atoms in a cubic lattice. There are two forms of diamond - hexagonal and cubic, with the latter being more common. It is considered metastable, meaning it is stable kinetically but not thermodynamically [41]. Diamond thin films' appeal stretches to unique realms like superconductivity and quantum computation via precise doping. Thus, diamond is highly desired due to its wide range of applications, including abrasives, coatings, electronics, photonics, and imaging devices in addition to biomedical uses [42-45].

1.2.2 Graphite

Graphite occurs naturally in various forms such as amorphous, crystalline, lumpy, or veined. Graphite's softness and flexibility are due to weak Van der Waals forces. As a result, it is employed as a lubricant across various industries. Graphite has a high ability to reflect visible light. Polycrystalline carbon forms possess a black color and small particle size that enable multiple light reflections within pores and between particles, resulting in gradual absorption. Graphite is widely utilized, such as in nuclear reactors using graphite rods [46], as electrodes in batteries, in steel reinforcement, and for anti-corrosion applications.

1.2.3 Graphene

A special transparent substance known as graphene has a large specific surface area [47], good thermal conductivity, good absorption, the quantum Hall effect, high optical transparency of about 97.7% [48] high carrier mobility, and high modulus of Young [47], etc. It is made up of a planar network made up of one layer of hexagon-shaped carbon atoms joined by links. Carbon is thus the lone fundamental unit of graphene. High thermal and electrical conductivity, distinctive optical behavior, superior mechanical qualities, remarkable chemical stability, and a sizable surface area are the results of this atomic structure in combination with graphene's electron distribution [49, 50]. By undergoing chemical and physical changes, graphene can be converted into graphene materials, such as reduced graphene oxide, graphene oxide, and single- and multilayer graphene, each of which has distinct characteristics. Carbon nanotubes or nanohorns can be produced by scrolling graphene [49, 51].

1.2.4 Quantum Dot

Quantum dot is one of the most analyzed nanomaterials in recent world of research. Amorphous or nanocrystalline nuclei with primarily sp2 hybridized carbon are found in quantum dots. CQDs are items of nanoscale dimensions. These objects are typically smaller than 20 nm, and they are almost always semiconductors where a process known as "quantum trapping" of particles takes place. The surface characteristics of QDs differ greatly based on the synthesis methods and precursors utilized, potentially including oxygen/nitrogen functional groups [52].

1.2.5 Fullerene

Fullerenes, also known as Buckminsterfullerene, are a unique carbon structure made up of an even number of sp2 hybridized carbon atoms. The atoms are arranged in 12 pentagonal and m hexagonal

rings, with m = (n − 20)/2, where n is the total number of carbon atoms. C60 (12 pentagons and 20 hexagons) is the smallest fullerene that follows the pentagon rule, which dictates that the most stable fullerenes are those where pentagons do not share edges [53].

The curvature of the structure leads to alterations in the properties of fullerenes, resulting in characteristics such as high electron affinity and increased chemical reactivity. This makes fullerenes more prone to additive reactions. Fullerenes are widely utilized in the chemical and medical sectors, serving purposes such as targeted drug delivery systems, nanosensors, antioxidants, and materials for solar panel construction [54].

1.2.6 Carbon Nanotubes and Nanofibers

CNTs are essentially graphene sheets rolled into cylindrical shapes. They are categorized into SWCNTs and MWCNTs based on the number of graphene layers, [55] with MWCNTs having nested cylinders and a 3.4 Å layer spacing. The configuration can also vary into "zigzag", "chair", or "chiral" nanotubes [56,58].

A single layer of graphene is rolled into a cylindrical shape to create single-walled carbon nanotubes, or SWCNTs. Since a catalyst is needed for the synthesis of SWCNTs, their manufacturing is more complicated and bulk synthesis is challenging. During functionalization, SWCNTs have a tendency to acquire additional flaws, which can affect their characteristics but facilitates future modification. SWCNTs typically have lower levels of purity. Because SWCNTs are less prone to build up in the body, they may be more suited for use in biomedical applications. Additionally, they have greater flexibility and may twist more readily. Because of their simplified structure, SWCNTs are comparatively easier to characterize and evaluate [57].

Multiple concentrically rolled graphene layers make up multi-walled carbon nanotubes (MWCNTs). Because MWCNTs may be made without a catalyst, bulk synthesis is made simpler and less expensive. Although MWCNTs have fewer flaws, they are more difficult to functionalize successfully. Higher purity MWCNTs are usually manufactured. Because MWCNTs are stiffer and more resistant to deformation, they tend to collect more in biological systems. The layered structure of MWCNTs makes characterisation difficult due to the complexity and inter-layer interactions [57].

When graphene sheets are curved at a certain angle (α), they form Carbon nanofiber (CNF), creating a stack of nanocones. CNF differs from carbon nanotubes (CNTs) by having an angle (α) that is not zero. CNF sizes can range from 3.5 nm to several hundred nanometers in diameter, with lengths up to several micrometers [59]. The small diameter significantly impacts the surface's mechanical and specific properties by affecting the number of structural defects. Various structures of carbon fibers include hollow- and filled-core, stacked nanocones; partitioned, stacked nanocones; and partitioned nanotubes [58].

Combining carbon tubes with appropriate polymers, like poly (p-phenylene vinylene) or its derivatives, results in composite materials with electroluminescent properties, which find applications in photovoltaic devices and light-emitting diodes [60]. Just like in graphene, the application of CNTs is constrained by challenges in dispersion and interaction with the polymer matrix, particularly due to their small diameter and high aspect ratio [61]. Nevertheless, the utilization of nanofibers and nanotubes in combination with other substances is also possible [62].

1.2.7 Q-Carbon

Q-carbon, which was found in 2015, is a newly discovered metastable phase of carbon [63]. Referred to as hardened carbon (Q-carbon, Q-C), it shows superior ferroelectric properties compared to diamond [64]. Q-carbon has distinctive mechanical, chemical, and physical characteristics, making it a focus in field-controlled electronics and biomedicine [65,66] due to its amorphous structure with 75–85% sp3 and remaining sp2 hybridized carbon atoms, resulting in unique properties like extraordinary Hall effect, field emission, and greater hardness than diamond [67,68].

1.2.8 Carbon Aerogel and Aeroraphite

Research has recently focused on carbon aerogels for energy applications. These aerogels have high electrical conductivity, mechanical strength, low density, large area, and controllable structure, and can be used as absorbents, catalysts, electrodes, or insulating materials [69-71]. They are 3D nanogrids with an open porous structure allowing the penetration of molecules and ions [72]. The interconnected solid phase particles consist of carbon grains with a network of interwoven graphite fibers [73]. The customizable porosity makes them ideal for extreme applications like space vehicles. Carbon aerogels also have high heat resistance and stability, retaining their structure at temperatures up to 2273 K [71].

1.2.9 Carbon Nanodiamond

Nanosized carbon particles known as carbon nanodiamonds have the same structural form as diamonds and can be created through various methods such as detonation, chemical vapor deposition, laser ablation, ultrasound cavitation, and high-energy ball milling of high-pressure and high-temperature microdiamonds [74]. Detonation is a widely used and cost-effective method that

can result in single-crystalline diamond nanoparticles averaging around 4-5 nm in size following a post-processing procedure involving purification, de-aggregation, and fractionation [75]. ND's outstanding optical and mechanical characteristics, such as high hardness, low friction coefficient, and wear resistance, along with its strong chemical and thermal resistance, position it as a top choice for in vivo imaging [76], targeted delivery [77], gene and drug transportation (even for water-insoluble medications) [78], creating nanorobots [74], and acting as a filler in tissue engineering scaffolds [79,80,81].

1.3 Molecular Electronics

The study of individual molecules' electrical characteristics and their potential application in the creation of new electronic devices is the goal of the field of molecular electronics. Fundamentally, the goal of molecular electronics is to build parts and circuits at the molecular scale by taking advantage of the special quantum mechanical properties of molecules. Using individual molecules as building blocks, molecular electronics seeks to produce electronic components such as transistors, diodes, and wires. A basic understanding of molecular electronics is the movement of charges via molecules. Research is still ongoing on phenomena including tunneling, hopping, and ballistic transfer. Using self-assembly techniques, which allow molecules to spontaneously arrange themselves into desired configurations, several molecular electronics devices are built. For specialized uses in molecular electronics, molecules can be created and manufactured with unique electrical characteristics. Applications for molecular electronics include molecular sensors, molecular-scale computation, high-density memory storage, and nanoscale energy conversion devices.

The idea of molecular rectifiers was first presented in a study by Aviram and Ratner (1974), which suggests that organic molecules could be used as electronic components like silicon diodes. They

postulate that rectification properties—which permit current flow in one direction but not the other—may result from asymmetric molecule structures. This revolutionary concept established the groundwork for molecular electronics and stimulated further investigation into nanoscale circuitry and molecular-scale electronic devices. Figure 1.4 illustrates the molecular structure and the tunneling mechanisms of the proposed device. [82].

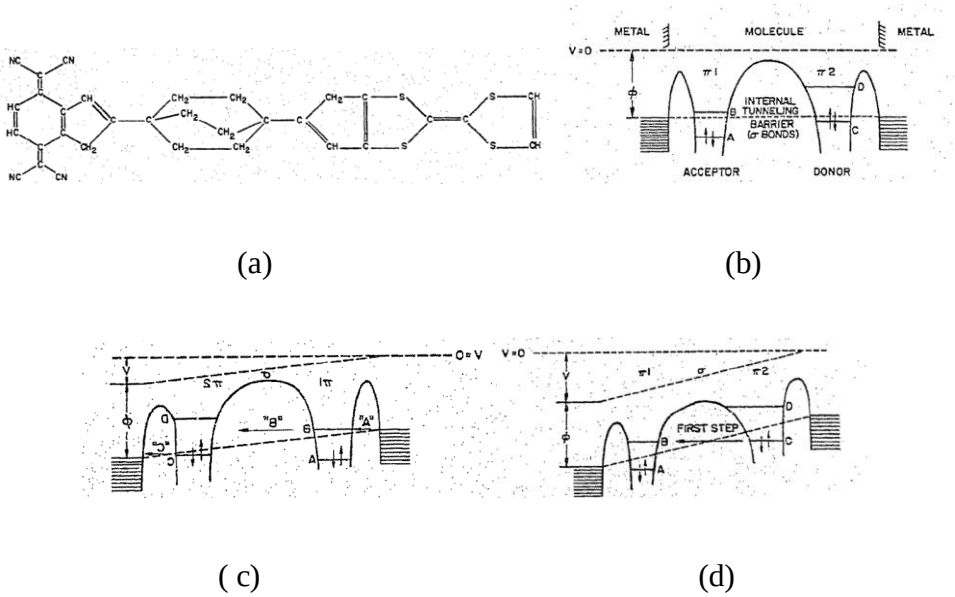

Figure 1.4: (a) The rectifier molecule; (b) Schematic of the energy versus distance of the device. B and D are the affinity levels and A and C are the highest occupied levels, of acceptor and donor, respectively; (c) Energy levels shift with applied voltage. “A”, “B”, and “C” are three tunneling processes; (d) Energy level shift with reverse applied voltage (adapted from [82])

Unimolecular rectification in donor-acceptor chains is investigated by Metzger (1999). The electrical behavior of single molecules bridging two electrodes is investigated in this work. Results point to asymmetric charge transport, which may have molecular electronics applications. The work advances nanotechnology and aids in the understanding of processes occurring at the molecular level [83]. Reed et al. (1997) illustrate the electrical conductance of a single atom

bridging two metal terminals, a key turning point in atomic hardware, explaining the potential of atoms as useful electronic components [84].

A technique for measuring single-molecule resistance by periodically creating molecular junctions is presented by Xu and Tao (2003). To test electrical resistance directly, they utilize a scanning tunneling microscope to make and destroy connections between a single molecule and gold electrodes. This method enhances the science of molecular electronics and sheds light on the electrical characteristics of individual molecules [85]. Nitzan and Ratner (2003) elucidate electron transport mechanisms in molecular wire junctions, providing insights into charge transfer phenomena crucial for molecular electronics, and advancing our understanding of nanoscale electrical conductivity [86].

Self-assembled monolayers (SAMs) of thiolates on metal surfaces are investigated by Love et al. (2005) as a platform for nanotechnology. Their article in Chemical Reviews explores the synthesis, characteristics, and uses of SAMs, emphasizing their importance in molecular electronics, surface modification, and nanoscale fabrication. An extensive summary of the developments in SAM-based nanotechnology is given in this study. Self-assembled monolayers (SAMs) are films formed by the spontaneous assembly of organic molecules, particularly thiolated compounds (e.g., alkane(di)thiols), from solution or gas phases onto curved or planar solid surfaces, as depicted in Figure 1.5 [87].

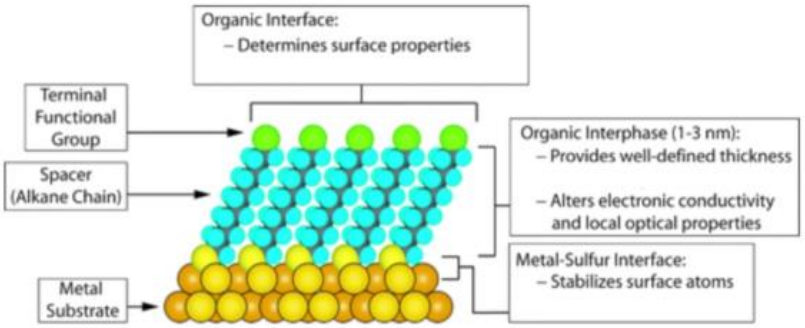

Figure 1.5: Illustration of SAM of alkanethiolates on a gold surface (adapted from [87])

SAMs of tiny molecules (thiols, silanes, etc.) and polymer SAMs (large chains of macromolecules) are the two types of SAMs that are usually researched. The SAMs produced by aliphatic and aromatic sulfur-containing compounds (benzene dithiol and alkanethiol, respectively) on gold surfaces have been the subject of the most research among the former group because their functional groups strongly react with the gold surface to produce SAMs with high density and homogeneity. The ordered monolayer is formed by the headgroups of SAMs chemisorbing on specified spots of gold (Au (111)) surfaces to create SAMs using thiols [88].

The mechanically controlled break junction (MCBJ) technique is a widely used method for forming single-molecular junctions [89, 90]. The study examined the electrical characteristics of 1, 4-benzene dithiol as it self-assembled between two gold electrodes where a metal wire has been adhered to a substrate is stretched until it narrows and eventually breaks, forming a tip-like structure, to produce nanogaps. Molecules can fill the gap between metal electrodes, as depicted in Figure 1.6 (a). Figure 1.6 (b) illustrates typical current-voltage and conductance-voltage traits. Employing MCBJ techniques allows for the creation of small contacts with adjustable nanometer-sized gaps. This enables trapping and electrically testing desired nanostructures [91].

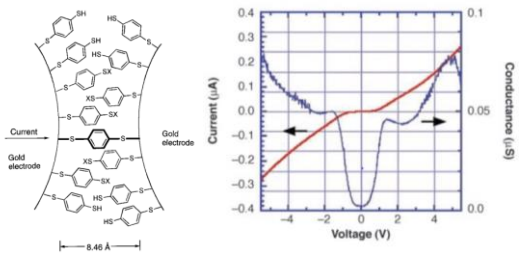

(a) (b)

Figure 1.6: Schematic of (a) A benzene-1,4- dithiolate SAM between two gold electrodes formed using the MCBJ technique. (b) Typical *I(V)* and *G(V)* characteristics (adapted from [91])

Lambert's presentation on molecular electronics offers a comprehensive outline of the field's different applications, from atomic wires to sensors and computing gadgets, highlighting its intriguing nature and innovative suggestions [92]. Ratner`s (2013) article explores the challenges and opportunities in molecular electronics, highlighting the interdisciplinary nature of the field and its potential for transformative advancements in nanotechnology and materials science [93].

Researchers have extensively investigated the electrical conductivity of molecular systems to comprehend their electronic characteristics and explore potential avenues for fabricating molecular electronic devices [94, 95, 96]. Electronic transport across molecular systems bridged between metallic electrodes has been modeled using two widely used theoretical approaches: the Landauer method and the Non-equilibrium Green's Function (NEGF) method [97].

The system is divided into three parts using the Landauer method: the left and right electrodes, in equilibrium at some electrochemical potential, μL, R; and the central region, which contains the molecule and some of the electrodes.

According to the Landauer technique, transport may be thought of as a scattering problem where the current is proportional to the transmission coefficient, and an incident carrier flux from one lead is dispersed and transmitted to the other lead by the center region.

$$I = \frac{2e}{\hbar}\int \frac{dE_i dE_f}{2\pi}\ T(E_i,E_f)\ [f_L(E_i)(1-f_R(E_f)) - f_R(E_i)(1-f_L(E_f))] \ \ldots\ldots\ldots(1.1)$$

Where I is current, e is the elementary charge, ħ is Planck's constant, $T(E_i, E_f)\ dE_f$ is the probability that an electron incident on the molecular target with energy, E_i will be transmitted with energy, E_f, $f_L(E)$ and $f_R(E)$ are the Fermi functions of the left and right leads.

The transport problem can be solved more broadly by using the NEGF method, which takes into account the effects of inelastic scattering and electron-electron interactions under non-equilibrium conditions [97].

Based on an explanation of the locations and species of each individual atom in the system, the Density Functional Theory (DFT) makes it possible to compute the attributes of a molecular system.

The most widely used approach to modeling electrical transport at the nanoscale is the self-consistent NEGF formalism in conjunction with DFT (DFT-NEGF) [98]. The electronic structure and Hamiltonian for the scattering region are first obtained using the DFT, and the charge density, transmission, and current of the molecular system are then solved using the NEGF method [98].

Numerous investigations have focused on simulating the electronic transport characteristics of molecular systems, with the benzene dithiol (BDT) molecule serving as the model system for studying molecular transport junctions [99-103].

Mao et al [103] conducted a study using DFT-NEGF on the Au-BDT-Au molecular junction, with device configuration as shown in Figure 1.7 (a). The molecular energy spectrum projection of the BDT molecule in the junction is shown in Figure 1.7 (b) [103]. The highest occupied molecular orbital (HOMO) results from the overlap between Sulphur atoms and the π orbital of the benzene ring moiety in the molecular projected self-consistent Hamiltonian (MPSH) of the BDT molecular junction (Figure 1.7 (b)).

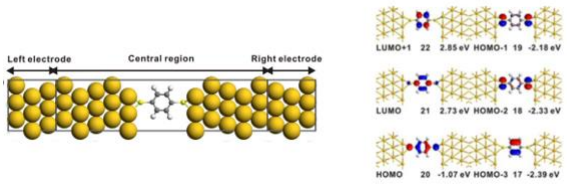

(a) (b)

Figure 1.7 (a) Device configuration of Au-BDT-Au molecular junction consisting of the central region and left/right electrodes. Two S atoms of BDT adsorb at hollow sites of the Au electrodes; (b) Molecular energy spectrum projection of BDT, with isovalue surface set at 0.05 au (adapted from [103])

Different types of conduction mechanisms in molecules can be categorized as either dependent on temperature or independent of temperature. Thermionic and hopping conduction are instances of thermally activated conduction mechanisms, typically resulting in superconductivity at elevated temperatures [104].

Hopping conduction is thought to be the main conduction mechanism in CNTs,[105] and pure CNT fibers have been demonstrated to display temperature-dependent *I-V* characteristics [106].

Fowler-Nordheim and direct tunneling are the main conduction mechanisms that are not affected by temperature [104]. The conduction in alkane(di)thiol molecules and SAMs linked to gold

electrodes is thought to occur through non-resonant tunneling, which accounts for the length-dependent conductivity of alkane(di)thiol molecules. The chain length of the molecule is like the width of the tunneling barrier [107]. This also clarifies the absence of temperature dependence in current seen in alkane(di)thiol molecules and SAMs [108, 109].

1.4 Background and Motivation

An interesting journey reflecting the convergence of chemistry, physics, and nanotechnology may be seen in the history of metal molecular junctions created using self-assembly processes. The advancement of these junctions has led to new developments in the fields of molecular sensors, nanoscale devices, and quantum computing, as well as advances in our understanding of molecular electronics. Researchers began looking into the potential of employing single molecules as useful electronic parts in circuits in the 1980s and 1990s. Since some molecules can spontaneously organize into distinct forms on surfaces, self-assembly techniques have become increasingly popular. In this method, non-covalent interactions like hydrogen bonding, van der Waals forces, and π-π stacking are used to generate molecular monolayers or thin films. Using self-assembly techniques, researchers like Mark Reed, Charles Lieber, and James Tour showed in the late 1990s and early 2000s that it was possible to create molecular-scale connections. Usually, a single molecule bridges two metal electrodes to form a nanoscale circuit at these junctions [110-114].

Metal-molecule junctions are extremely promising for a variety of uses, such as quantum computing, molecular electronics, and nanoscale sensors. To enhance the functionality and performance of these molecular-scale devices, researchers are investigating new materials, design approaches, and production processes. In spite of tremendous advancements, there are still a number of obstacles and restrictions in the field of metal-molecule junctions. These include the necessity for precise control over molecular orientation and electrical coupling, as well as

problems with reproducibility, scalability, and molecular stability and degradation. Furthermore, consideration must be given to molecular-scale quantum phenomena and how they affect device performance in the design and optimization of metal-molecule junctions.

The primary goal of this study is to move beyond earlier work on metal-molecule junctions and toward the development of molecular electrical circuits with a variety of network architectures, all accomplished using efficient self-assembly techniques. It includes an in-depth understanding of various electrical characteristics using a variety of analytical and computational modeling methodologies.

1.5 Overview of Thesis

In-depth studies on two-terminal electron transport have been carried out to advance the field of molecular electronics. Both two-terminal and three-terminal heterojunctions with a single molecule or molecular self-assembled monolayer (SAM) structure can be combined and merged with a variety of molecules and materials to get the necessary electronic properties. [115-117]. Motivated by prior work on metal nanoparticle-molecular systems, in this study, electrical and electronic properties of nanoscale graphene-dithiol molecular networks comprising a balanced quantity of dithiol molecules are investigated and analyzed.

1.5.1 Objectives and Scopes

The main objective of this project is to design and analyze graphene-BDT structures under DFT-based simulations. The major points of this project are as follows.

1. To model the graphene-BDT structure on Material Studio software for DFT-NEGF-based simulations.

2. To research the methodologies of molecular behavior and transmission during the experimented simulations.
3. To study different parameters that play a crucial role in the simulations.
4. To evaluate the outcome of the simulations with the expected results and how that affects other sectors.

1.5.2 Report Outline

In this project, BDT as Molecular Junction and Graphene have been constructed in Material Studio software. Linear chains have been constructed using these molecules and their electrical properties have been simulated using Quantum Mechanical Computational Method. This thesis investigates the properties of linear chains. The research investigated is organized as follows:

Chapter 1 presents a comprehensive analysis of Carbon Nanotubes (CNT) and Molecular Electronics. The electronic properties of BDT-graphene molecular networks were modeled using DFT-NEGF-based simulation methods.

Chapter 2 discusses the self-assembled metal molecular network methodology including properties of Graphene, BDT, and various quantum mechanical computational methods.

Chapter 3 is focused on model simulation of constructed structure and analysis. DOS, Molecular Orbital, and Transmission spectrum have been obtained from simulation and analyzed in this chapter.

Chapter 4 is about the discussion of the results of this project and outlines potential future work.

Chapter 2 - Self-Assembled Metal Molecular Network Methodologies

2.1 Introduction to Unit Structure of Self-Assembled Metal Molecular Networks and Methodologies

The self-assembled metal molecular network studied in this work is constructed by benzene (1,4) dithiol and graphene clusters. Also, a 1-unit, 2-unit, and 3-unit linear chain has been structured to study the impact of presenting multiple graphene clusters in the chain. The electronic and transport properties of metal-molecular networks were studied using various software previously. In this section, unit structures such as BDT and graphene were investigated along with a discussion about their properties. The calculation of quantum mechanical systems mostly relies on the time-independent Schrödinger wave equation, and this section discusses the different methods and approximations developed to solve it.

2.2 Graphene and its Properties

A lot of interest has been shown recently in using graphene, a one-atom-thick planar sheet of atoms bonded to silicon in a honeycomb crystal lattice, as a potential next-generation electronic material because of its remarkable qualities, which include high current density, ballistic transport, chemical inertness, high thermal conductivity, optical transmittance, and super hydrophobicity at the nanoscale [118,119].

Graphene-based materials have potential in nanotechnology for various applications which is presented in Figure 2.1. By adjusting the structure and incorporating carbon nanotubes or C60 molecules, the lithium storage capacity of graphene nanosheets can be enhanced, making them

viable for rechargeable lithium-ion batteries. Graphene can be used in ultracapacitors, solar cells, water filters, highly flexible OLEDs, and transistors [120].

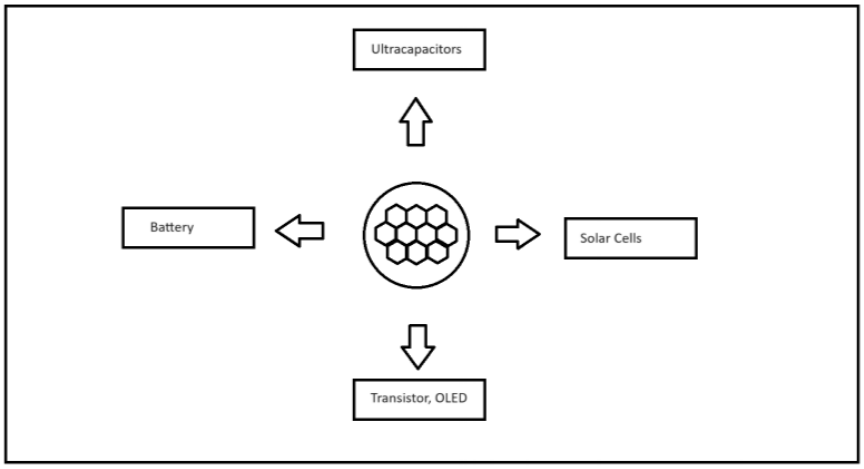

Figure 2.1: Applications of graphene

2.2.1 Structure and Composition of Graphene

A single layer, or monolayer, of closely spaced carbon atoms in a hexagon-shaped honeycomb lattice is known as graphene. It is an allotrope of carbon with a molecular bond length of 0.142 nm that has the shape of a plane of sp^2-bonded atoms [4]. Figure 2.2 shows the sp^2 carbon hybridization [121].

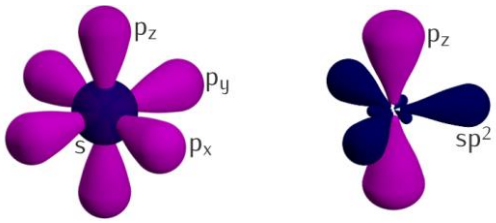

Figure 2.2: sp^2 Carbon hybridization [121]

During a standard sp^2 hybridization between two adjacent carbon atoms on the graphene layer, the sp^2(2s, 2px, and 2py) hybridized orbitals form an in-plane σ bond, while the 2pz orbitals, which

are perpendicular to the planar structure, generate an out-of-plane π bond. The covalent σ bond that forms has a small distance between atoms of around 1.42Å, surpassing the strength of sp3 hybridized carbon-carbon bonds found in diamonds. This attribute contributes to the exceptional mechanical properties of monolayer graphene such as a Young's modulus of 1 TPa and an intrinsic tensile strength of 130.5 GPa. A conduction band and valence band with zero band gap are created in monolayer graphene because of the half-filled π band, allowing electrons to move freely. Additionally, the π-bonds create a faint Vander Waals attraction among neighboring layers of graphene in bilayer and multi-layer graphene. The stability of the planar ring is caused by the resonance and delocalization of the electrons [120].

Table 2.1: Physiochemical properties of graphene and its derivatives [122]

Physiochemical Property	Estimated Value
High Surface Area	~2630m^2g^{-1}
Excellent electrical conductivity	~1738 siemens/m
Strong Mechanical strength	Young's Modulus ~1100GPa, Fracture strength ~125GPa
Thermal Conductivity	5000 $Wm^{-1}K^{-1}$
Ease of functionalization	π -π Stacking interaction Electrostatic interaction

2.2.2 Electronic Properties of Graphene

Long mean free routes allow the electrons in graphene to move freely without interfering with disorder and electron-electron interactions. Because of this, graphene has different physical structures and electrical characteristics from other typical metals and semiconductors.

The honeycomb lattice structure is a triangular lattice with a basis consisting of two atoms. Graphene simulation, particularly with the use of density functional theory (DFT), can be used to predict the electrical structure of graphene. DFT is used to study and compute the adsorption

energy of graphene and other materials (such as lithium, sodium, hydrogen, and potassium), as well as the geometry, work function, dipole moment, and density of states (DOS) of each adatom-graphene system.

Graphene's strong ambipolar electric field effect clearly demonstrates its remarkable properties. Charge carriers can be continuously exchanged between electrons and holes at concentrations of n of 10^{13} cm^{-2}, and they can have large mobilities μ above 15,000 cm^2 V^{-1} s^{-1} at ambient conditions. Despite the large n (10^{13} cm^{-2}) in electrically and chemically doped devices, graphene exhibits a consistently high mobility.

Another indicator of the system's exceptional electronic quality is the Quantum Hall Effect (QHE). The QHE in graphene is visible at room temperature because its temperature range is ten times wider than that of other 2D materials. The behavior of massless fermions in a magnetic field at the high-field limit, as Shubnikov-de Haas oscillations (SdHOs) advance to the QHE, sheds more light on their peculiar reaction.

The transparency or opacity of suspended graphene depends solely on the fine-structure constant, $\alpha=e^2/hc\approx7.299\times10^{-3}$ (where c is the speed of light). This factor, commonly associated with quantum electrodynamics, determines the interaction between light and relativistic electrons [123].

2.3 BDT and its Properties

Benzene-1,4-dithiol has the chemical formula $C_6H_6S_2$ and belongs to the organosulfur compounds category. This includes a benzene ring with two thiol groups. The diprotic compound's conjugate base acts as a chelating agent in coordination chemistry and a precursor for creating different organosulfur compounds [124].

Table 2.2: Basic properties of BDT [124]

Physiochemical Property	**Estimated Value**
Synonym	1,4 Benzenedithiol, Benzene-1,4 dithiol
Formula	$C_6H_6S_2$
Molar mass	142.24g/mol
Density	1.24 g/cm3
Solubility in water	Soluble in basic water
Boiling point	119-120 C (246-248 F, 392-393 K) at 17 mmHg
Melting point	22-24 C (72-75 F, 295-297 K)
Appearance	Powder or crystal
Color	White to Orange to Green

2.3.1. Structure and Composition of BDT

1,4-Benzenedithiol is a solid crystalline substance with a sulfur scent that ranges in color from white to yellow. It exhibits minimal volatility when at room temperature. It dissolves a little in water but dissolves very well in many organic solvents. 1,4-Benzenedithiol is utilized in various significant applications. Figure 2.3 presents the Molecular structure of BDT

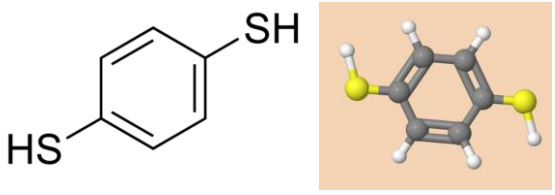

Figure 2.3: Molecular structure of BDT

Often, it is utilized as a middle step in organic synthesis for creating sulfur-containing compounds. In addition, it is utilized in electrochemistry as both a corrosion inhibitor for metals and a modifier for electrodes. Furthermore, it serves as a ligand for dyes and photosensitive materials.

One way to make 1,4-Benzenedithiol involves oxidizing benzothiophene disulfide using sodium manganate, followed by treating the resulting compound with calcium hydroxide, and ultimately acidifying the mixture to produce 1,4-Benzenedithiol [125].

Benzene-1,4 dithiol (BDT) is a type of aromatic dithiol that can create a self-assembled monolayer (SAM) on various surfaces. BDT is utilized as a connector to aid in the creation of acrylate-based light-sensitive epoxidized soya bean oil for 3D printing uses. Gold-based nano constrictions can be developed by treating the surface with BDT, resulting in decreased flicker noise compared to the untreated surface. This molecule can be employed in electronic devices within single-molecule junctions. It has also been utilized in the fabrication of nanomaterials [126].

2.3.2. Electronic Properties of BDT

Typically, the transport via a molecule sandwiched between two metallic electrodes is measured in order to analyze the electrical properties of molecular devices. Naturally, the transport properties that arise are a reflection of both the molecule and the metal-molecule interaction. The local electronic structure at the various molecular locations has a significant influence on a molecular device's characteristics since transport is generally limited to a small number of valence orbitals. Understanding the device thus requires an understanding of the specifics of the chemical bonding, such as hybridization or charge transfer, and consideration of structural relaxation brought on by the metal-molecule contact [127].

The ring plane of the benzene-1,4-dithiol molecule forms π bonding and π* antibonding orbitals from the p orbitals of sulfur and carbon, and in-plane orbital overlap forms σ bonding and σ*

antibonding orbitals. The antibonding orbitals remain unoccupied while the σ and π orbitals are completely occupied. σ states emerge at lower energies than π states because they are more susceptible to bonding–antibonding splitting due to their mediation of direct orbital overlap. The conductance of the molecular contact exhibits Ohmic behavior for tiny biases due to a smooth density of states close to the Fermi energy. Two conduction peaks are seen as the bias increases, and they can be linked to resonant tunneling via either the π* or, at higher bias, the π orbitals [127].

The benzene dithiol has a conductance value of 0.011 G_0, ($G_0 = 2e^2/h$). BDT consists of alkanedithiol chains. These molecules have a significant energy gap between their HOMO and LUMO, making them highly insulating. However, they are also chemically inert and simple, making them ideal for testing experimental techniques or theoretical methods [128].

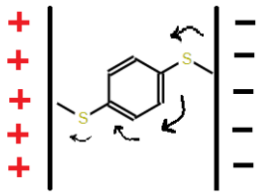

Figure 2.4: Expected chemical mechanism to transfer charge from surface to surface. [adapted from [129]]

Using Benzene 1,4 dithiol in the crosslinking step is considered to increase the conductivity between two non-contacting nanostructures by conveying charges [129]. Figure 2.4 demonstrates the chemical mechanism to transfer charge from surface to surface area.

2.4 BDT-Graphene Linear Chains

The researchers started experimenting with BDT (1,4 – benzenedithiol) bridged by gold electrodes to comprehend the characteristics of molecular electronics. If the leads consist of metals like gold,

it is important to take into account a three-dimensional configuration like face-centered cubic when analyzing the electronic transport characteristics. The spin relaxation length in gold is excessively low for moving spin along with complex production and evaluation processes. Graphene shows promising aspects considering the fabrication process along with extended spin relaxation length which is the motivation to study benzene molecules connected to graphene nanoribbon leads [130].

2.4.1 Understanding BDT-Graphene Structures

BDT, a basic conjugate molecule, has potential applications in molecular electronics equipment like mechanically adjustable break-junctions [131]. Lately, innovative molecular junctions have been developed and constructed using BDT sandwiched between p-doped graphene and Au film as electrodes, demonstrating improved charge properties related to transportation [132]. The molecule 1,4-Benzenedithiol bonds to the surface as thiolates through a sulfur-gold bond [133].

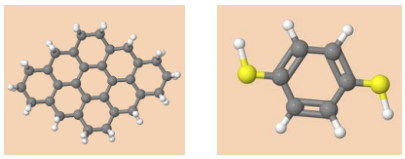

(a) (b)

Figure 2.5: (a) Graphene Cluster (b) 1,4 Benzene dithiol

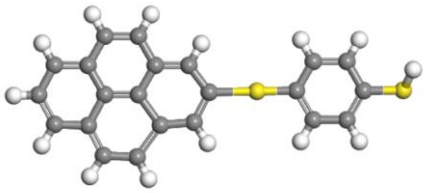

Figure 2.6: BDT-Graphene Chain

Figure 2.5(a-b) shows the graphene cluster and BDT molecule, and Figure 2.6 shows the BDT-Graphene linear chain. While complexes were being formed, the BDT molecule attached to gold atoms or graphene clusters through S atoms within the thiol groups. Monolayer graphene cluster shows slight changes in shape in complexes because of the impact of molecules, metal elements, imperfections, and doped atoms. Different complexes are formed with various configurations. In BDT/Au-G-Au and BDT/Au-G_N (N-doped graphene) complexes, the molecules' major axes align parallel to the graphene plane, while in BDT/Au-G_{MV} (Monovacancy graphene) complexes, the molecular axis is nearly perpendicular to the graphene [134].

2.5 Quantum Mechanical Computational Methods

Quantum mechanical (QM) techniques are becoming more and more crucial in forecasting the configurations and characteristics of different condensed-phase systems. Ab initio quantum chemistry techniques are computational chemistry approaches that rely on quantum chemistry principles. Ab initio quantum chemistry methods aim to find solutions to the electronic Schrödinger equation by considering the nuclei positions and electron count to provide valuable insights into electron densities, energies, and system properties [135]. MO theory, also known as MOT or molecular orbital theory, is a technique that employs quantum mechanics to explain the electronic configuration of molecules [136]. Quantum Chemical Methods can be categorized into two groups depending on whether wave function methods or density functional theory (DFT) is utilized. The most basic approach using wave functions is called Hartree-Fock (HF), where the wave function for multiple electrons is simplified to just one Slater determinant (the mathematical representation of wave functions in quantum mechanics). Semiempirical methods offer a quicker way to address the size restrictions of DFT [137]. Non-equilibrium Green’s function techniques

are commonly employed for computing current and charge densities in nano-sized conductors, including molecules and semiconductors, under bias conditions [138].

2.5.1 Molecular Orbital (MO) Theory

The molecular orbital theory transformed the examination of chemical bonding by estimating the states of bonded electrons, known as molecular orbitals, as linear combinations of atomic orbitals (LCAO). Making these estimations involves using the density functional theory (DFT) or Hartree-Fock (HF) models to solve the Schrödinger equation [136].

In the LCAO technique, every molecule possesses a group of molecular orbitals. The molecular orbital wave function ψ_j is hypothesized to be able to be expressed as a basic weighted combination of the n atomic orbitals χ_i, as shown in the equation: [139]

$$\psi_j = \sum_{i=0}^{n} c_{ij}\, \chi_i \qquad \textbf{(2.1)}$$

To be useful as approximation molecular orbitals, atomic orbital combinations must meet three basic conditions.

1. The atomic orbital combination needs to be in the correct irreducible representation of the molecular symmetry group in order to have the proper symmetry.
2. Additionally, atomic orbitals need to overlap in space.
3. For atomic orbitals to merge into molecular orbitals, their energy levels must be comparable [140].

The molecular orbitals generated from atom-to-atom bonds are represented by a linear combination of atomic orbitals (LCAO) in molecular orbital theory. They are frequently separated

into three categories: non-bonding, anti-bonding, and bonding. Typical orbitals for bonding are pi (Π) orbitals, which have a nodal plane along the bond axis, and sigma (σ) orbitals, which are symmetric about the bond axis. Delta (δ) orbitals and phi (φ) orbitals, which have two and three nodal planes along the bond axis, respectively, are less common. An asterisk is added to represent antibonding orbitals [141].

2.5.2 Hartree-Fock Method

The Hartree–Fock (HF) scheme is the most basic form of ab initio electronic structure calculation; it does not explicitly account for the instantaneous Coulombic electron-electron repulsion. In the computation, just its mean field, or average influence, is taken into account. Because this is a variational process, the approximate energies that are acquired and stated in terms of the wave function of the system are always greater than or equal to the precise energy. As the size of the basis increases, these approximate energies tend to a limiting value known as the Hartree-Fock limit [142].

The HF wave function and energy are erroneously introduced by the absence of instantaneous electron correlation, which has a significant impact on the kinetic barrier prediction and the London dispersion force description. It is still possible to systematically improve the HF solution in spite of this error. In one way, the many-body perturbation theory leads to the Møller–Plesset (MPn) methods [143]. In another, the configuration interaction (CI) methods [144] are derived from expressing the wave function as a linear combination of Slater determinants, i.e., the HF one plus those representing single, double, triple, etc., excitations.

Despite the enhanced quality of the post-HF techniques, their computational expense significantly limits their applicability due to the system size. These computations in surface modeling are

primarily utilized to refine less precise (yet more cost-effective) techniques to verify their adequacy in depicting the electronic makeup of the modeled surfaces [137].

2.5.3 Semi-empirical methods

Even though DFT methods offer significant cost advantages compared to wave function methods, simulations using DFT are still constrained by the size of systems, typically up to hundreds or even thousands of atoms, and require high-performance computing for massively parallel calculations. Semiempirical techniques provide a quicker option for surpassing the size constraints of DFT. These techniques stem from the pure QC techniques but make use of various approximations, such as excluding bioelectronics integrals, and incorporate empirical factors to address errors caused by the approximations and consider electron correlation effects. Because of these simplifications, semiempirical methods are quicker than ab initio methods, allowing for the analysis of large chemical systems that would be impossible to handle with pure quantum chemistry methods. Yet, the effectiveness of the semiempirical techniques greatly relies on the appropriateness of the parameterization for the particular scenario being analyzed. In other words, the results may be highly inaccurate if the simulated system does not align with the training set that was used to parameterize the method [137].

2.5.4 Density Functional Theory (DFT)

Density functional theory (DFT) is a computational method in physics, chemistry, and materials science used to study the electronic structure of atoms, molecules, and condensed phases, mainly focusing on the ground state of many-body systems. By utilizing this theory, functions, which are functions of another function, can be employed to determine the characteristics of a many-electron system. In DFT, these functionals are based on the electron density that varies in space [145].

Despite originating from the Thomas-Fermi model, density functional theory was formally established by Walter Kohn and Pierre Hohenberg through the two Hohenberg-Kohn theorems (HK) [146]. The second HK theorem establishes an energy functional for the system and demonstrates that the lowest energy state electron density minimizes this function. Walter Kohn and Lu Jeu Sham further advanced the HK theorem to create Kohn-Sham DFT (KS DFT). In this structure, the challenging problem of many-body interaction among electrons in a fixed external potential becomes a solvable problem of non-interacting electrons in an effective potential. The efficient potential accounts for the external potential and the impact of Coulomb interactions among electrons, such as exchange and correlation interactions. Modeling the last two interactions presents a challenge in KS DFT. The local-density approximation (LDA) is the most basic approximation, using precise exchange energy for a uniform electron gas derived from the Thomas-Fermi model and correlations to fit the energy for a uniform electron gas. Solving non-interacting systems is quite straightforward since the wavefunction can be depicted as a Slater determinant of orbitals [145].

In typical many-body electronic structure calculations, the molecules or clusters being studied have their nuclei considered to be stationary (following the Born-Oppenheimer approximation), creating a constant external potential V through which the electrons move. An immobile electronic state can be defined by a wavefunction $\Psi(r_1, \ldots, r_N)$ that meets the time-independent Schrödinger equation for multiple electrons [145].

$$\hat{H}\Psi = [T + V + \hat{U}\,]\Psi = [\sum_{i=1}^{N}\left(-\frac{\hbar^2}{2m_i}\nabla_i^2\right) + \sum_{i=1}^{N} V(r_i) + \sum_{i<j}^{N} U(r_i, r_j)\,]\,\Psi = E\Psi \qquad \textbf{(2.2)}$$

Where $\hat{H}$ represents the Hamiltonian and E denotes the total energy of the N-electron system. T represents the kinetic energy. V represents the potential energy caused by positively charged

nuclei in the external field, while $\hat{U}$ denotes the energy of interaction between electrons. The individuals in charge *T* and $\hat{U}$ are universal operators that remain consistent across all N-electron systems. The value of *V* varies depending on the system. Due to the presence of the interaction term $\hat{U}$, this complex equation involving multiple particles cannot be broken down into simpler equations for individual particles. Numerous advanced techniques exist for solving the many-body Schrödinger equation by expanding the wavefunction in Slater determinants.

In this case, DFT offers a more flexible option by allowing the systematic mapping of the many-body problem onto a single-body problem without $\hat{U}$. The electron density n(r) is the main variable in DFT, and it is determined for a normalized Ψ [145].

$$n(r) = N \int d^3 r_2 \ldots \int d^3 r_N \Psi^*(r, r_2, \ldots., r_N)\Psi(\mathrm{r}, r_2, \ldots., r_N) \quad \textbf{(2.3)}$$

Kohn–Sham equations of this auxiliary noninteracting system can be represented as :

$$\left[-\frac{\hbar^2}{2m}\nabla^2 + V_s(\boldsymbol{r})\right]\varphi_i(\boldsymbol{r}) = \varepsilon_i\varphi_i(\boldsymbol{r}), \quad \textbf{(2.4)}$$

which yields the orbitals φ_i that reproduce the density n(**r**) of the original many-body system [147]

$$n(\boldsymbol{r}) = \sum_{i=1}^{N}|\varphi_i(\boldsymbol{r})|^2 \quad \textbf{(2.5)}$$

The effective single-particle potential can be written as

$$V_s(\boldsymbol{r}) = V(r) + \int \frac{n(r\prime)}{|r-r\prime|}\, d^3r' + V_{XC}[n(\boldsymbol{r})], \quad \textbf{(2.6)}$$

Where the first term is the external potential denoted as V(r), the second term represents the Hartree term that accounts for electron-electron Coulomb repulsion, and the final term, VXC, denotes the exchange-correlation potential. In this case, VXC incorporates all the multiple-particle interactions. As the Hartree term and VXC are influenced by n(r), which is influenced by the φi,

which are in turn influenced by Vs, the issue of solving the Kohn-Sham equation must be approached iteratively in a self-consistent manner. Typically, one begins by making an initial assumption for n(r), then computes the corresponding Vs and solves the Kohn-Sham equations for the φi. Using this information, a revised density is determined, and the process is restarted. This process is then continued until reaching convergence [145].

2.5.5 Density Functional Non-equilibrium Green's Function (DFT-NEGF)

The NEGF method was first developed in the 1960s by Martin's seminal work. Schwinger, along with Kadanoff, Baym, Keldysh, and additional researchers. Following the emergence of mesoscopic physics in the 1980s, the Landauer approach was integrated with this method, resulting in the widely utilized "NEGF-Landauer method" in nanoelectronics for device modeling and technology advancement [148].

Another frequently applied method for studying charge transport in metal-molecule-metal junctions relies on the DFT-NEGF principle [132]. In short, this method involves placing a molecule between two leads which are semi-infinite displayed in Figure 2.7. The NEGF method is a revision of the mesoscopic transport theory created by Landauer, takes into account the impacts of inelastic (electron-phonon) scattering and electron-electron interactions in a non-equilibrium state (when a bias is applied) and provides a broader method for addressing the transportation issue [149].

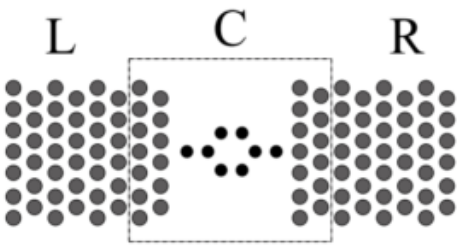

Figure 2.7: Schematic of a device set up for calculation charge transport using NEGF principles

The most common approach is the combination of the NEGF formalism with DFT in a self-consistent manner (DFT-NEGF) technique for simulating electronic flow in nano-sized materials [149]. The initial application of the DFT is used to derive the Hamiltonian and electronic structure of the scattering region before calculating the NEGF to determine the charge density, transmission, and current of the molecular system. After resolving the ground state issue through DFT, the Green's function of the central area is calculated. The Green's function at energy E is given by [149]

$$G(E) = [(E+i\eta)\, S-H-\Sigma_L-\Sigma_R]^{-1} \qquad \textbf{(2.7)}$$

H and S represent the Hamiltonian and overlap matrix for the scattering region. Determined by DFT, η is a small positive value, and ΣL, R are self-energies that take into consideration the impact of the electrodes on the scattering region. Subsequent to this, the fresh density of charge and electric potential are determined. The amount of charge or electronic density is acquired in the following way:

$$\rho = \frac{1}{2\pi} \int_{-\infty}^{\infty} [f(E, \mu_L)\, G\Gamma_L G^{\dagger} + f(E, \mu_R)\, G\, \Gamma_R G^{\dagger})]dE \qquad \textbf{(2.8)}$$

The electrochemical potentials of the electrodes are denoted as $\mu L, R$, while f(E, μ) represents the Fermi-Dirac function which characterizes the energy population. The electronic density obtained from Green's function is utilized in the following DFT calculation, and the process is reiterated until DFT and NEGF achieve self-consistency. The transmission function can be derived from Green's function.

$$T(E) = Tr\,(\Gamma_L G \Gamma_R G^{\dagger}) \qquad \textbf{(2.9)}$$

Finally, the current can be obtained using the Landauer-Büttiker formula as [149]

$$I = \frac{2e}{h}\int_{\mu_L}^{\mu_R} T(E)dE = \frac{2e}{h}\int_{\mu_L}^{\mu_R} (Tr(\Gamma_L G \Gamma_R G^{\dagger})\, dE \qquad \textbf{(2.10)}$$

2.6 Conclusion

In our study, we have used Density Functional Non-equilibrium Green's Function (DFT-NEGF) for geometry optimization and energy analysis. The study of self-assembled metal molecular networks using Density Functional Theory (DFT-NEGF) yields valuable insights into their electronic characteristics and behavior. Through DFT simulations, precise predictions of charge distribution, HOMO-LUMO gaps, and electron transport mechanisms within these networks can be made. Employing a combination of self-assembly and DFT analysis presents an effective strategy for creating materials with specific electronic properties. By optimizing metal-ligand interactions and structural arrangements, these networks can be customized for diverse applications in molecular electronics and catalysis. Overall, incorporating DFT-NEGF into the examination of self-assembled metal molecular networks enhances our comprehension and advancement of functional nanomaterials.

Chapter 3 - Modeling the Electronic Properties of BDT-Graphene Molecular Networks

3.1 Introduction to Simulated Structures, Modeling Tools, and Methods

In quantum mechanical systems, the majority of computations rely on the time-independent Schrödinger wave equation and the diverse techniques and approximations devised to resolve it. In this chapter, we focused on using DFT-based DMol^3 analysis for modeling the electronic properties of dithiol molecules-metal cluster network.

3.2 Details of Simulated Nanostructures and Modelling Methods

Numerous studies have focused on modeling the electronic transport properties of molecular systems, with the BDT molecule, due to their stability and presence of delocalized π electron, often serving as the key model for exploring molecular transport junctions [150, 151].

3.2.1 Simulated Nanostructures

Researchers have extensively studied the electronic and transport properties of a BDT molecule bridged between two gold electrodes [152]. The general consensus is that delocalized molecular orbitals near the Fermi energy play a crucial role in facilitating electron transport through the molecular junction [153].

Inspired by previous research, we modeled molecular systems comprising 1,4- benzenedithiol molecules interconnected with single-layer graphene. Multiple metal-molecule nanojunctions were formed by connecting the molecules and metal clusters to form nanoscale networks.

Figure 3.1(a-b) illustrates the creation of linear chains, made up of numerous molecular junctions by joining benzenedithiol molecules and graphene nanosheet. As seen in Figure 3.1 (c-e), linear chains of varying lengths were identified by the quantity of graphene nanosheet units they held.

(a) Benzene (1,4) dithiol

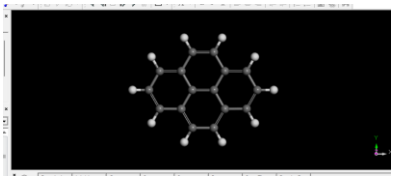

(b) Single Layer Graphene

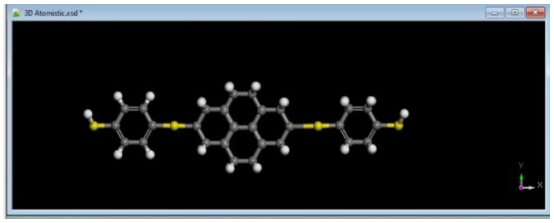

(c) 1-unit linear chain

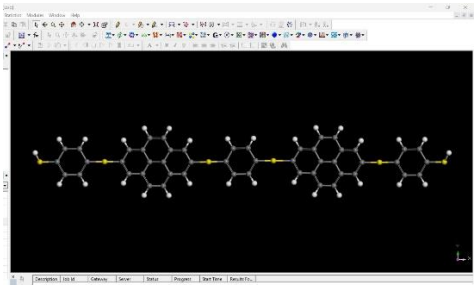

(d) 2-unit linear chain

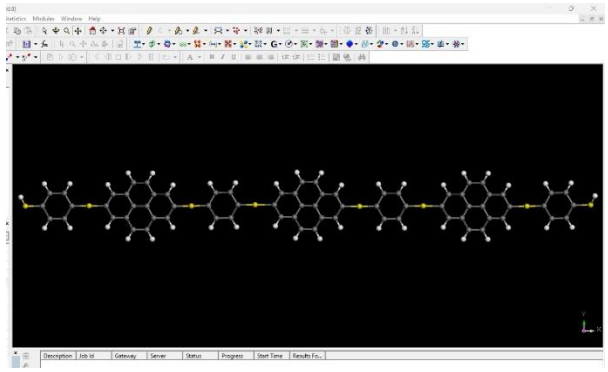

(e) 3-unit linear chain

Figure 3.1 (a-b) LDA VWN-optimized building blocks and starting structures for (c-e) Benzenedithiol-Graphene nanosheet linear chains of various lengths. Here, yellow, white, and grey colors denote sulfur, hydrogen, and carbon atoms, respectively.

We have also conducted a VAMP simulation on benzene dithiol molecules and single layer graphene.

3.2.2 Modelling Methods (DMol^3, VAMP)

DMol^3

With the aid of a software program called DMol^3, one can determine the electronic characteristics of molecules, surfaces, clusters, and crystalline solid materials using DFT. In order to use them, one must solve the DFT equations for each individual atom. This yields a set of numerical functions on the atomic basis set [154]. Fine geometry optimization calculations were performed on BDT and single layer graphene nanostructure using LDA VWN; BDT and single layer graphene were then bonded together to form linear chains. The electronic wave functions were expanded in a double numerical polarization (DNP) basis set. All electrons were included in the calculation. The SCF tolerance was set to 10^{-6} and a smearing value of 0.005 Ha was used for the calculations. Also, Energy analysis calculations were conducted for better understanding without using spin unrestricted. GGA PW91 has been used for energy analysis with a basis set of DND 3.5. The SCF tolerance was set to 10^{-6} and a smearing value of 0.005 Ha was used for the calculations.

VAMP

VAMP is a semiempirical molecular orbital package that can predict geometries, heats of formation, and a wide range of molecular properties. Semiempirical techniques use the same Linear Combination of Atomic Orbitals-Self Consistent Field (LCAO-SCF) theory as ab initio methods, but they simplify the process by omitting or approximating many complex integrals. Empirical parameters and functions are introduced to correct the errors caused by these simplifications, and they are adjusted to match experimental data. This is why the term

"semiempirical molecular orbital theory" refers to the methods used, which are parameterized to match experimental results. VAMP includes numerous improvements in geometry optimization and two-electron integral calculations [155].

3.3. Results and Analysis

3.3.1 Density of States (DOS) of simulated nanostructures

BDT

After constructing a molecular or crystal structure, it typically requires refinement to achieve a stable geometry. This refinement process, known as optimization, involves an iterative procedure where the atomic coordinates are adjusted until the structure's energy reaches a stationary point—where the forces acting on the atoms are zero. The term "geometry optimization" is generally understood to mean "geometry minimization" [155]. Figure 3.2 shows the geometry optimization steps and optimization convergence graph for benzene 1,4 dithiol.

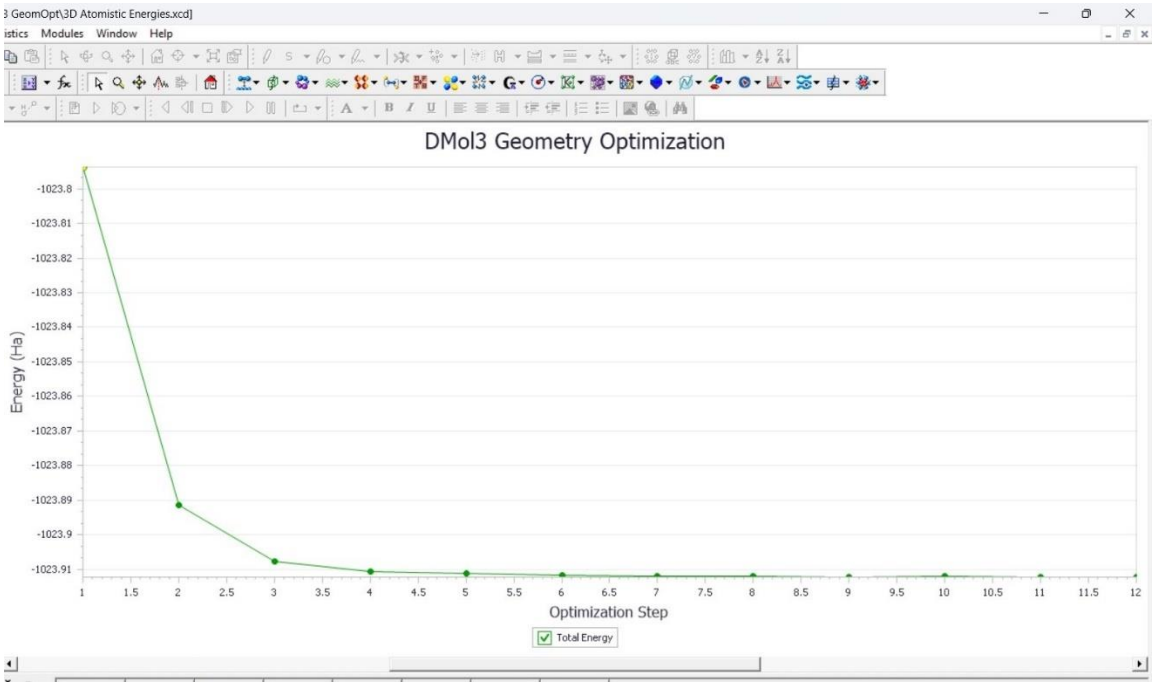

(a)

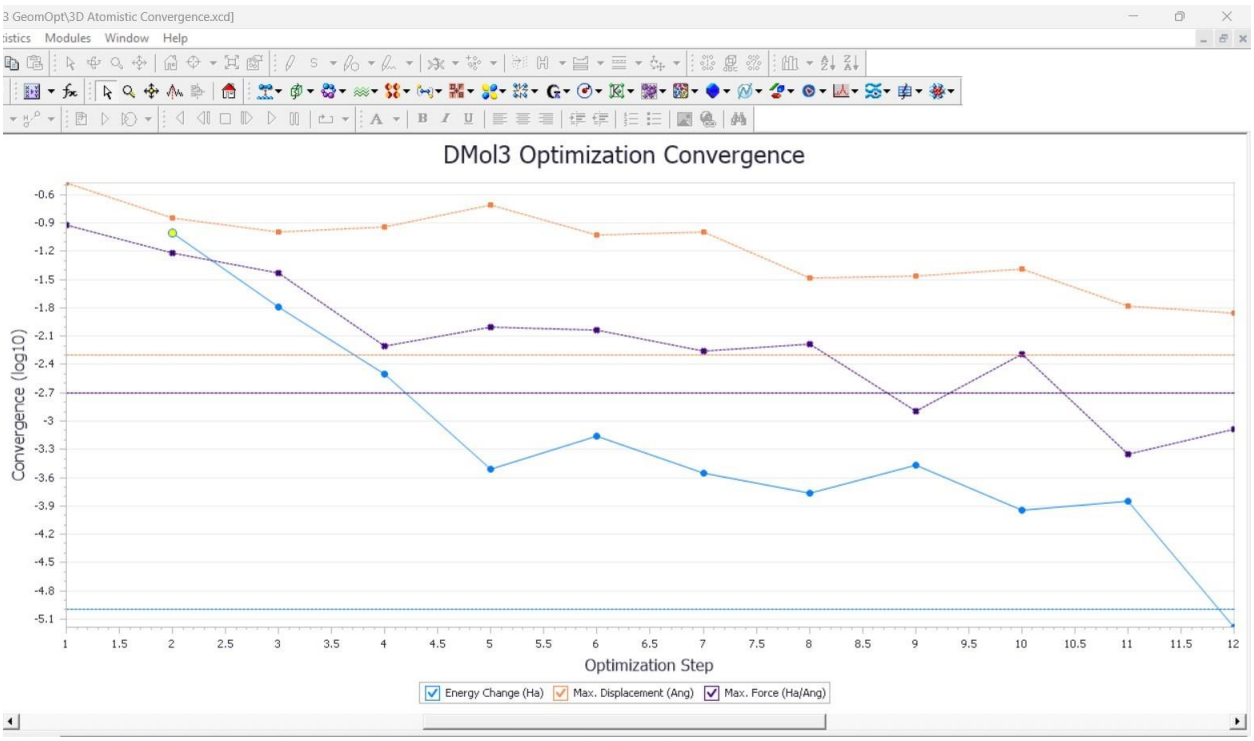

(b)

Figure 3.2: (a) Geometry Optimization Step Graph and (b) Optimization Convergence Graph of benzene 1,4 dithiol

Plots showing the density of states (DOS) in a system give information on how many states are available for electrons to occupy at different energy levels. The DOS, with artificial broadening added to each state, is a convolution of all the orbitals or states of the system as a function of energy.

On the other hand, over a range of energies, the projected density of states (PDOS) plot projects the total system orbitals onto the base orbitals or functions of particular atoms within the molecular system. This makes it possible to record the contributions made by various atomic orbitals to the total DOS. The total and projected density of state information of building blocks and linear networks are shown and analyzed below.

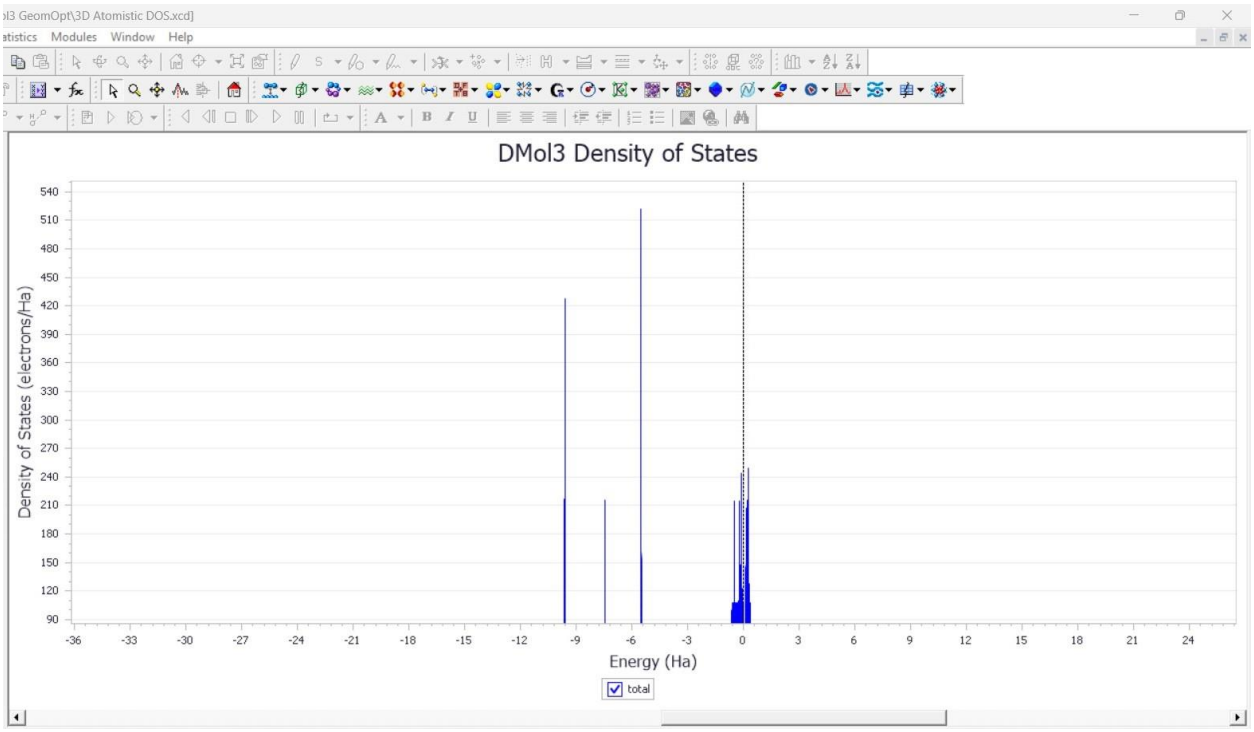
DMol3 Density of States
Density of States (electrons/Ha)
Energy (Ha)
total

(a)

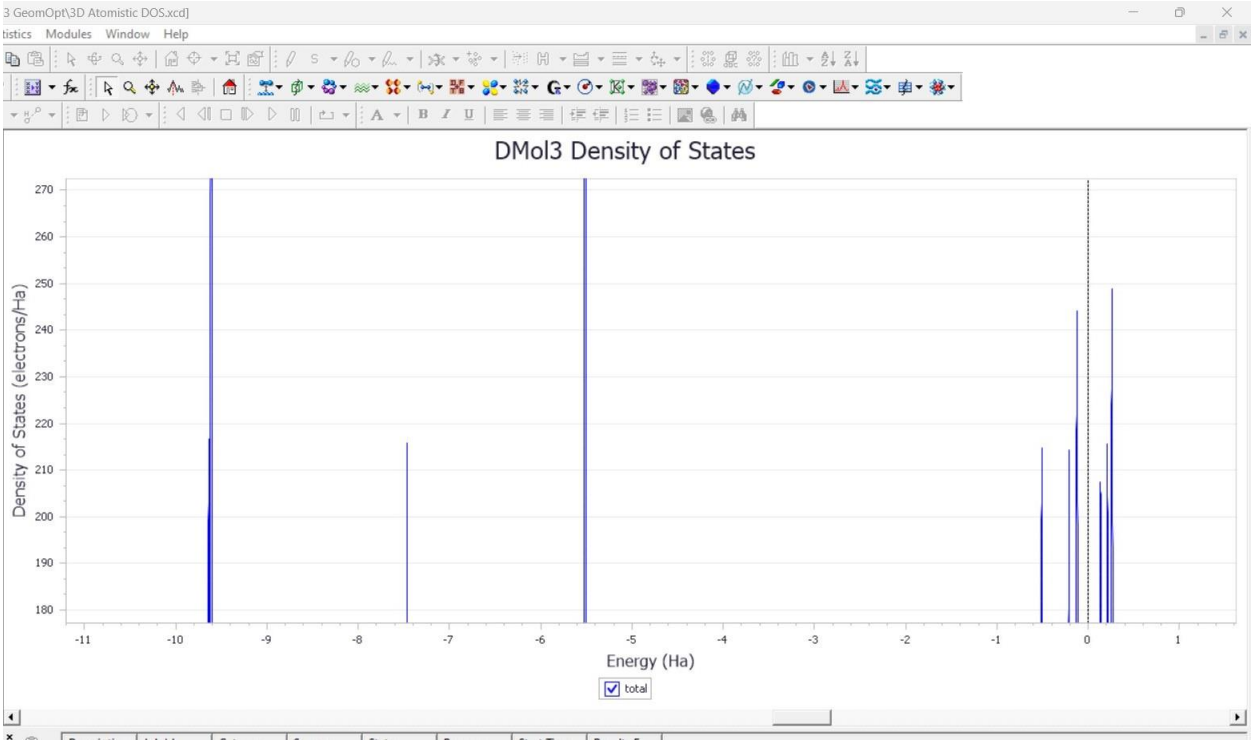
DMol3 Density of States
Density of States (electrons/Ha)
Energy (Ha)
total

(b)

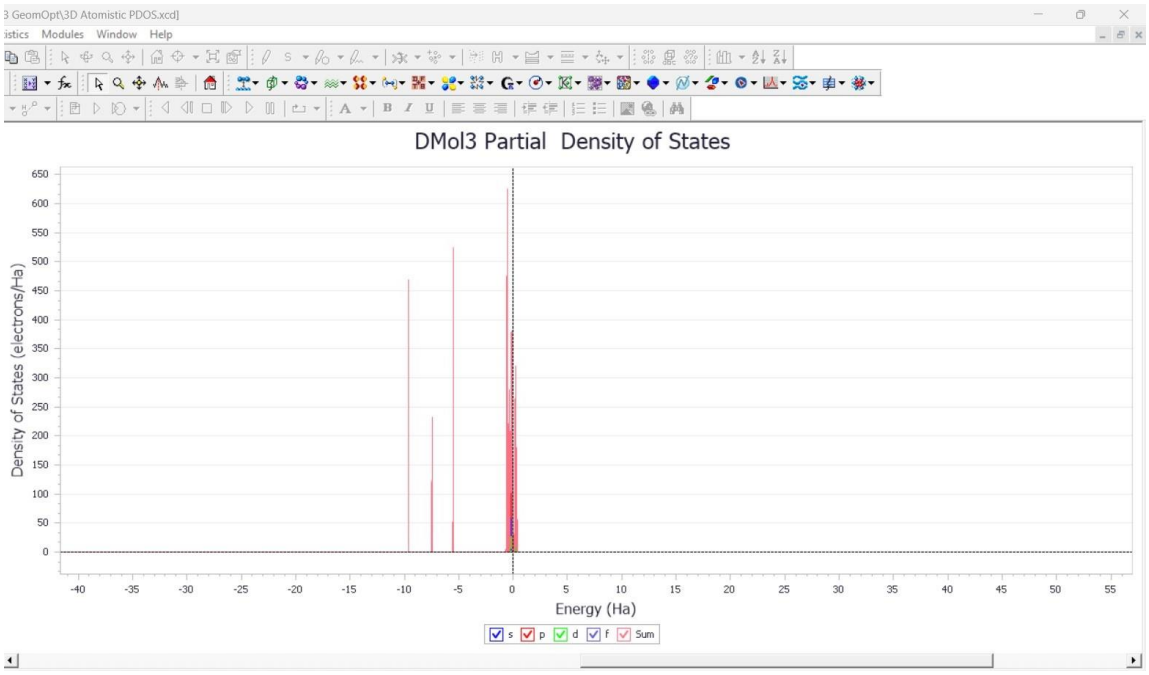

(c)

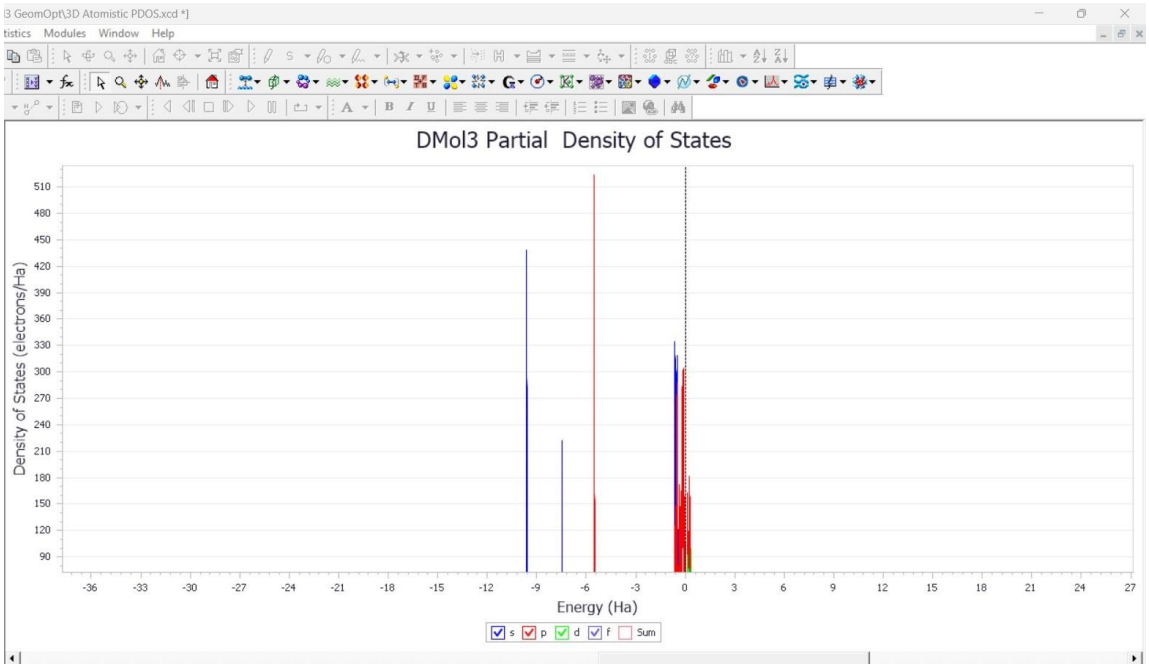

(d)

Figure 3.3: DOS and PDOS plot of BDT from Geometry Optimization (a) DOS plot (b) Magnified view of DOS plot near Fermi Energy (c) PDOS plot with sum (d) PDOS plot without sum

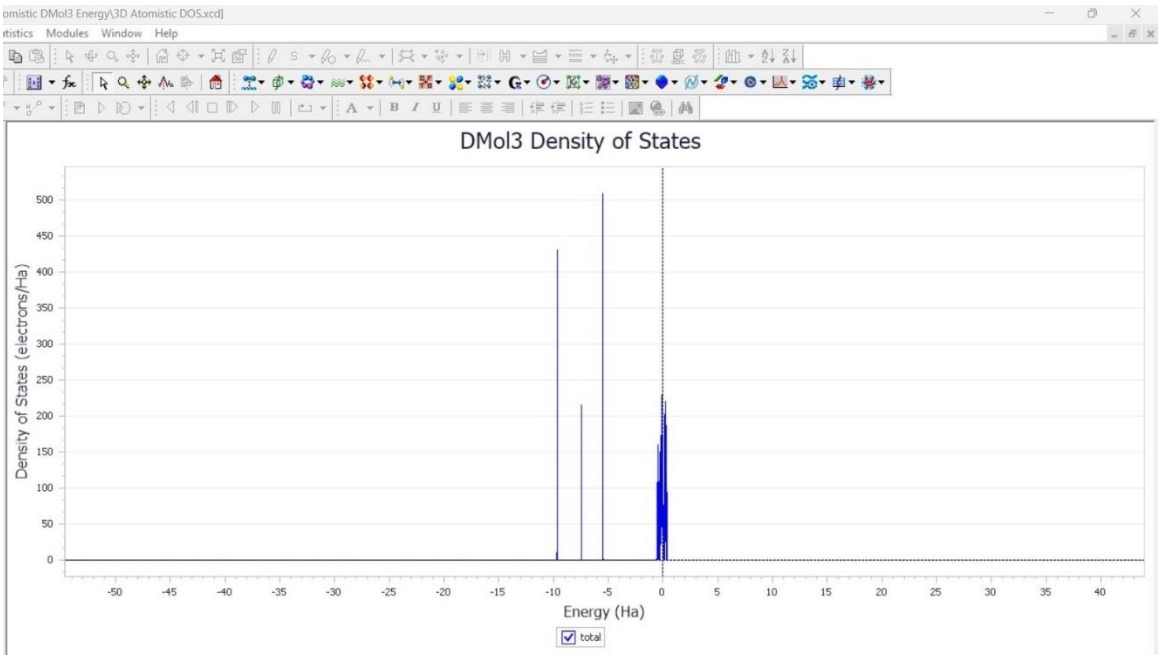
DMol3 Density of States
Density of States (electrons/Ha)
Energy (Ha)
total

(a)

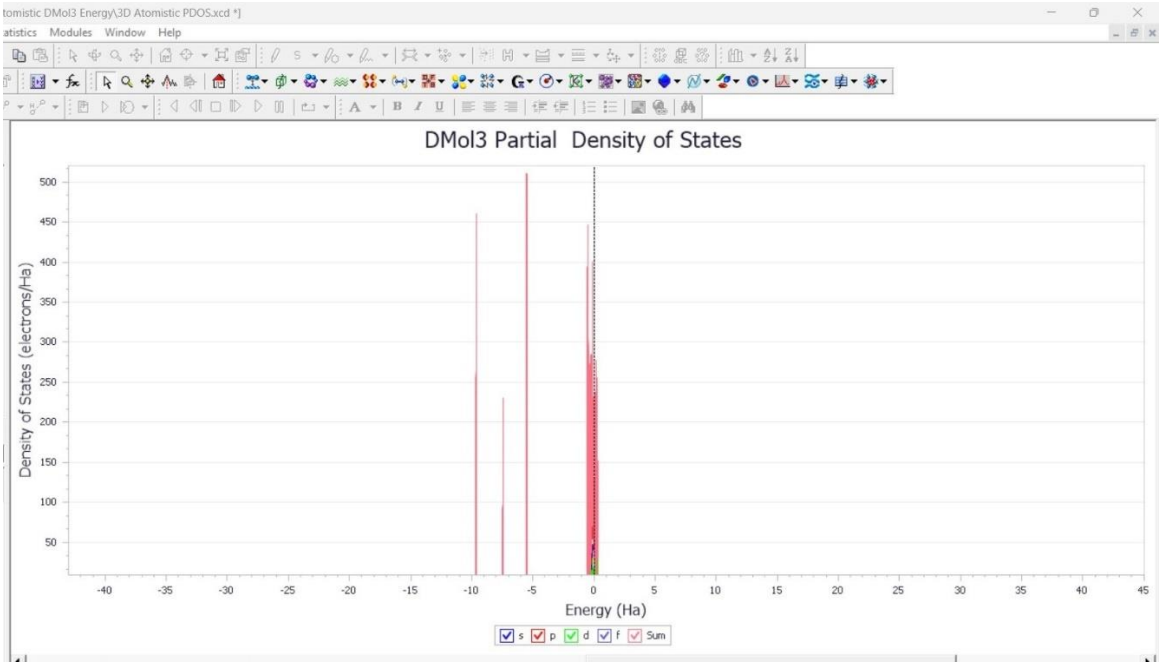
DMol3 Partial Density of States
Density of States (electrons/Ha)
Energy (Ha)
s p d f Sum

(b)

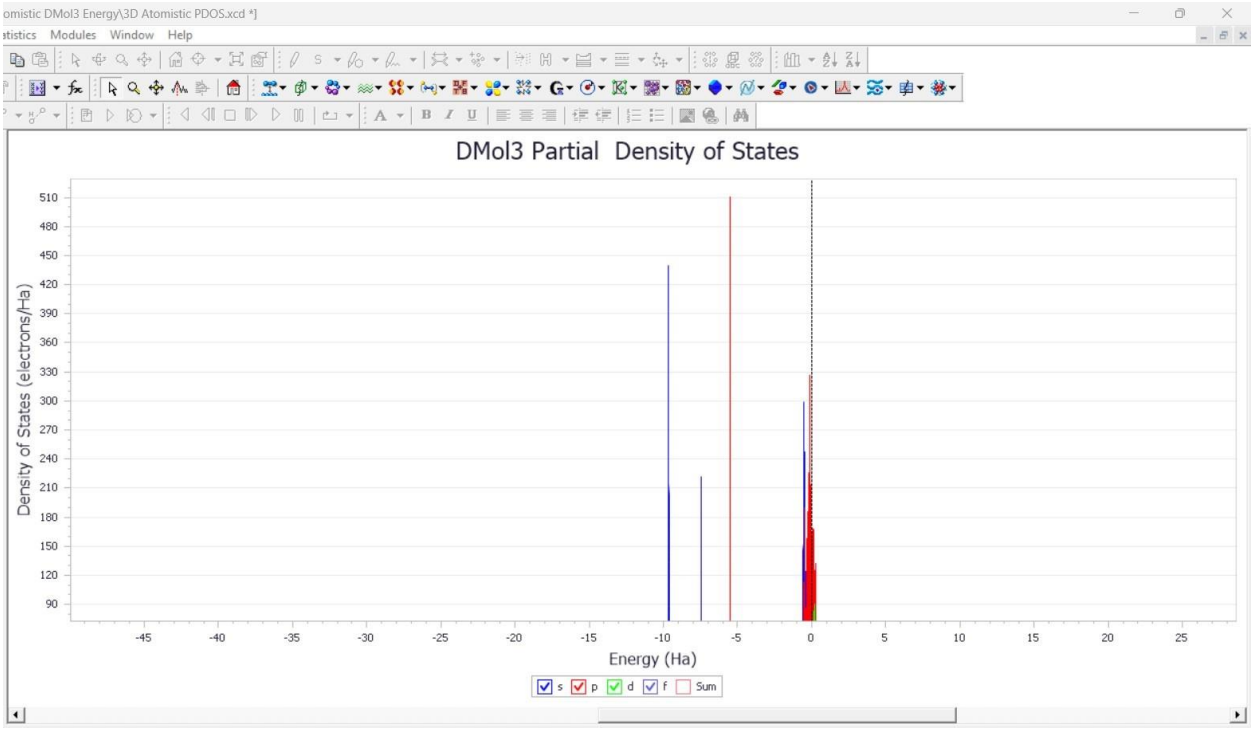
DMol3 Partial Density of States
Density of States (electrons/Ha)
Energy (Ha)
s p d f Sum

(c)

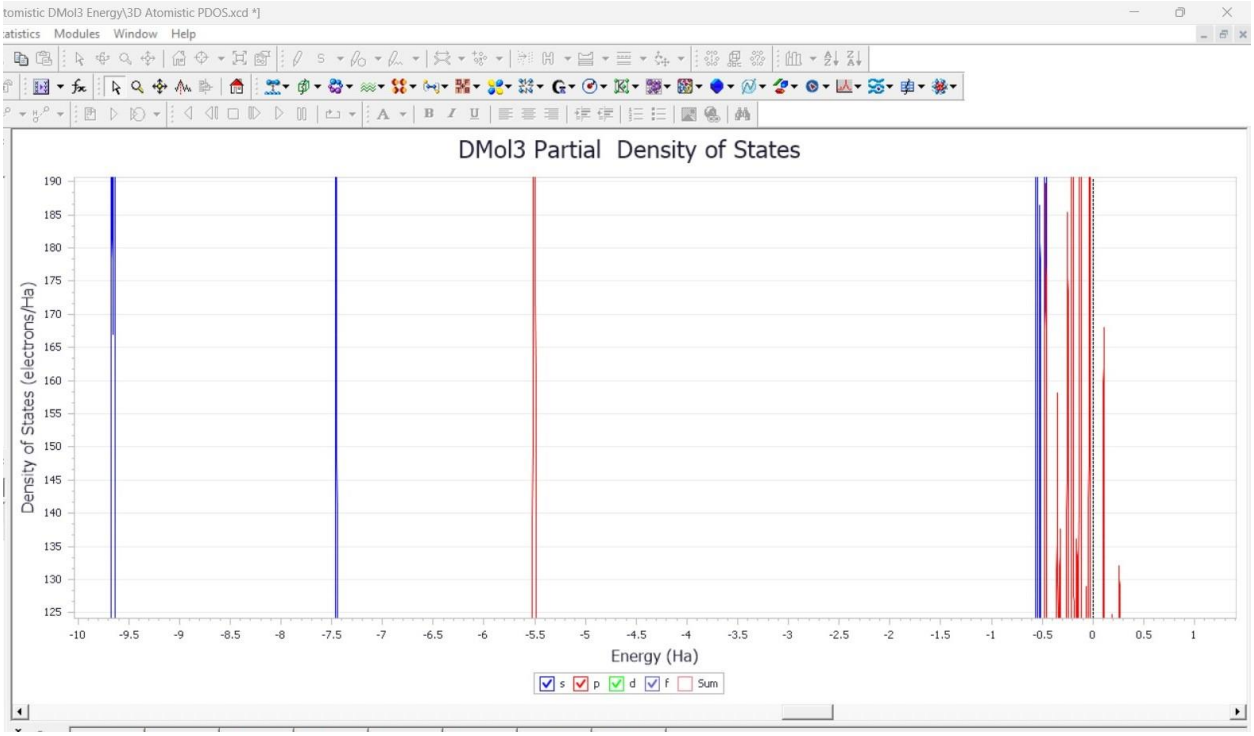
DMol3 Partial Density of States
Density of States (electrons/Ha)
Energy (Ha)
s p d f Sum

(d)

Figure 3.4: DOS and PDOS plot of BDT from Energy Analysis (a) DOS plot (b) PDOS plot (c) PDOS plot without sum (d) Magnified view of PDOS plot without sum near Fermi Energy

Figure 3.3 and Figure 3.4 show the total DOS and PDOS of BDT obtained from Geometry Optimization and Energy Analysis respectively. The PDOS peaks in both Figure 3.3 and 3.4 between the Fermi energy (represented by the vertical dashed line in the plot) can be seen at ~-0.6Ha and ~0.3Ha and those peaks likely correspond to HOMO and LUMO energies respectively. The various peaks in the PDOS plot correspond to the orbital overlap and energetical shift [156]. In both analyses, DOS and PDOS show similar properties. If HOMO and LUMO are far from Fermi level with a high energy gap, it indicates that the hybrid interface states (HIS) are not shifted and new states are generated by interfacial hybridization [157].

DOS and PDOS charts here provide an example of the structure of fragment orbitals that pertain to molecular orbitals. An anti-bonding interaction promotes that negative values and non-binding interactions indicate values around zero, whereas a bonding interaction confirmed the PDOS's positive value [158].

HOMO-LUMO gap of BDT using DFT without scaling is relatively small, near 4.2 eV. But theoretically it is 10.33eV. If scaling has been used, then the HOMO-LUMO gap would be around 8.5eV for BDT [159].

Graphene Nanosheet

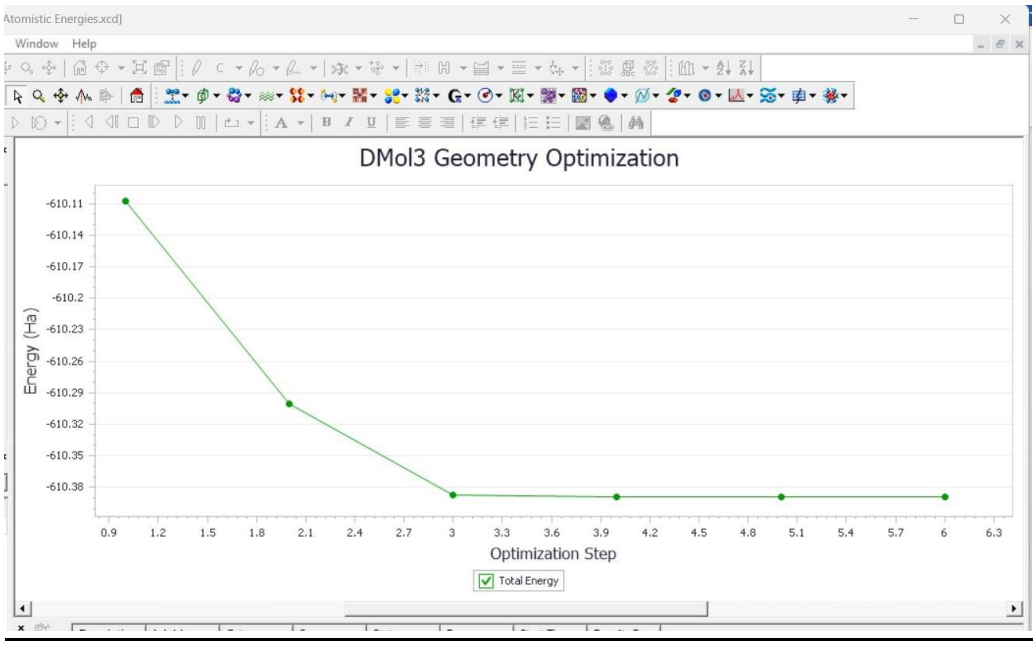

(a)

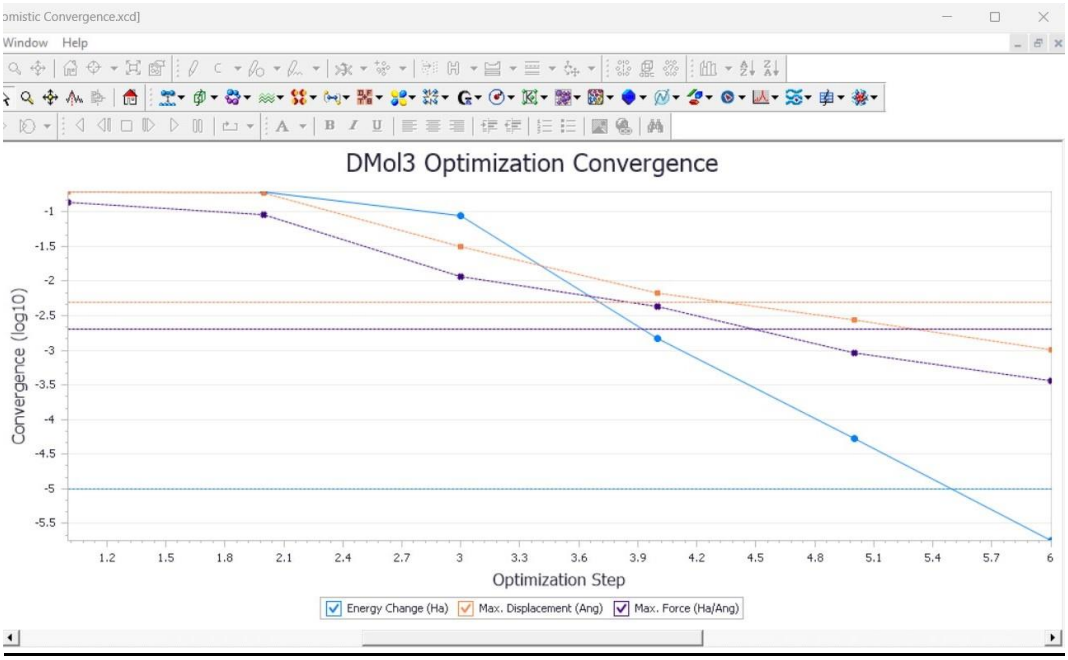

(b)

Figure 3.5: (a) Geometry Optimization Step Graph and (b) Optimization Convergence Graph of graphene nanosheet

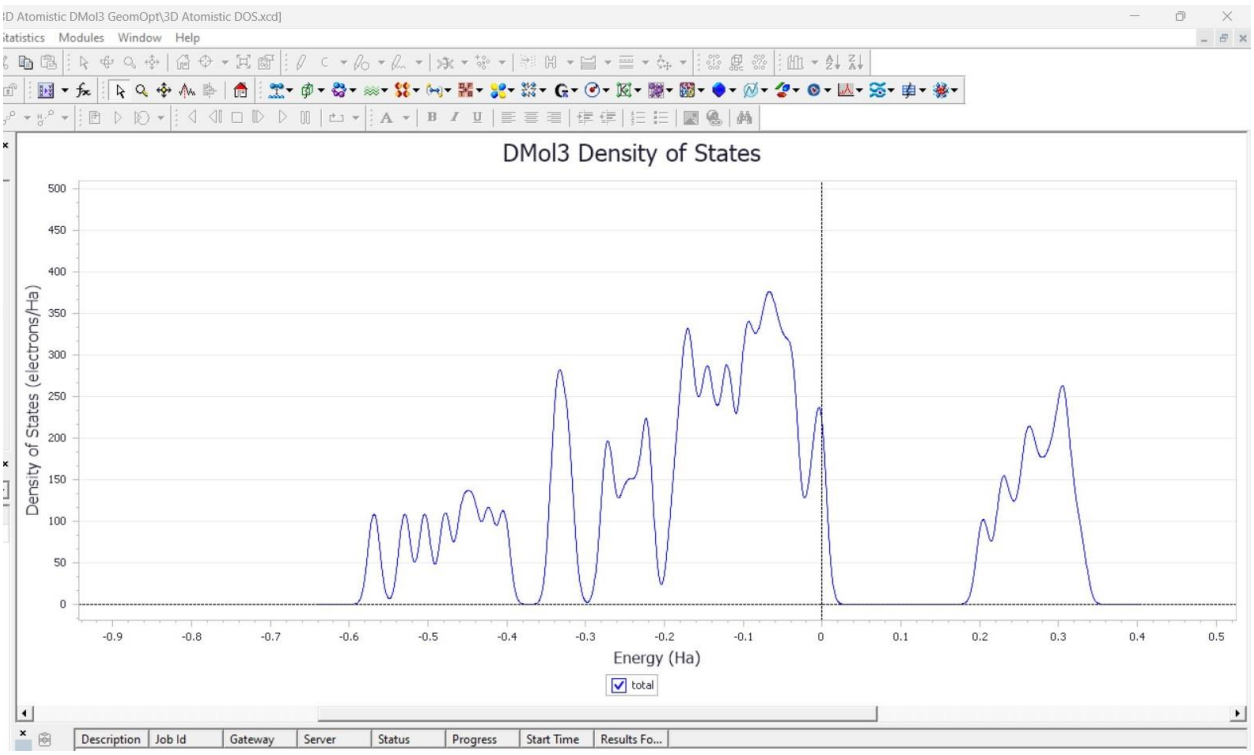
DMol3 Density of States
Density of States (electrons/Ha)
Energy (Ha)
total
Description
Job Id
Gateway
Server
Status
Progress
Start Time
Results Fo...

(a)

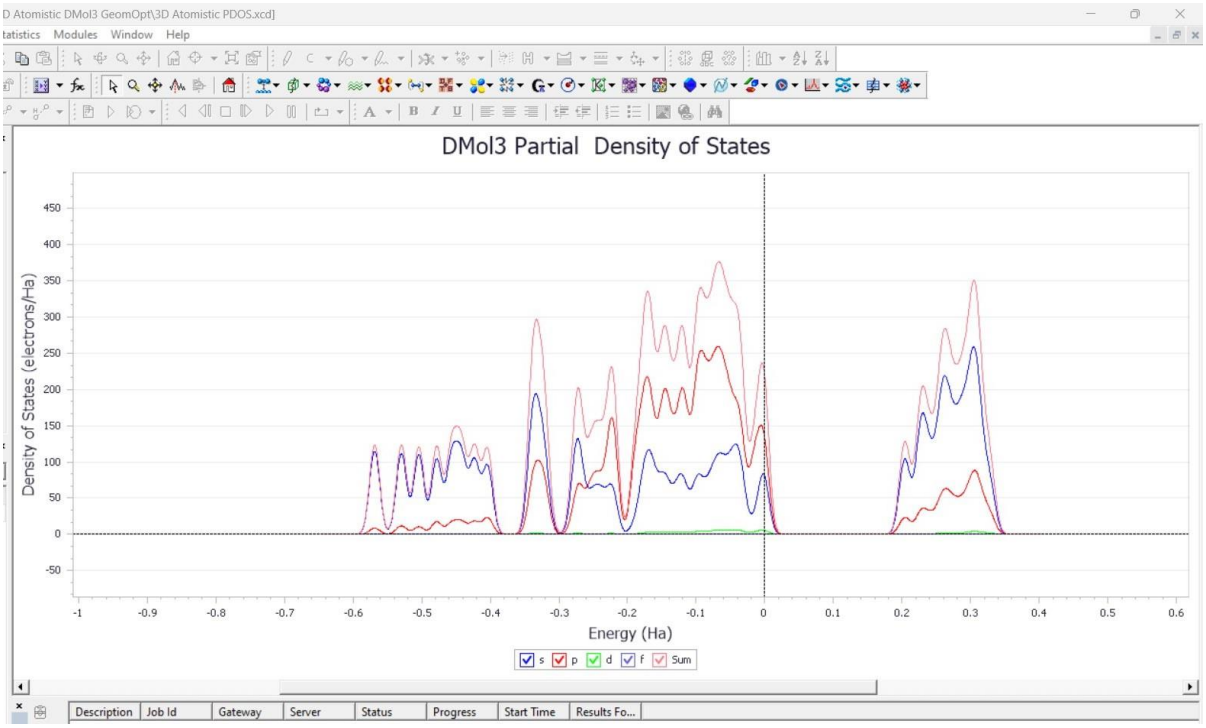
DMol3 Partial Density of States
Density of States (electrons/Ha)
Energy (Ha)
s
p
d
f
Sum
Description
Job Id
Gateway
Server
Status
Progress
Start Time
Results Fo...

(b)

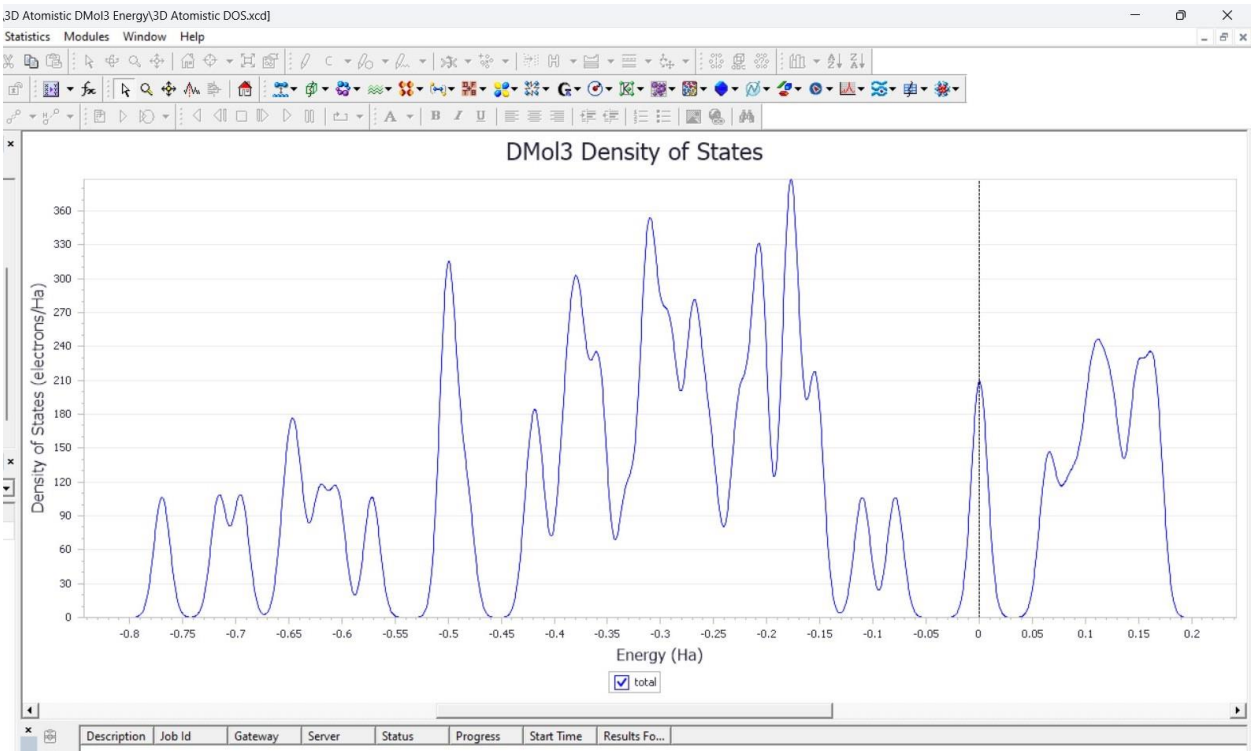

(c)

Figure 3.6: DOS and PDOS plot of Graphene nanosheet from Geometry Optimization and Energy Analysis (a) DOS plot from Geometry Optimization (b) PDOS plot from Geometry Optimization (c) DOS plot from Energy Analysis

Figure 3.5 shows the geometry optimization and convergence graph of graphene nanosheet. Figure 3.6 shows the total DOS and PDOS of Graphene nanosheet obtained from Geometry Optimization and Energy Analysis respectively. The DOS plot shows the valence band edge and conduction band edge around the Fermi-level energy. The PDOS peaks in Figure 3.6 (b) between the Fermi energy (represented by the vertical dashed line in the plot) can be seen at ~-0.6Ha and ~0.4Ha and those peaks likely correspond to HOMO and LUMO energies respectively. In both analyses, DOS and PDOS show similar properties. Here we can see that the valence band edge of graphene nanosheet is entirely composed of the p-orbitals, while the conduction band edge is made of the d-

orbitals. The PDOS graph also demonstrates that the majority of the valence and conduction bands surrounding the Fermi level are made up of carbon atoms in 2p states.

The valence and conduction bands consist solely of the π and π* bands. Given that each carbon atom's 2pz orbital contains one electron, the valence band is fully occupied while the conduction band remains unoccupied. It is also established that the electronic characteristics of a material are primarily influenced by the states close to the Fermi level. Hence, the electronic behavior of graphene is chiefly determined by the 2pz orbitals. Additionally, the partial density of states (PDOS) reveals that the carbon atoms' 2s and 2p orbitals contribute to the lower-lying valence bands within graphene's electronic structure. These lower valence bands are indicative of robust in-plane covalent bonds (σ bonds). The σ bond framework contributes to the remarkable mechanical properties of graphene [160].

Regarding graphene, it has been demonstrated that overlooking quasiparticle effects leads to an underestimation of the Fermi velocity (by 17%) in the 2eV energy range near the Fermi level, while not impacting the nonexistent band gap [161]

1-Unit Linear Chain

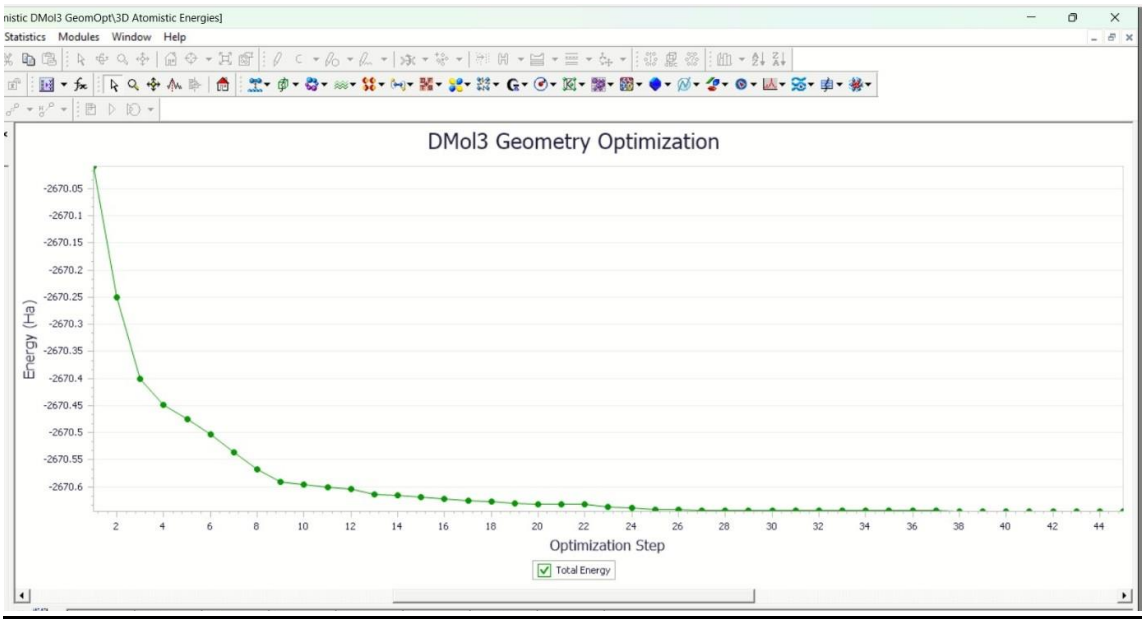

(a)

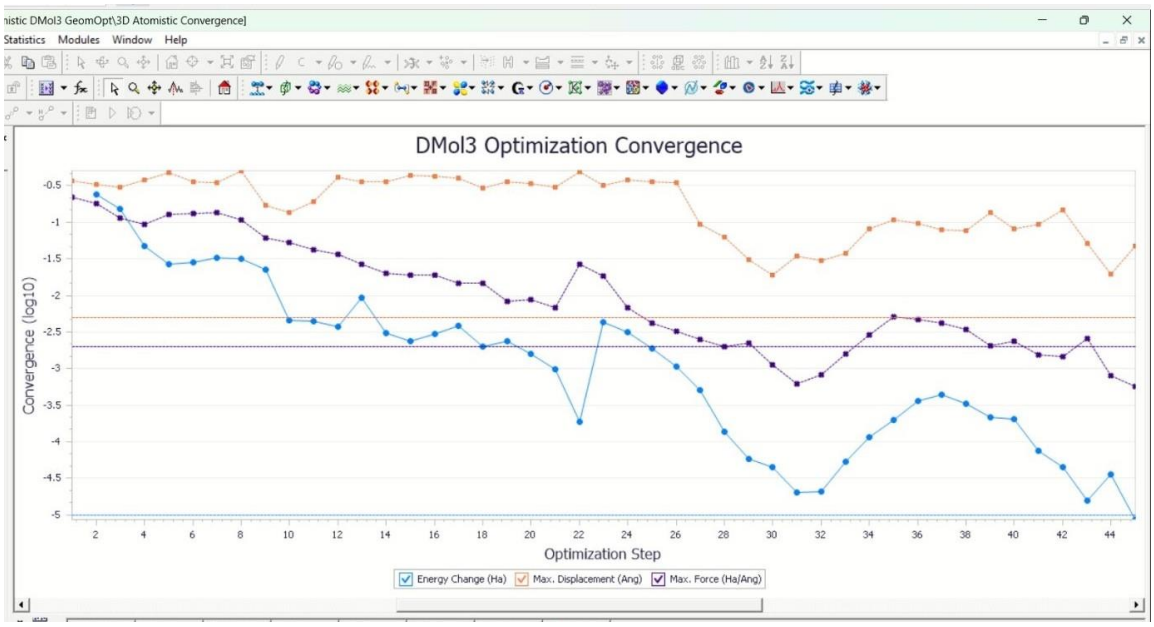

(b)

Figure 3.7: (a) Geometry Optimization Step Graph and (b) Optimization Convergence Graph of the 1-unit linear chain

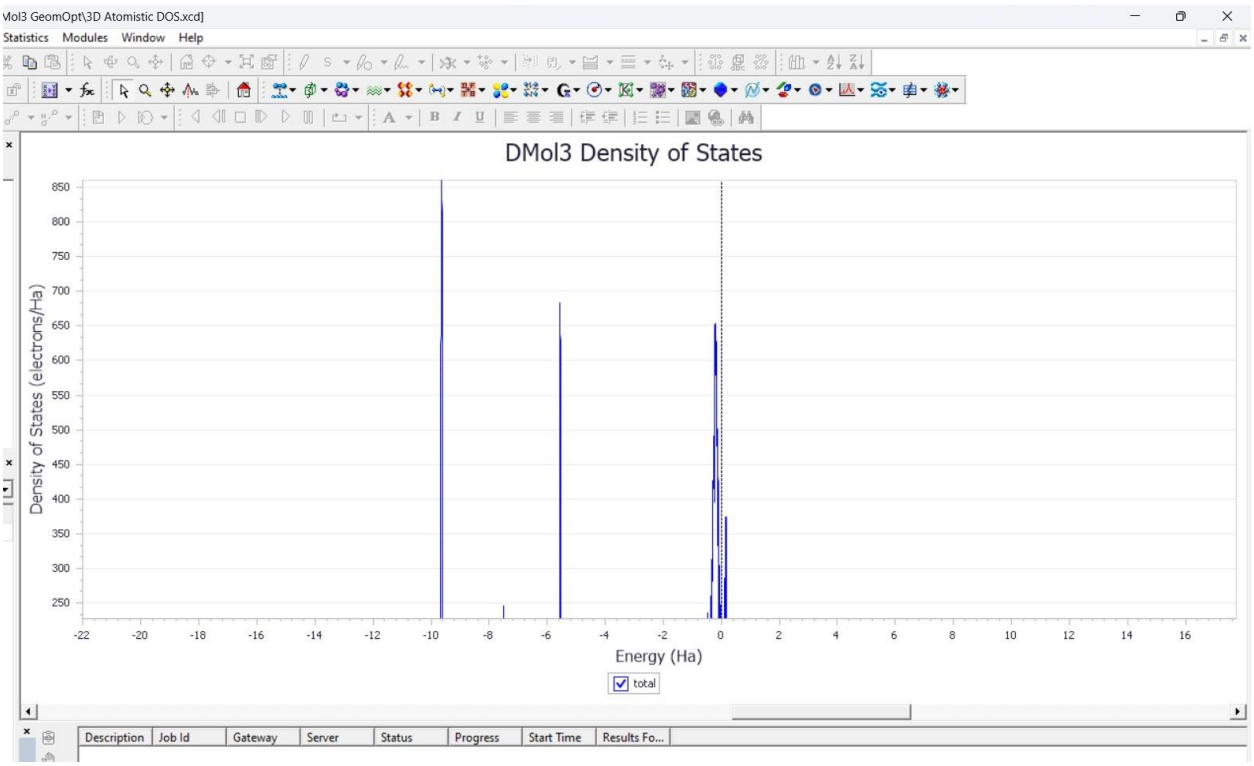
Statistics Modules Window Help
DMol3 Density of States
Density of States (electrons/Ha)
Energy (Ha)
total
Description
Job Id
Gateway
Server
Status
Progress
Start Time
Results Fo...

(a)

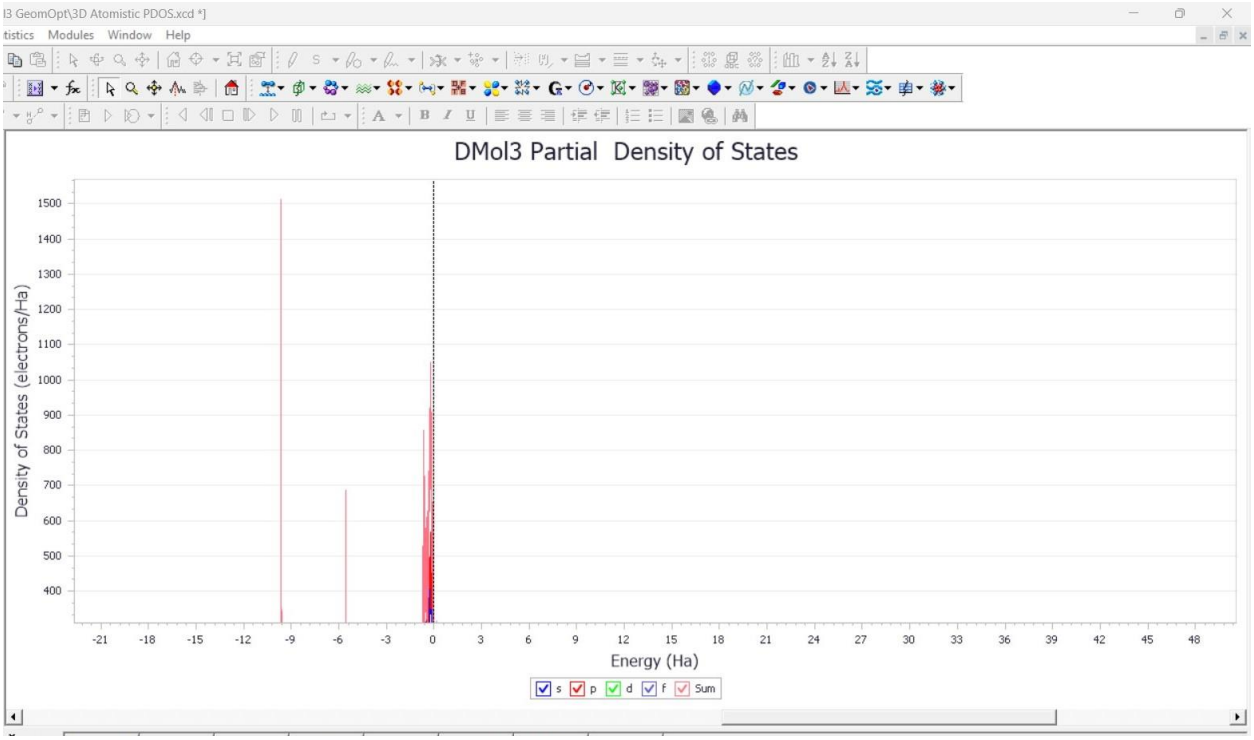
Statistics Modules Window Help
DMol3 Partial Density of States
Density of States (electrons/Ha)
Energy (Ha)
s
p
d
f
Sum

(b)

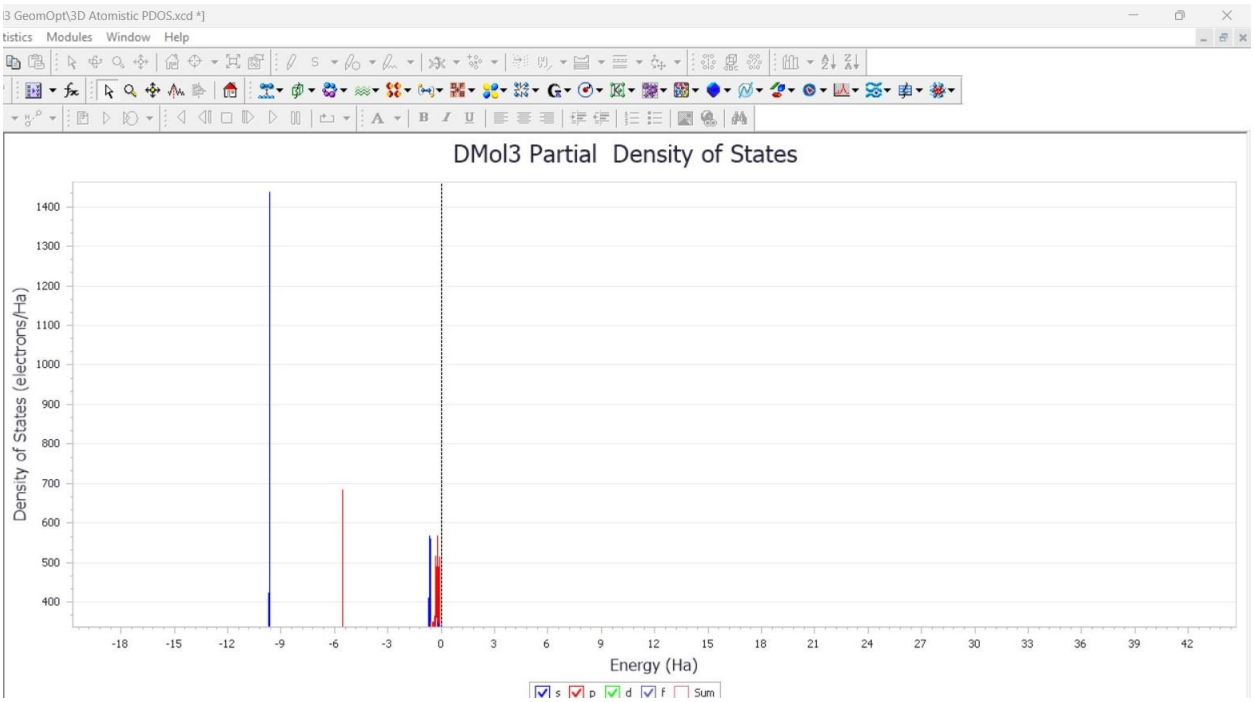

(c)

Figure 3.8: DOS and PDOS plot of 1-unit Benzenedithiol-Graphene linear chain from Geometry Optimization (a) DOS plot of 1-unit Benzenedithiol-Graphene linear chain (b) PDOS plot with sum (c) PDOS plot without sum

Figure 3.7(a-b) demonstrates the Geometry Optimization Step Graph and Optimization Convergence Graph of the 1-unit linear chain. PDOS plots of the isolated molecular networks against the total DOS of the linear molecular networks are shown in Figure 3.8 above. Figure 3.8(a) shows the total DOS of a 1-unit linear chain and Figure 3.8(b) and (c) represent the PDOS of an isolated 1-unit linear chain. The PDOS peaks in Figure 3.8 between the Fermi energy (represented by the vertical dashed line in the plot) can be seen at ~-0.6Ha and ~0.3Ha and those peaks likely correspond to HOMO and LUMO energies respectively. The various peaks in the PDOS plot correspond to the orbital overlap and energetical shift [156]. In both analyses, DOS and PDOS show similar properties.

2-Unit Linear Chain

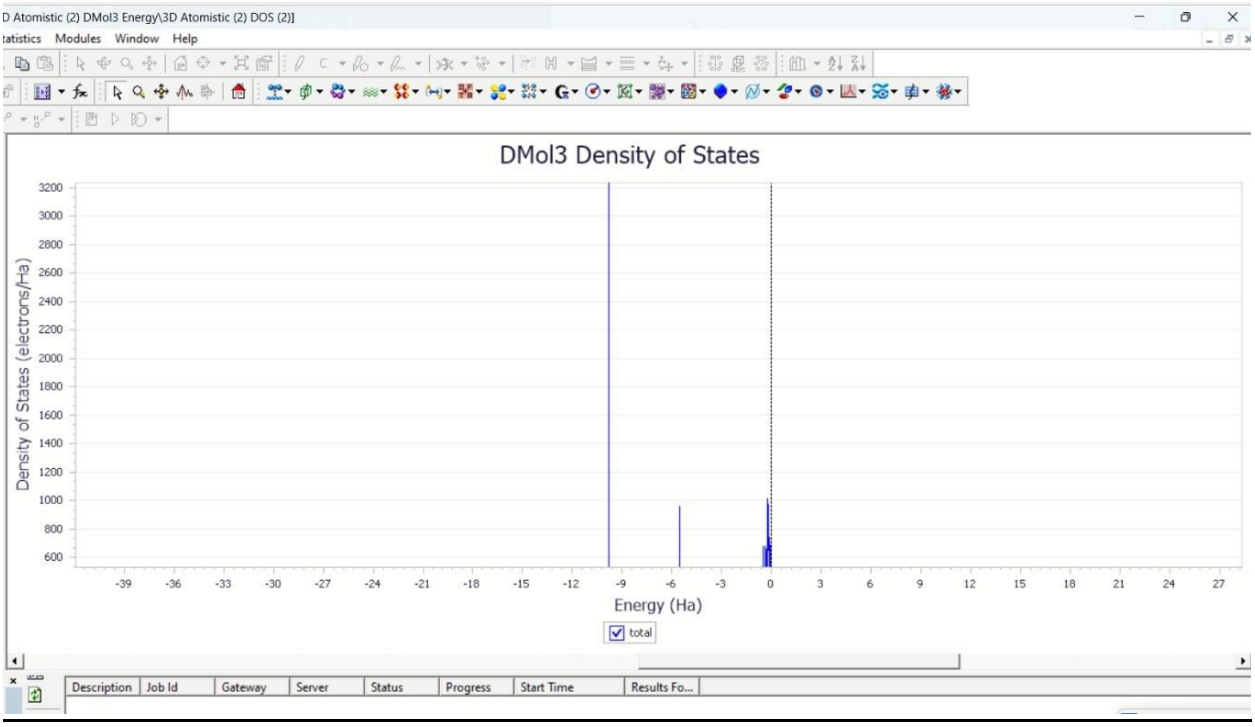

Figure 3.9: DOS plot of the 2-unit Benzenedithiol-Graphene linear chain from Geometry Optimization

Figure 3.9 shows the DOS plot of the 2-unit Benzenedithiol-Graphene linear chain from geometry optimization. Multiple peaks have been observed between ~-0.6Ha and ~0Ha. There are two more peaks visible around ~-5Ha and ~-9.6Ha. Those peaks most likely correspond to the energies of the HOMO and LUMO, respectively [156].

3-Unit Linear Chain

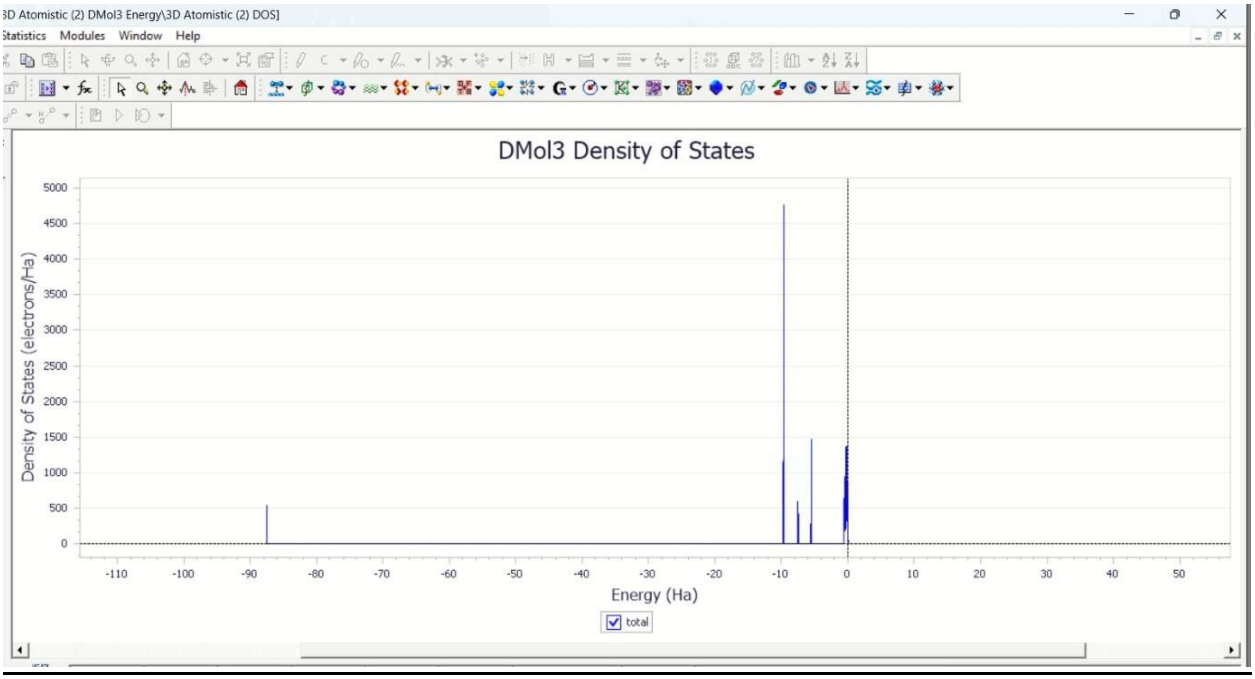

Figure 3.10: DOS plot of the 3-unit Benzene dithiol-graphene linear chain from Geometry Optimization

Figure 3.10 shows the DOS plot of the 3-unit Benzene dithiol-graphene linear chain from geometry optimization. Multiple peaks have been observed between ~-10Ha and ~0Ha. There are three prominent peaks visible around ~-10Ha, ~-8Ha and ~-6Ha. Those peaks most likely correspond to the energies of the HOMO and LUMO, respectively [156].

3.3.2 Molecular orbital visualizations of the nanostructures

BDT

The energetic alignment of frontier molecular orbitals—the highest occupied molecular orbital (HOMO) and the lowest unoccupied molecular orbital (LUMO)—with the Fermi level of the metal electrodes, which is typically controlled by tunneling transport, has been shown to affect

conductance in DFT-based studies of electron transport through molecules [162]. Therefore, a comprehension of electron transport in molecular systems requires an understanding of molecular orbitals. Plotting the isosurfaces of the LDOS at energies corresponding to peaks in the PDOS plots allowed for the visualization of molecular orbitals in this work. Figure 3.11 shows the electron density of benzene dithiol. Data on the stability and reactivity of molecules are included in the FMO investigations. The movement of charges within the molecule is seen by the HOMO and LUMO plots [158].

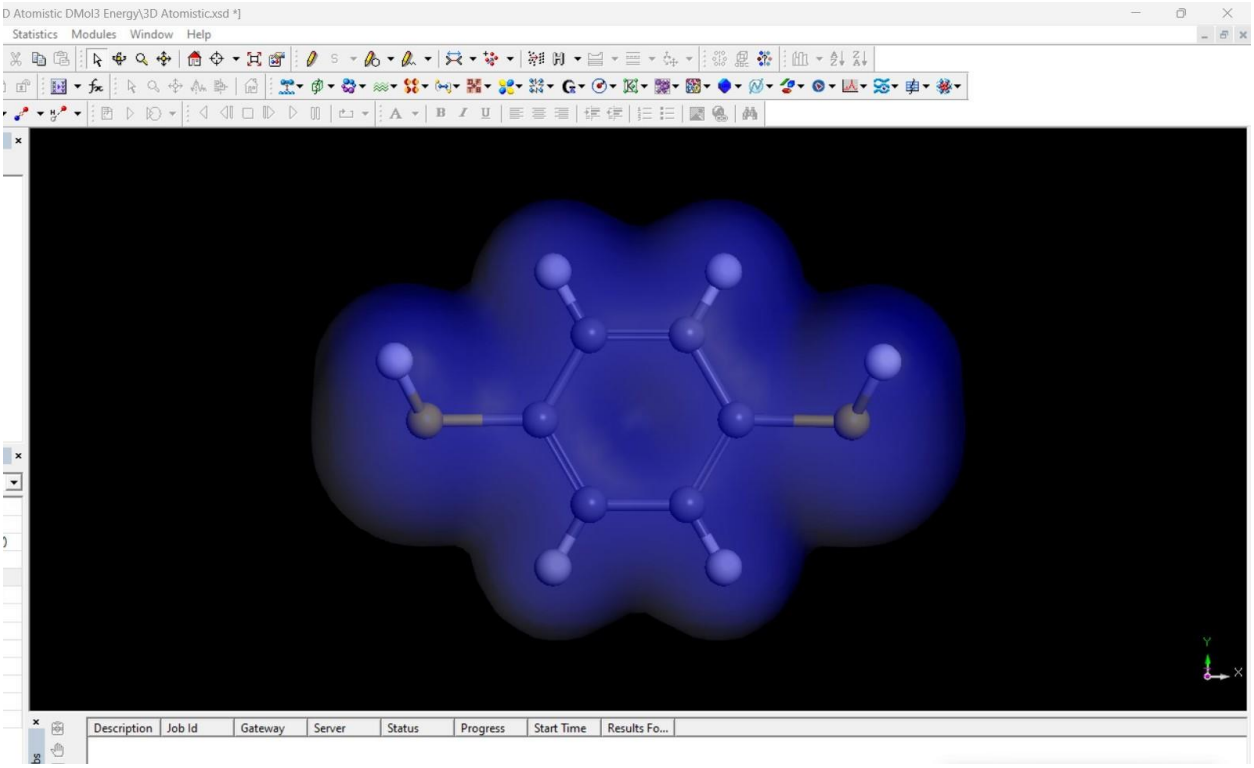

Figure 3.11: Electron density of BDT

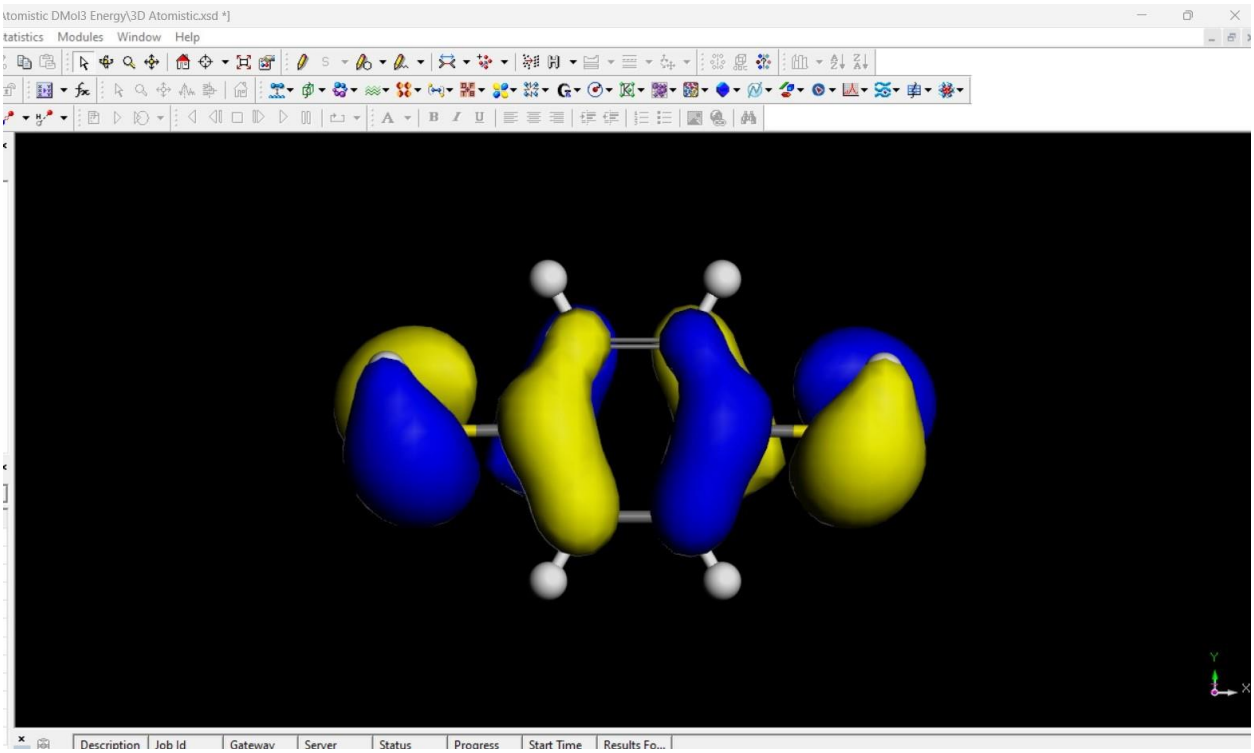
Modules
Window
Help
Description
Job Id
Gateway
Server
Status
Progress
Start Time

(a) HOMO

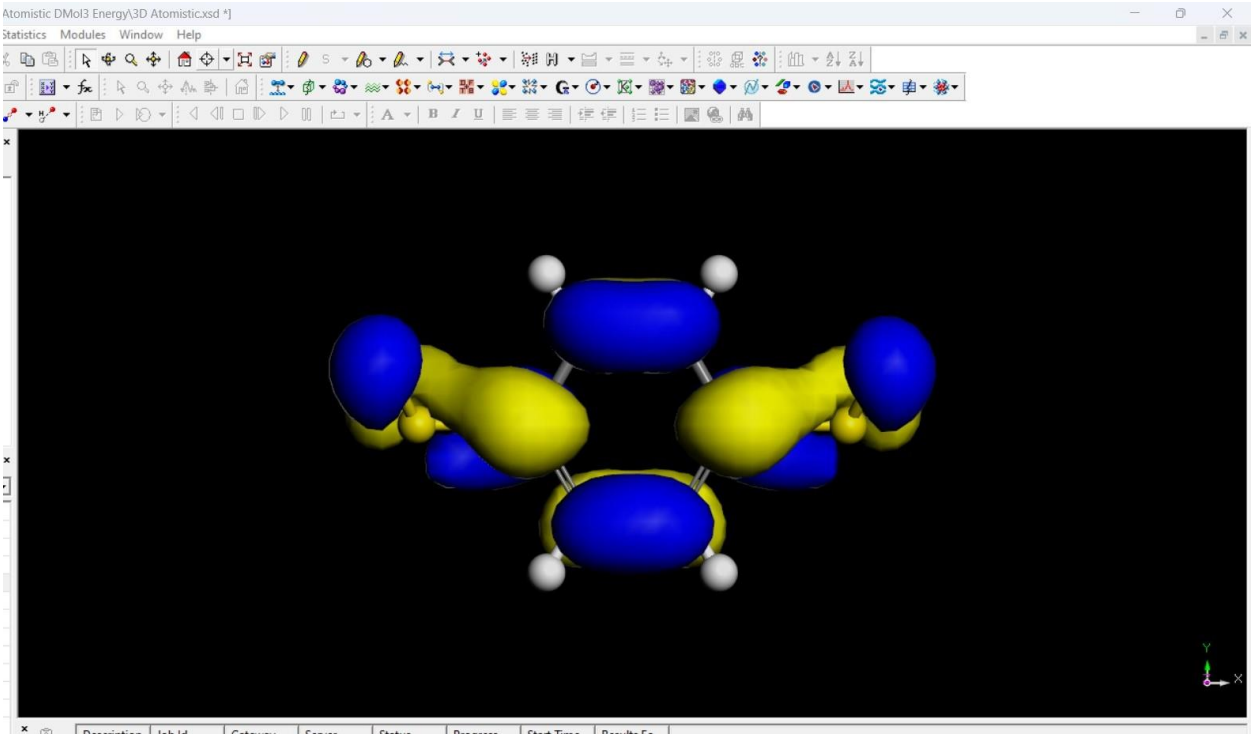
Modules
Window
Help

(b) LUMO

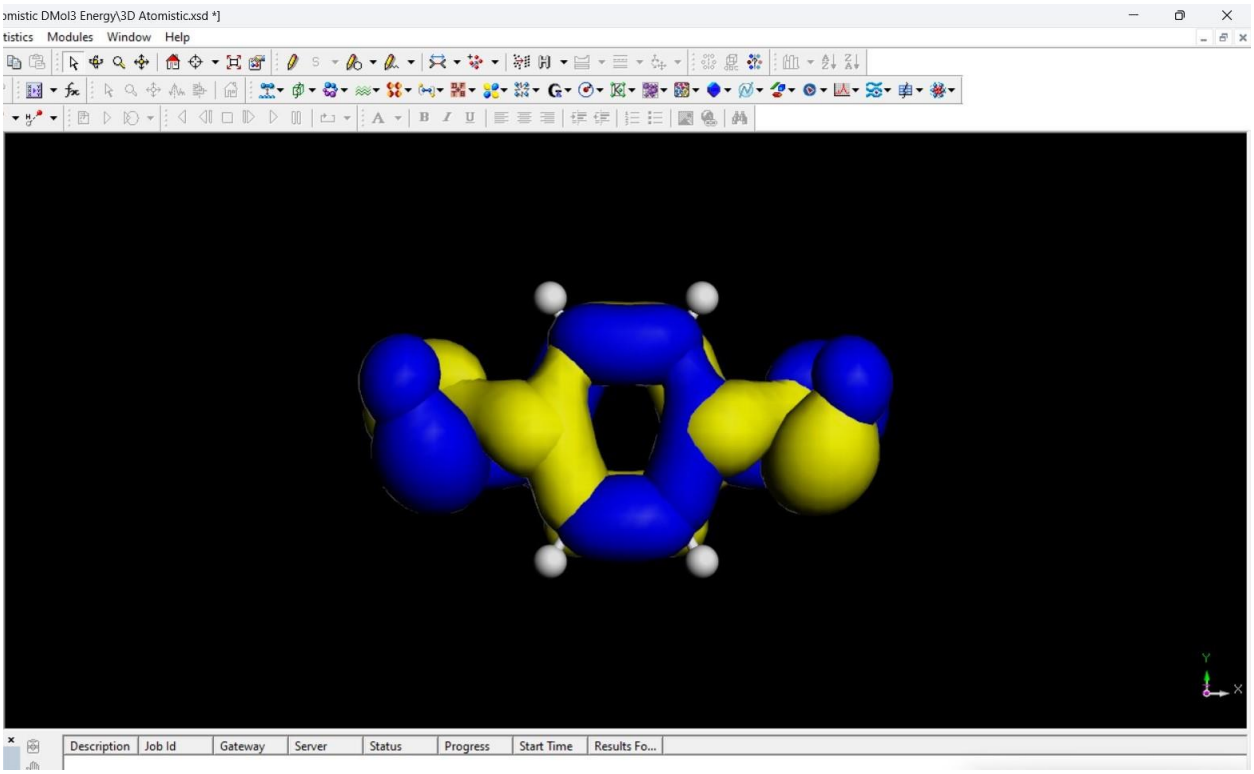

(c) HOMO-LUMO

Figure 3.12: Frontier Molecular Orbitals of benzene dithiol (a) HOMO (b) LUMO (c) HOMO-LUMO from Energy Analysis

Figure 3.12 shows the frontier molecular orbitals of benzene dithiol where HOMO, LUMO, and a combination of HOMO-LUMO is given.

The molecule's HOMO and LUMO are identified as having blue (positive position) and yellow (negative position) colors, respectively. The carbon molecule's HOMO is situated above the benzene ring. The C-S atom is where LUMO is located. The simplicity of adding an electron to the receptor molecule's empty orbital is indicated by a high E_{HOMO} value. It will be more able to admit electrons if its E_{LUMO} value is lower since it will have less resistance to doing so. The ionization potential (I) = - E_{HOMO} and electron affinity (A) = - E_{LUMO} are connected to the HOMO

and LUMO energy levels. The difference between the HOMO and LUMO energy values is used to calculate the energy gap (Eg) [158].

From the geometry optimization simulation, the HOMO is 0.1853 Ha and LUMO is 0.0599Ha. Again, from the energy analysis, the HOMO is 0.1990 Ha and LUMO is 0.0945 Ha. The difference between HOMO and LUMO is 0.1254 Ha (3.1eV) and 0.1045 Ha (2.84eV) respectively for both cases. A more significant change of 2.5–2.6 eV rather than simply 1 eV is produced as a result of polarization and chemical bonding of the S atom to the surface [163] which is reflected in our experimental result. The BDT molecule has the highest reactivity and reduced solidity due to its low I, A, and Eg energy levels.

Graphene Nanosheet

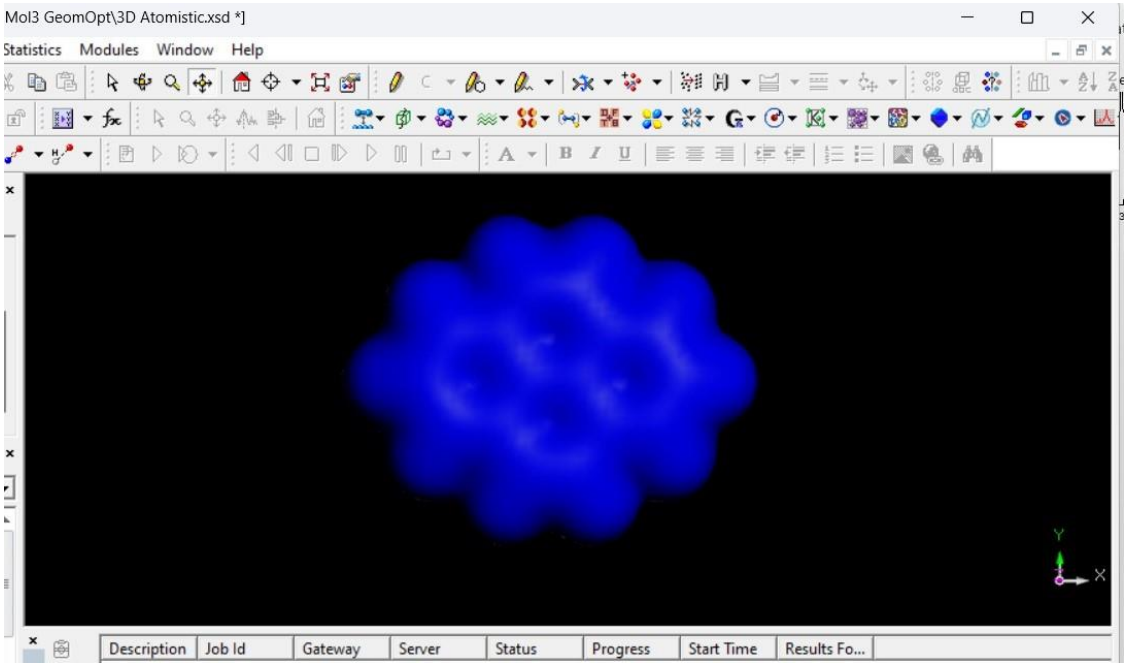

Figure 3.13: Electron Density of Graphene Nanosheet

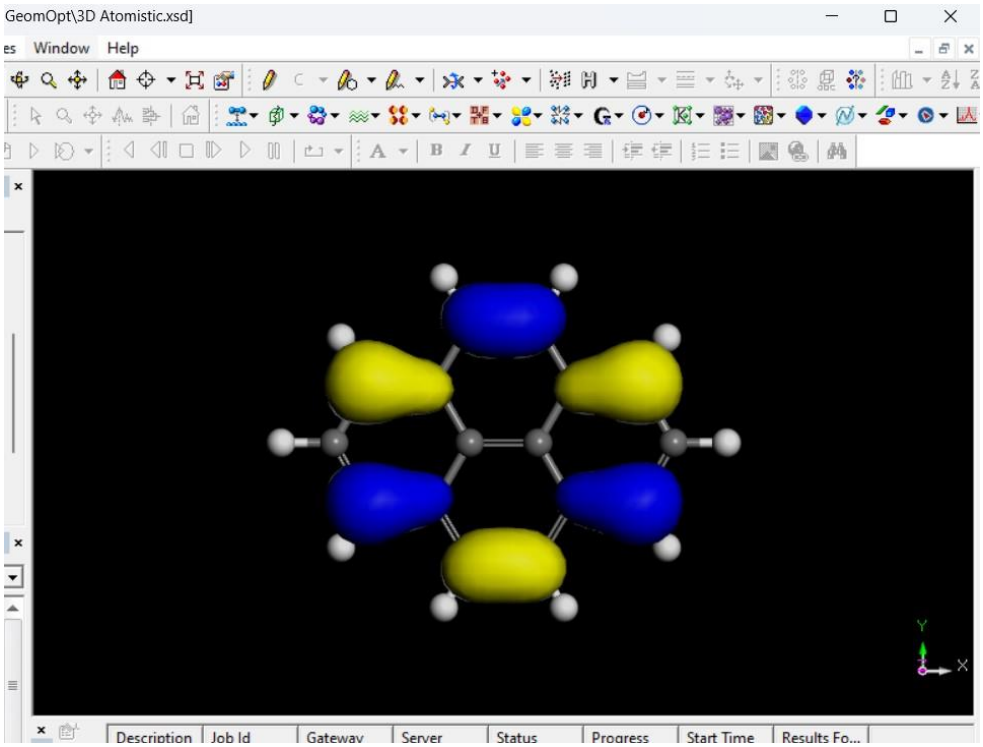
GeomOpt\3D Atomistic.xsd]
Window
Help
Description
Job Id
Gateway
Server
Status
Progress
Start Time
Results Fo...

(a) HOMO

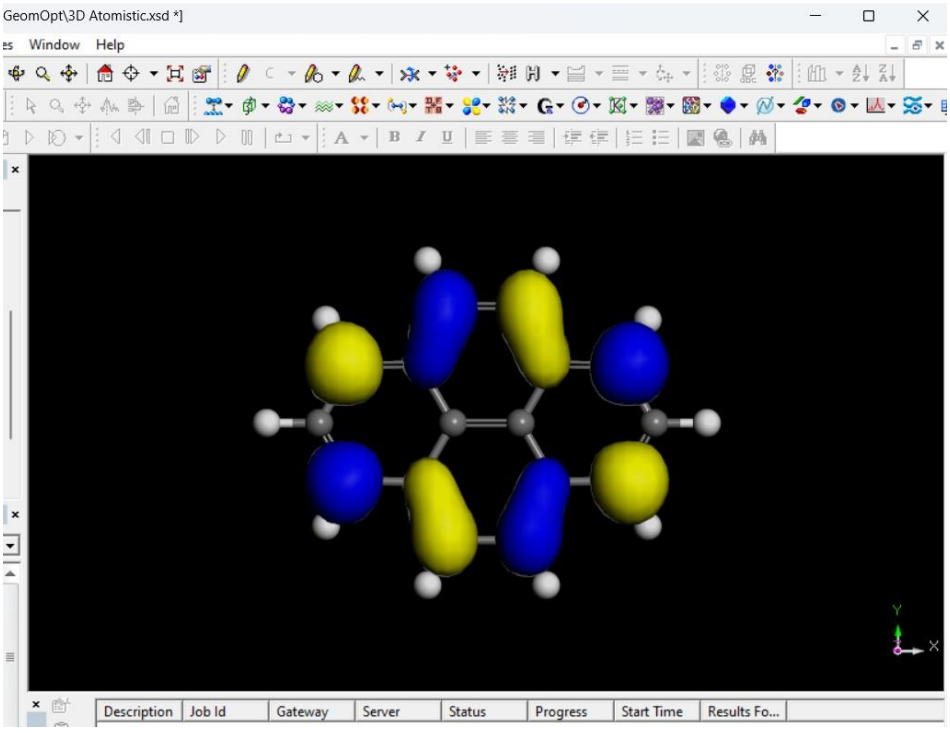
GeomOpt\3D Atomistic.xsd *]
Window
Help
Description
Job Id
Gateway
Server
Status
Progress
Start Time
Results Fo...

(b) LUMO

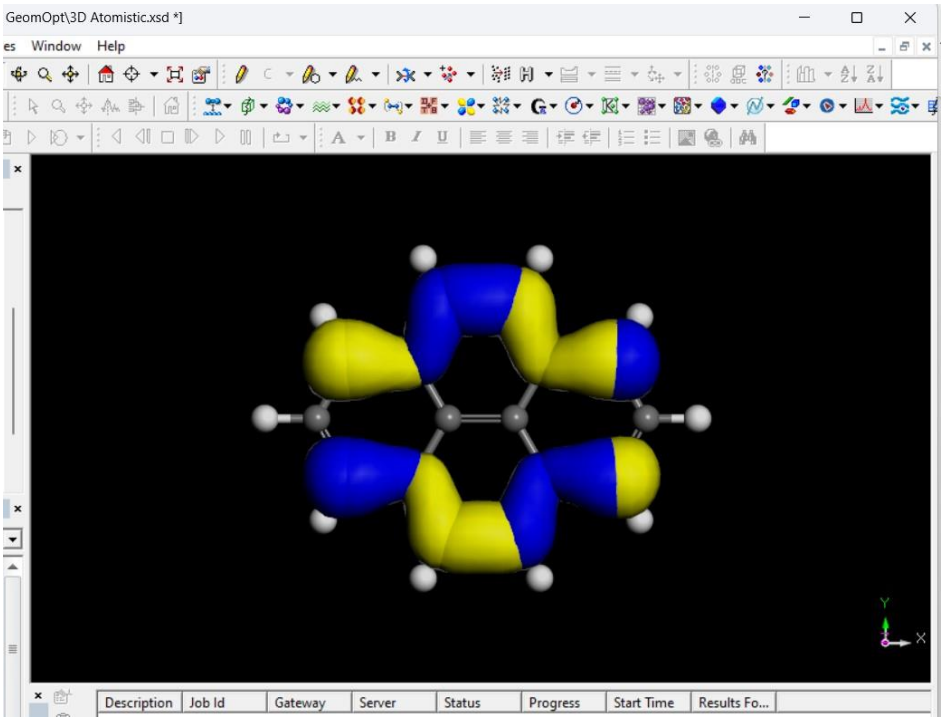

(c) HOMO-LUMO

Figure 3.14: Frontier Molecular Orbitals of Graphene Nanosheet (a) HOMO (b) LUMO (c) HOMO-LUMO from Energy Analysis

The HOMO indicates the capacity to donate an electron, while the LUMO serves as an electron acceptor, denoting the ability to receive an electron [164]. As illustrated in Figures, the charge density for the HOMO orbital is concentrated around the C=C bond and the entire molecular ring, whereas the LUMO features a charge distribution throughout the whole structure, excluding the hydrogen atoms. Next, we evaluate the energy levels of the HOMO and LUMO, along with the band gap energy, to describe the potential charge-transfer interactions within the molecules.

Figure 3.13 presents the electron density of the graphene cluster and Figure 3.14 shows the frontier molecular orbitals of the graphene cluster where HOMO, LUMO, and a combination of HOMO-

LUMO is given. From the energy analysis, the HOMO is 0.1906 Ha and LUMO is 0.0927 Ha. The difference between HOMO and LUMO is 0.0979 Ha (2.664eV). The present graphene quantum dot usually fluoresces green or blue and has a HOMO-LUMO gap between 2.2 and 3.1 eV. It is uncommon to get graphene quantum dots with a HOMO-LUMO gap smaller than 2.2 eV [165]. These values demonstrate the improvement of graphene properties, thereby enabling the use of the complexes being examined as acceptor materials in optoelectronic devices, owing to their strong electron affinity.

1- Unit Linear Chain

In certain energetically near orbitals, the spatial distributions of molecular orbitals show significant overlap, which permits the orbitals to combine, and form delocalized electron transport channels. In some instances, on the other hand, the charge density stays concentrated around particular atoms, impeding electron passage across the linear chain. HOMO orbitals in 1-unit benzene dithiol graphene linear chain will overlap to form an electron transport channel but LUMO orbitals are more clustered around certain atoms and do not extend across the linear chain. So, it can be expected that the molecular network would be highly conducting at certain energies and not at others. As chain length increases, the HOMO-LUMO gap shrinks, lowering the barrier to electron transport through the molecule and pointing to an increased possibility for charge movement as these networks grow [166].

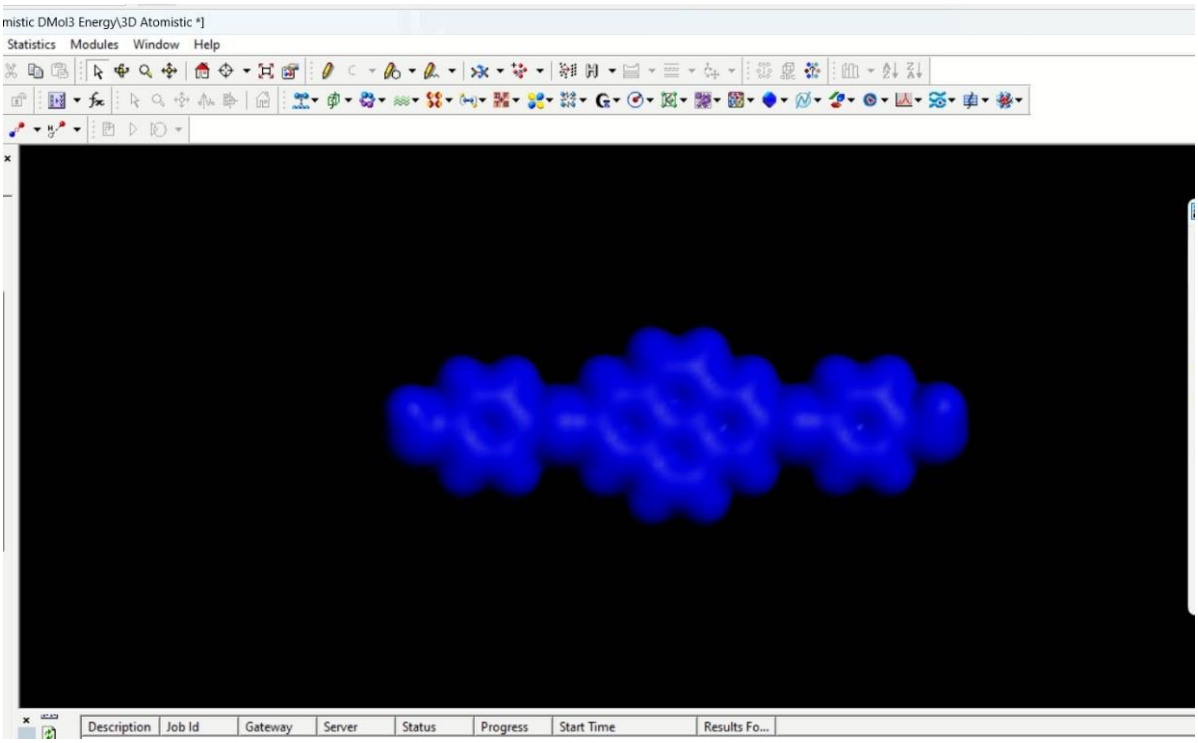
mistic DMol3 Energy\3D Atomistic *]
Statistics Modules Window Help
Description Job Id Gateway Server Status Progress Start Time Results Fo...

(a)

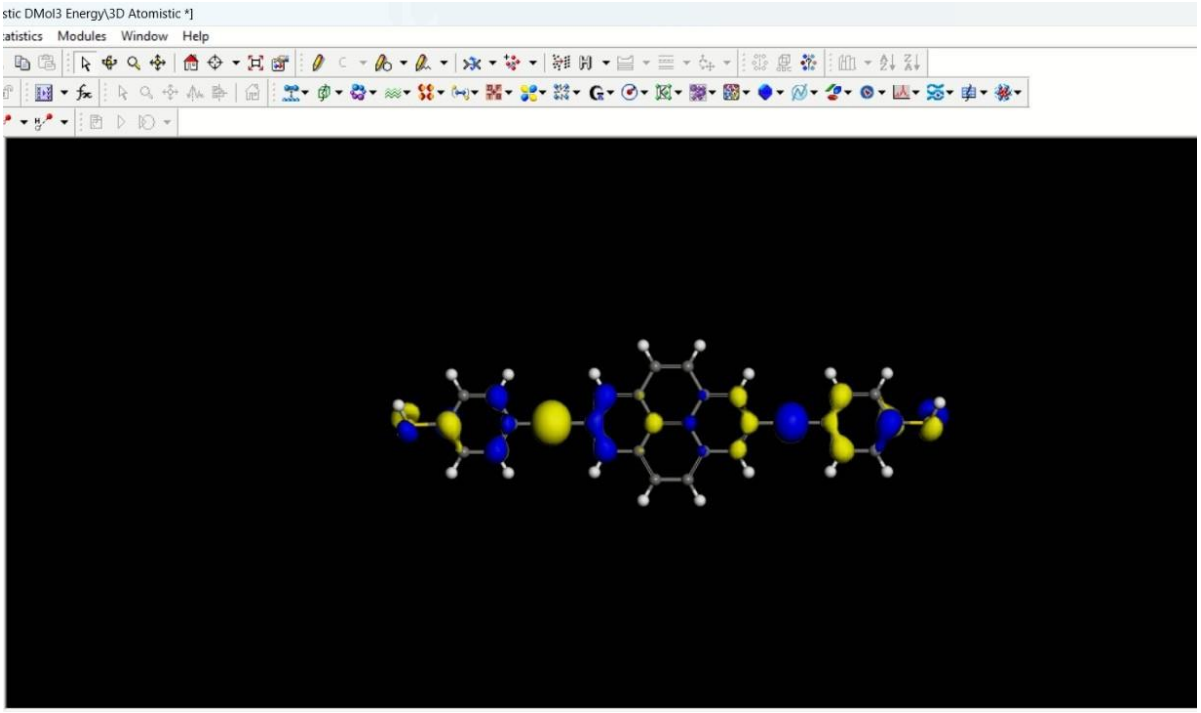
stic DMol3 Energy\3D Atomistic *]
tatistics Modules Window Help

(b)

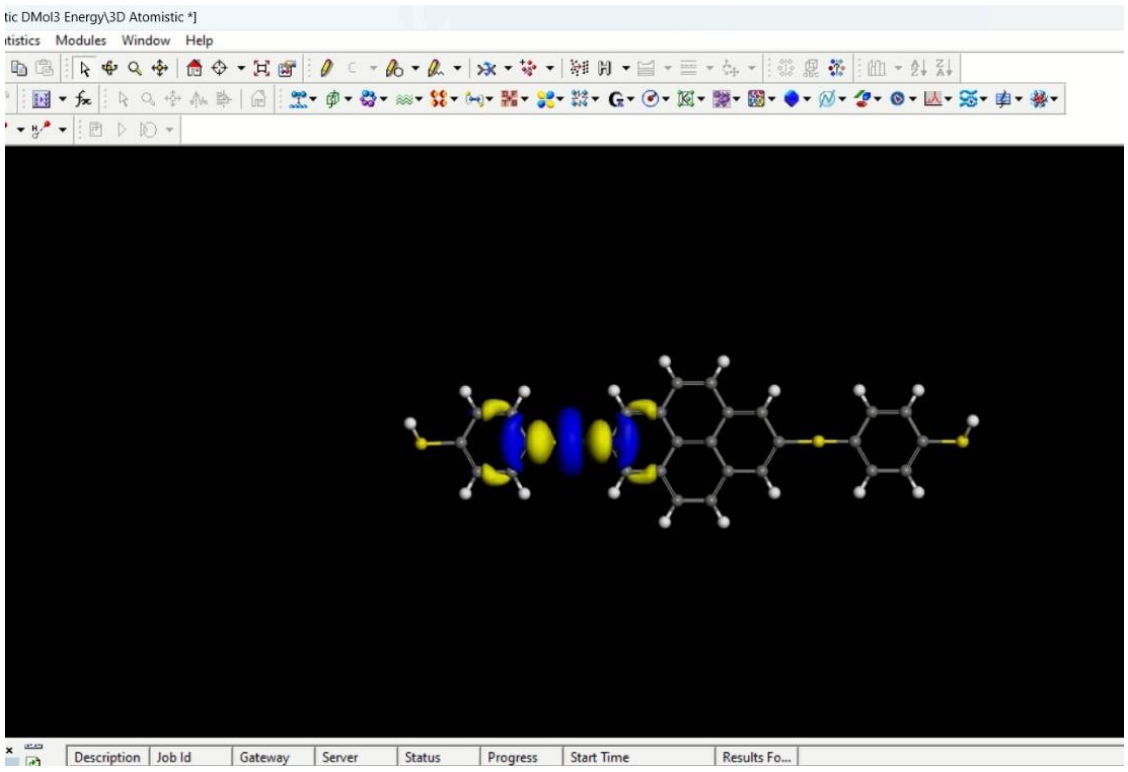
tic DMol3 Energy\3D Atomistic *]
tistics Modules Window Help
Description Job Id Gateway Server Status Progress Start Time Results Fo...

(c)

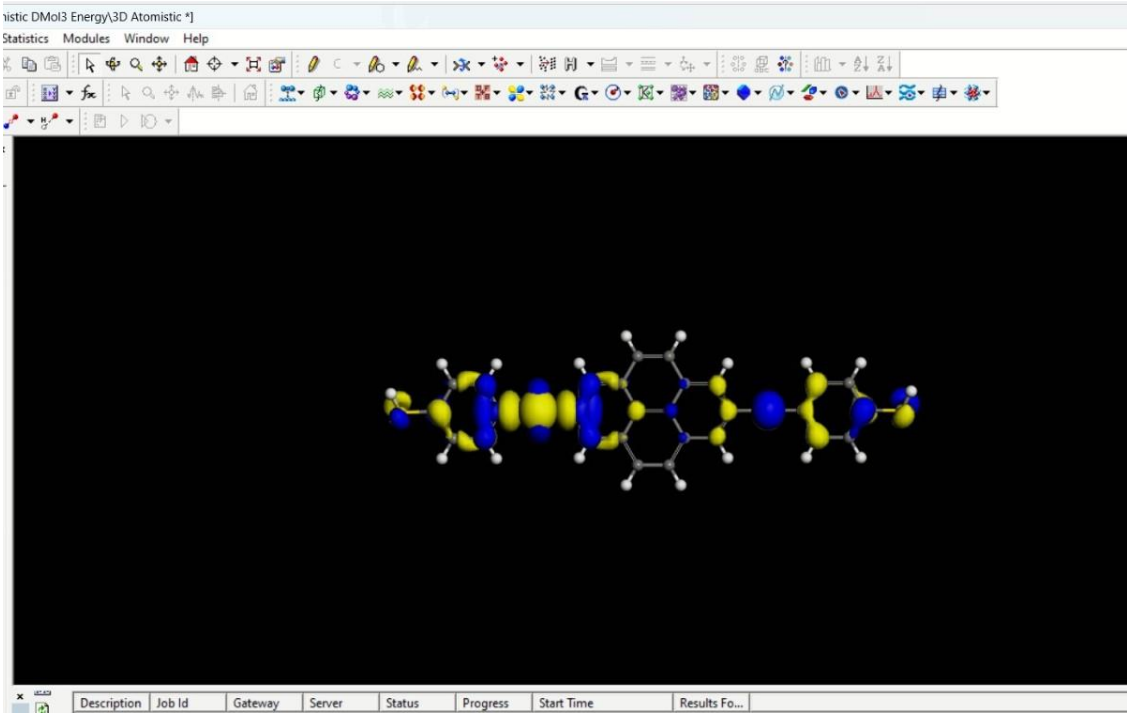
istic DMol3 Energy\3D Atomistic *]
Statistics Modules Window Help
Description Job Id Gateway Server Status Progress Start Time Results Fo...

(d)

Figure 3.15: Frontier Molecular Orbitals of the 1-unit linear chain (a) Total Electron Density (b) HOMO (c) LUMO (d) HOMO-LUMO

Figure 3.15 shows the frontier molecular orbitals of the 1-unit linear chain where electron density and a combination of HOMO-LUMO are given. From the geometry optimization simulation, the HOMO is 0.1791 Ha and LUMO is 0.0925 Ha. Again, from the energy analysis, the HOMO is 0.1803 Ha and LUMO is 0.1611 Ha. The difference between HOMO and LUMO is 0.0866 Ha (2.35eV) and 0.01911 Ha (0.52eV) respectively for both cases. The HOMO-LUMO gap of the 1-unit linear chain has been shrunk here compared to their individual HOMO-LUMO gap.

2- Unit Linear Chain

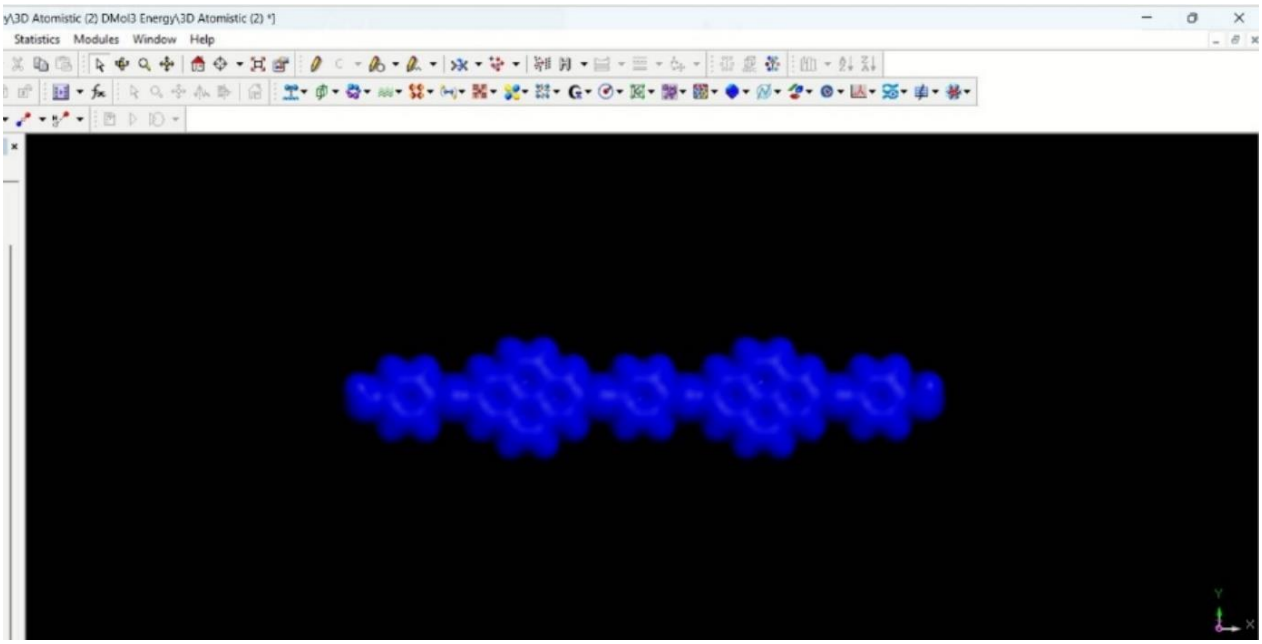

(a)

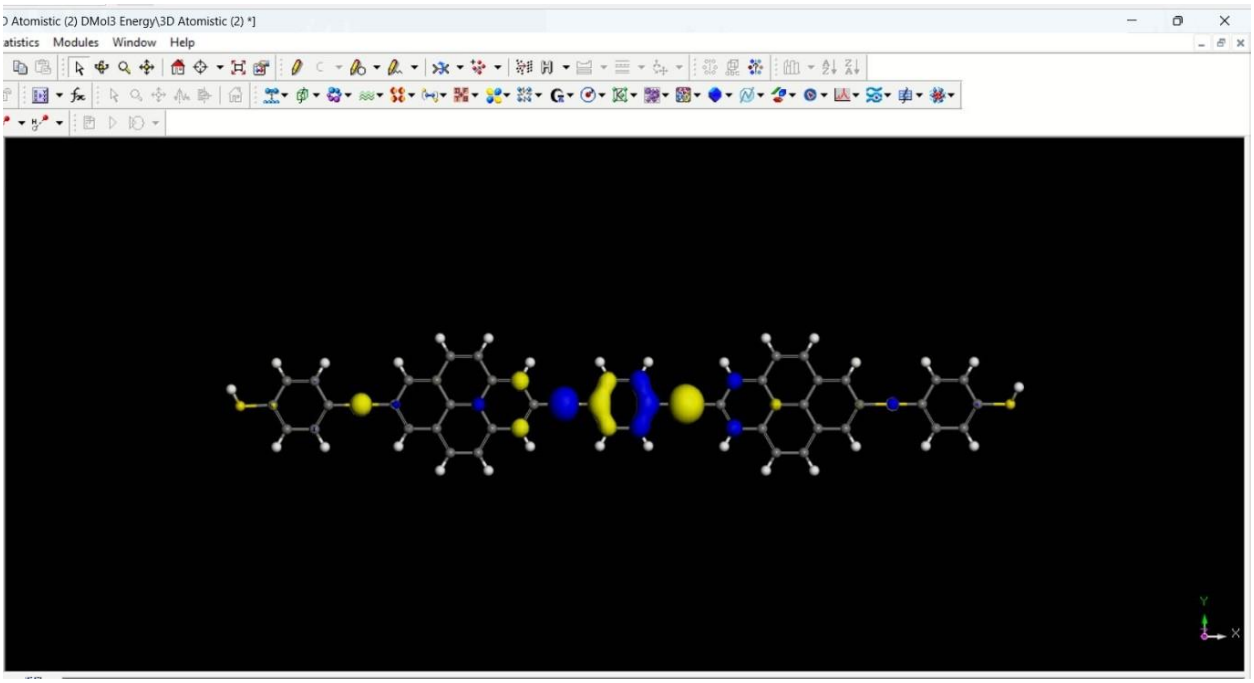
) Atomistic (2) DMol3 Energy\3D Atomistic (2) *]
atistics Modules Window Help

(b)

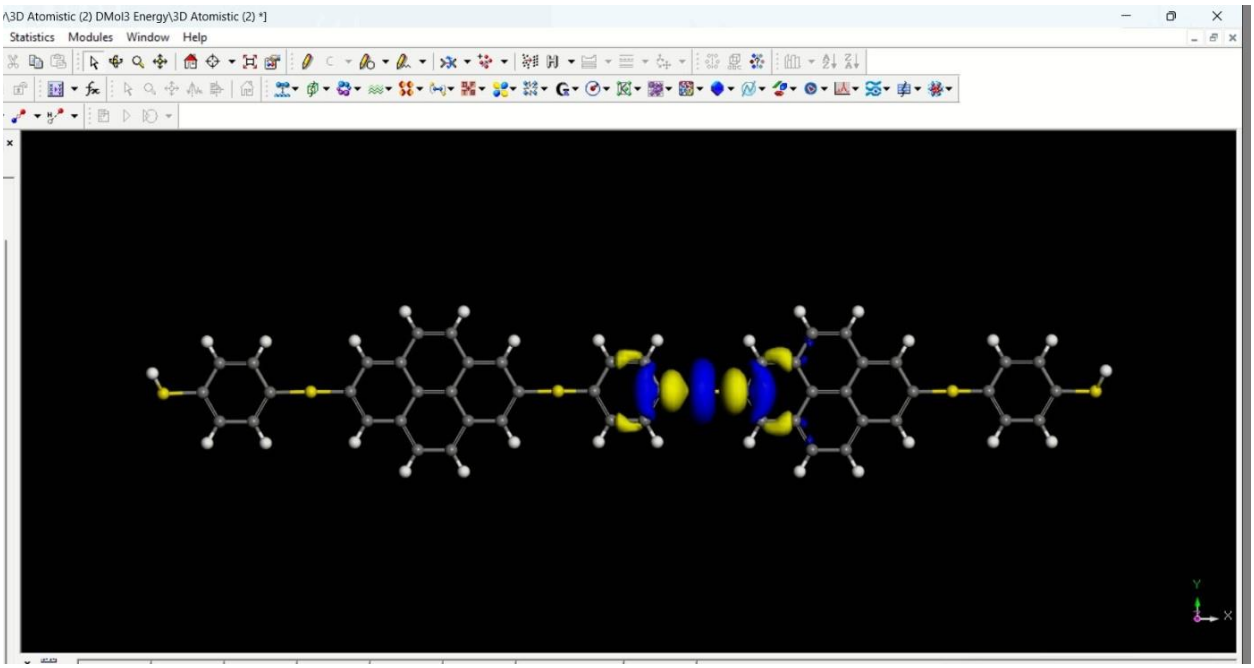
\3D Atomistic (2) DMol3 Energy\3D Atomistic (2) *]
Statistics Modules Window Help

(c)

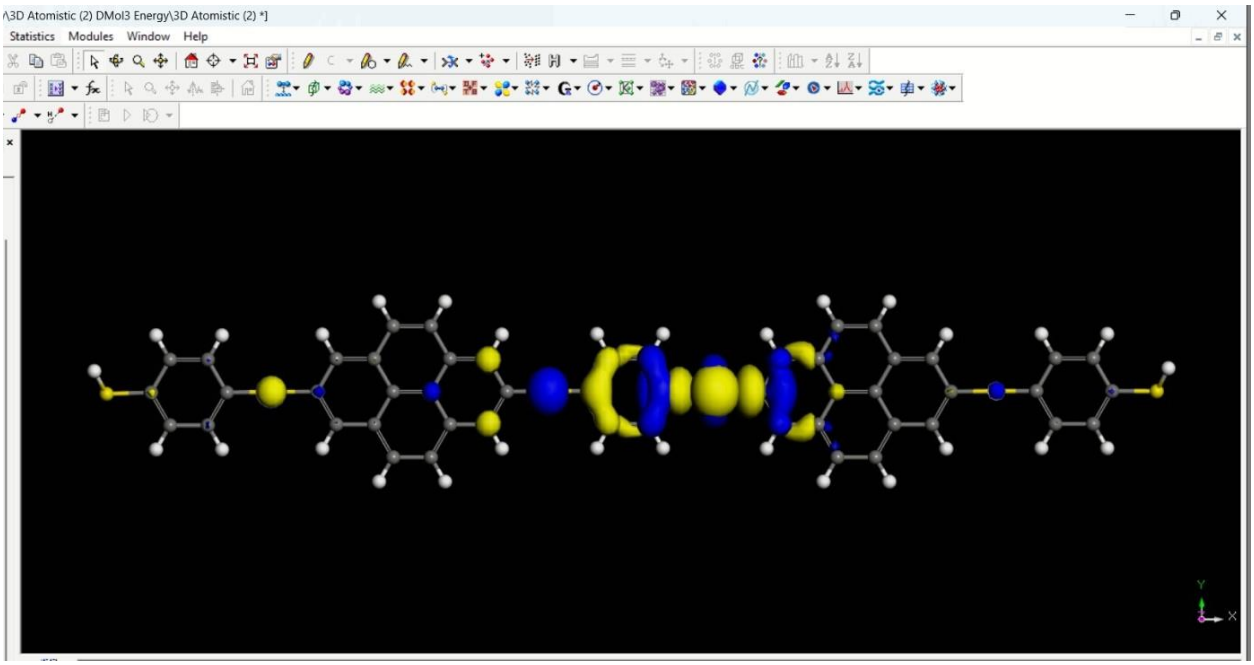

(d)

Figure 3.16: Frontier Molecular Orbitals of the 2-unit linear chain (a) Total Electron Density (b) HOMO (c) LUMO (d) HOMO-LUMO

Figure 3.16 shows the frontier molecular orbitals of the 2-unit linear chain where electron density and a combination of HOMO-LUMO are given. From the energy analysis simulation, the HOMO is -0.163843 Ha and LUMO is -0.156075 Ha. The difference between HOMO and LUMO is 0.007768 Ha (0.211378eV). The HOMO-LUMO gap of the 2-unit linear chain has been shrunk here compared to their individual HOMO-LUMO gap and 1-unit linear chain.

3- Unit Linear Chain

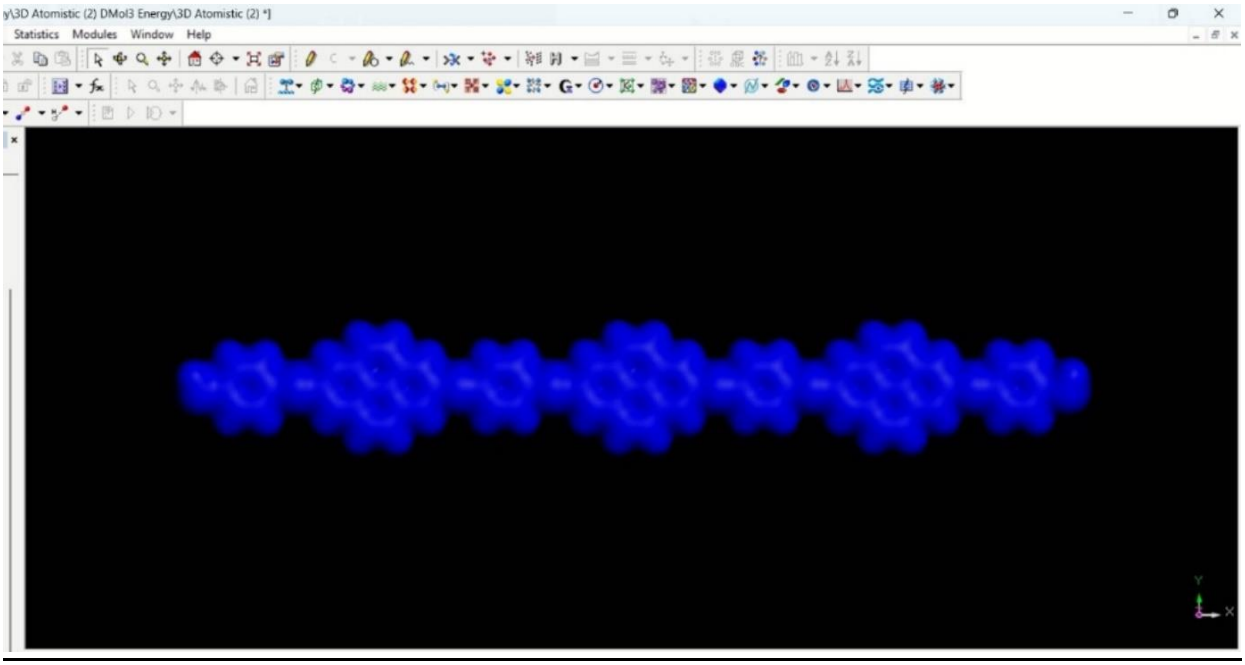
y\3D Atomistic (2) DMol3 Energy\3D Atomistic (2) *]
Statistics Modules Window Help

(a)

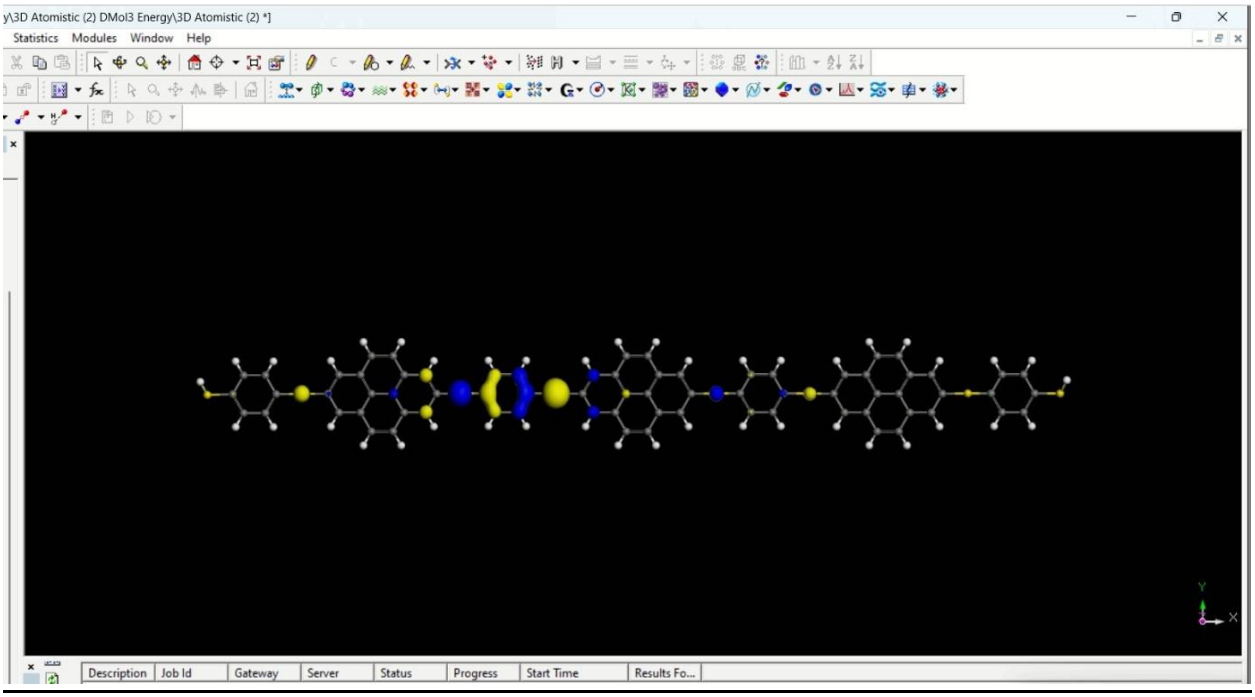
y\3D Atomistic (2) DMol3 Energy\3D Atomistic (2) *]
Statistics Modules Window Help
Description
Job Id
Gateway
Server
Status
Progress
Start Time
Results Fo...

(b)

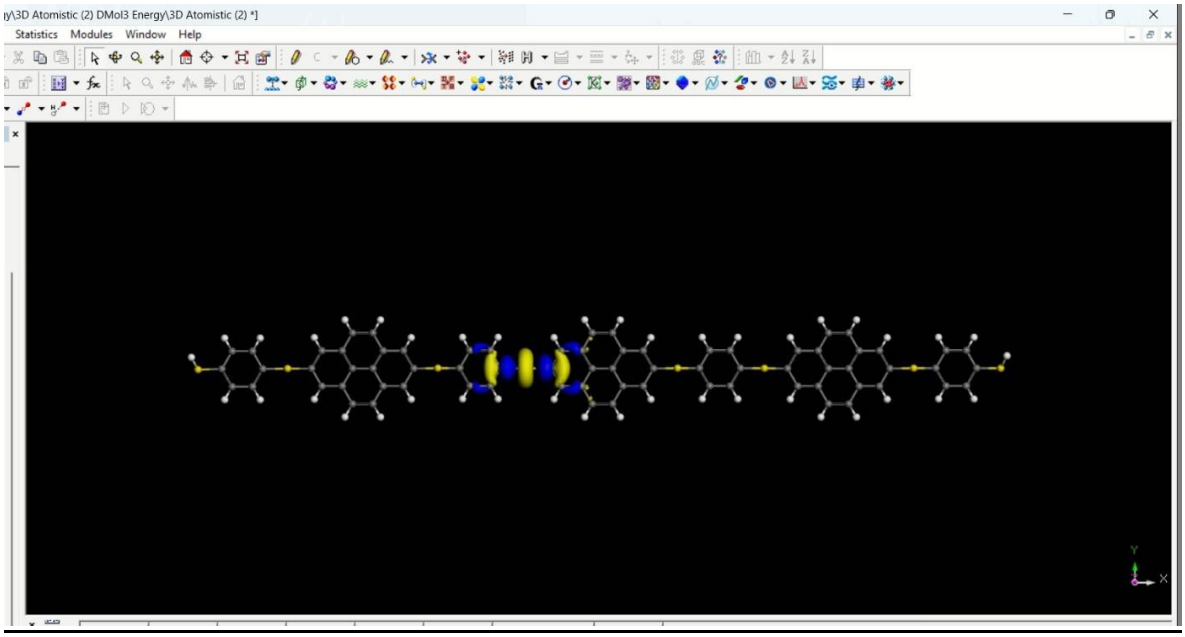

(c)

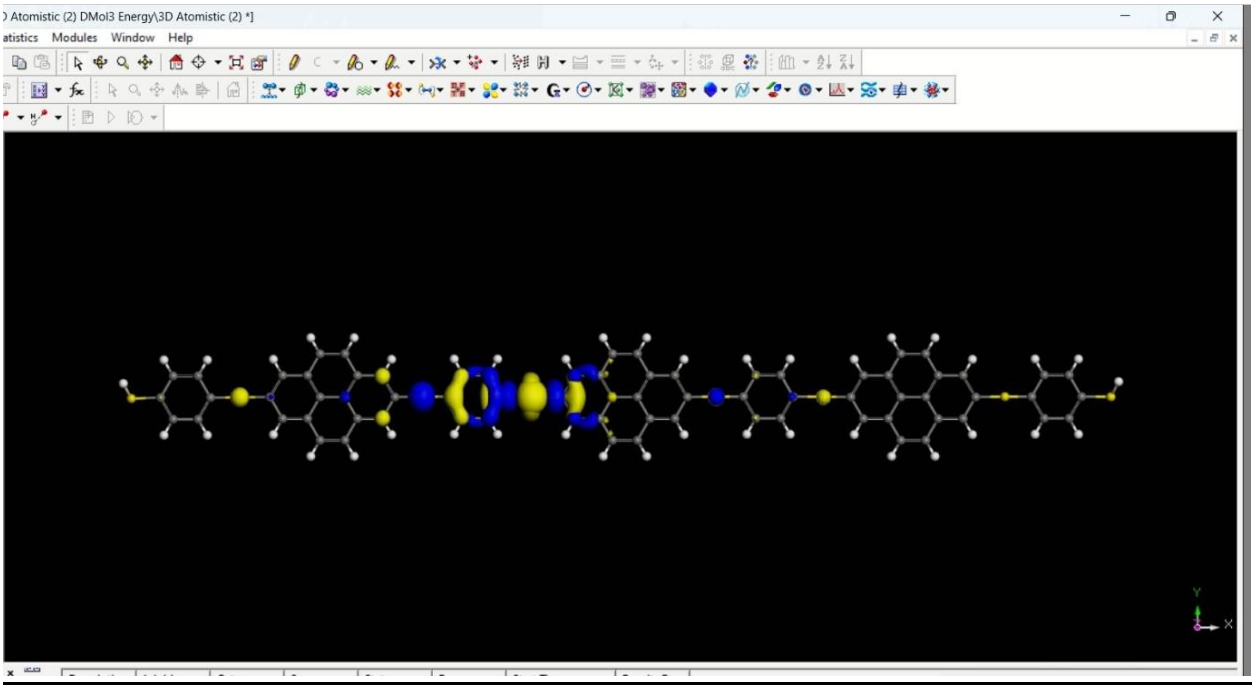

(d)

Figure 3.17: Frontier Molecular Orbitals of the 3-unit linear chain (a) Total Electron Density (b) HOMO (c) LUMO (d) HOMO-LUMO

Figure 3.17 shows the frontier molecular orbitals of the 3-unit linear chain where electron density and a combination of HOMO-LUMO are given. From the energy analysis simulation, the HOMO is -0.167351 Ha and LUMO is -0.159499 Ha. The difference between HOMO and LUMO is 0.007852 Ha (0.213663eV). The HOMO-LUMO gap of the 3-unit linear chain has been shrunk here compared to their individual HOMO-LUMO gap and 1-unit linear chain.

3.3.3 Transmission properties of nanostructures

Numerous theoretical investigations have examined the electron transmission spectrum of Au/BDT/Au junctions. The estimated electronic structure of Au/BDT/Au shows a valley between the peaks associated with HOMO and LUMO in the electron transmission spectrum and the density of states. There are no peaks in the Au/BDT/Au electron transmission spectra that are less than 0.5 eV from the Fermi level [167]. The TranSIESTA simulation package has been used for performing calculations on benzenedithiol for transmission properties. Figure 3.18 shows the electron transmission plot of benzene dithiol which resembles the previous investigation [168-170].

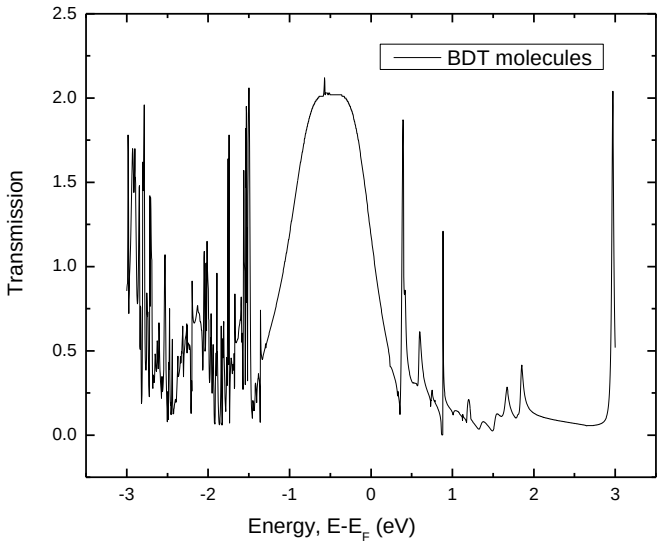

Figure 3.18: Transmission plot of BDT

The transmission spectra's peaks are likely a result of delocalized molecular orbitals that create pathways for charge carriers to move through the chains. Below the fermi energy level, the transmission peaks probably correspond to delocalized molecular orbitals such as HOMO and HOMO-1, which overlap and extend across the entire chain, providing effective conduction pathways. Conversely, the fewer transmission peaks above the fermi energy level can be attributed to the presence of localized molecular orbitals at higher energies, like LUMO and LUMO+1, leading to a significant reduction in the transmission coefficient [171]. The transmission spectra show wide peaks, which are probably caused by numerous overlapping molecular orbitals that combine to create paths for electron transport.

Band Structure helps to understand the electronic properties of graphene nanosheet. DFT is used to calculate the band structure and density of states. Numerous academic publications have reported that DFT is inaccurate in determining a semiconductor's band gap. Nonetheless, DFT provides a qualitative comprehension of the electrical structure [162].

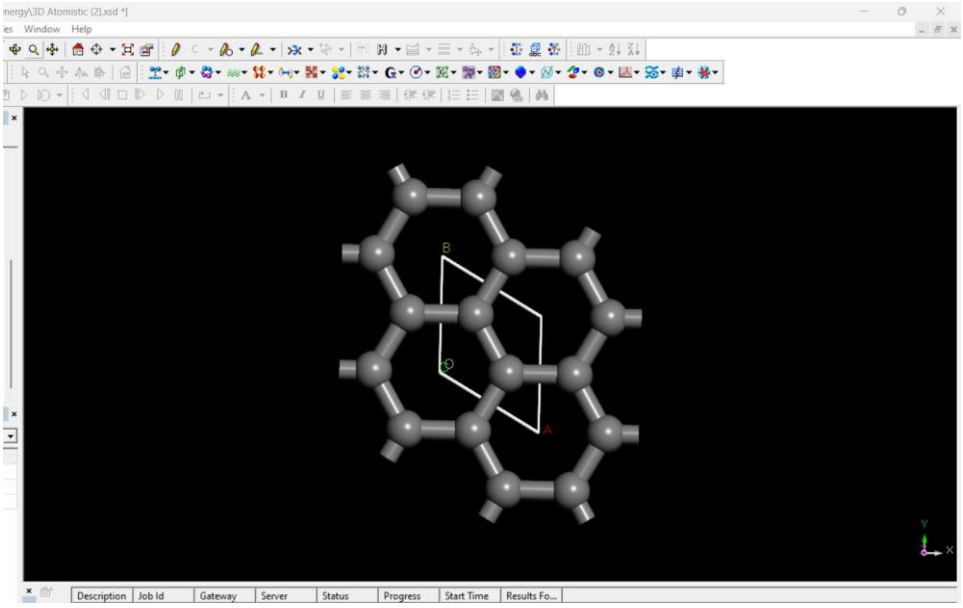

(a)

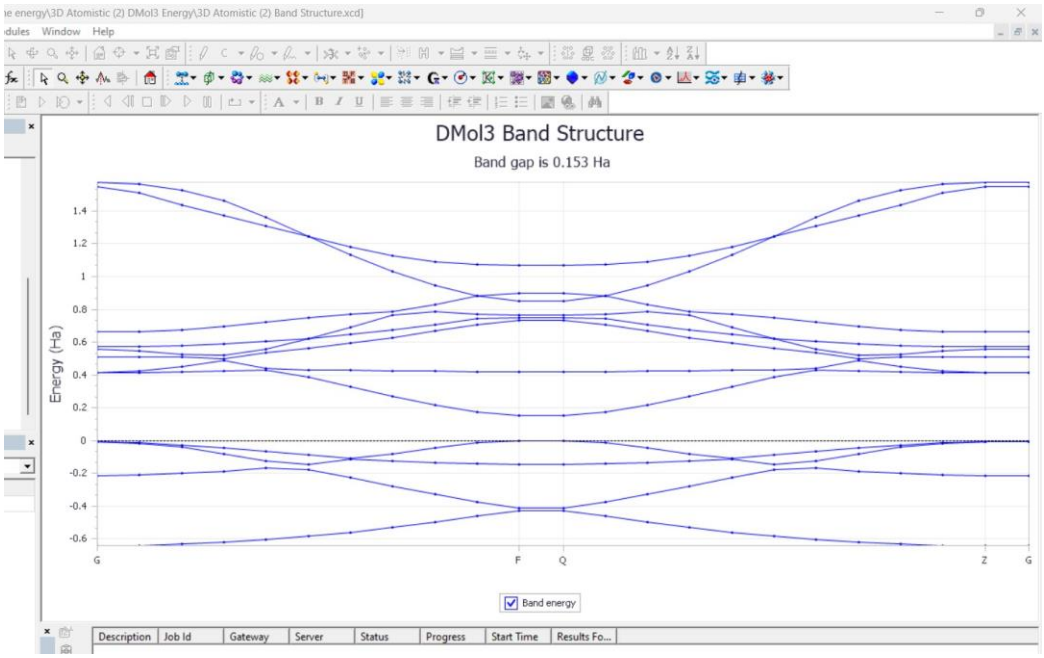

(b)

Figure 3.19: (a) Graphene Cluster (b) Band Structure of Graphene Cluster

Figure 3.19 (a-b) represents the band structure of the graphene cluster. The 'p' orbital maximum states are detected at around -0.4 to -0.1 Ha and 0.1 to 0.2 Ha. The density of states shows perfect overlap between the 's' and 'p' orbitals. We have also eobserved that band gap of graphene from our experiment is 0.153 Ha (4.1633eV). It has been reported that the band gap of graphene is 2.04eV. For single molecular adsorption on graphene, H_2 showed a greater affinity for the center site of the hexagonal ring [173].

3.3.4 Comparative Study of VAMP Analysis

After completing the construction of a structure, it is essential to carry out refinement to achieve a stable geometry. This refinement process, known as optimization, involves iteratively adjusting the atom coordinates to minimize the energy of the structure until it reaches a stationary point, where the forces on the atoms are zero. One can initiate an energy minimization to look for a

relative minimum on the energy hypersurface. This procedure will result in a geometry that closely mirrors the physical structure of the system at its equilibrium state [155].

An experimental VAMP Analysis including geometry optimization and Energy analysis has been done on Benzene dithiol and Graphene nnanosheet. This analysis was performed to explore the different electrical and optical properties of those molecules in the VAMP model. A tabular comparison has been shown below between the Benzene dithiol (BDT) and Graphene nanosheet. In both cases, Hamiltonian was set at AM1, multiplicity was Auto, and spin was set at RHF with zero charge.

Table 3.1: Comparison between experimental result VAMP Geometry Optimization of BDT molecule and Graphene

Parameters	Benzene dithiol (BDT)	Graphene Nanosheet
VAMP Geometry Optimization Graph	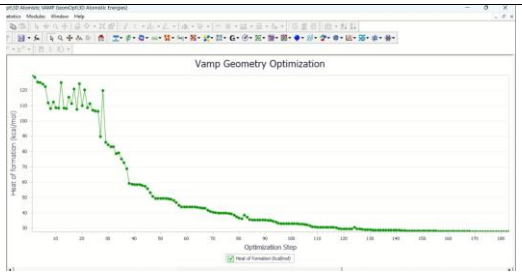	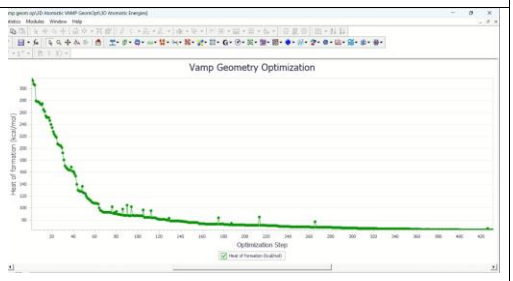
VAMP Optimization Convergence Graph	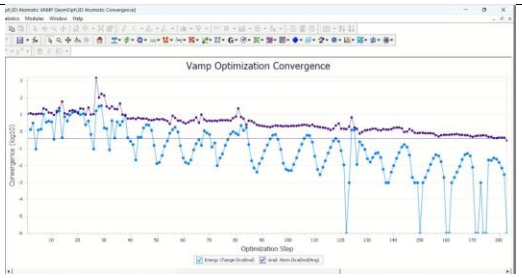	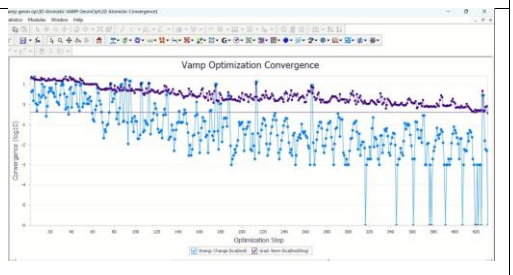

Electronic Properties	* Heat of formation = 27.685594 Kcal/mol * Electronic energy = -5231.807760 eV * Core-core repulsion = 3992.492637 eV * Total energy = -1239.315124 eV * Gradient norm = 0.443609 * RMS force = 0.073935 * Ionization potential = 8.270391 eV * 21 filled levels * Molecular weight = 142.233 * SCF calculations = 8357 * Computation time = 33.34 seconds * Calculation performed on 21.09.2024 - 09:39:06	* Heat of formation = 63.308299 Kcal/mol * Electronic energy = -13556.148785 eV * Core-core repulsion = 11370.715397 eV * Total energy = -2185.433387 eV * Gradient norm = 0.432282 * RMS force = 0.050945 * Ionization potential = 8.116981 eV * 37 filled levels * Molecular weight = 202.255 * SCF calculations = 35137 * Computation time = 416.37 seconds * Calculation performed on 21.09.2024 - 11:56:37
HOMO	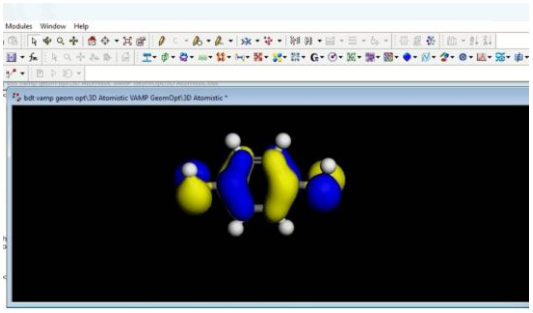	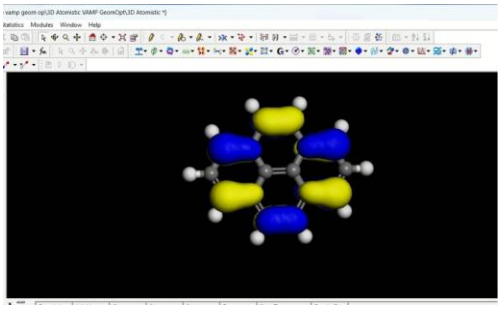
LUMO	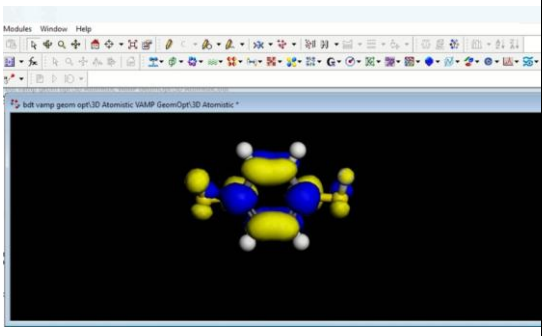	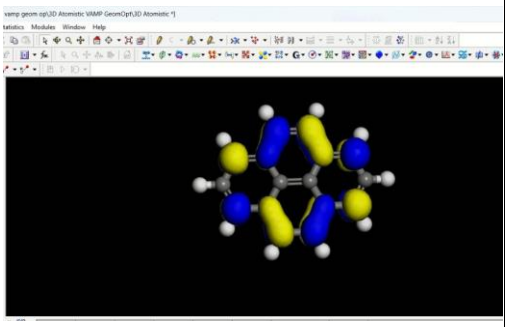
HOMO-LUMO	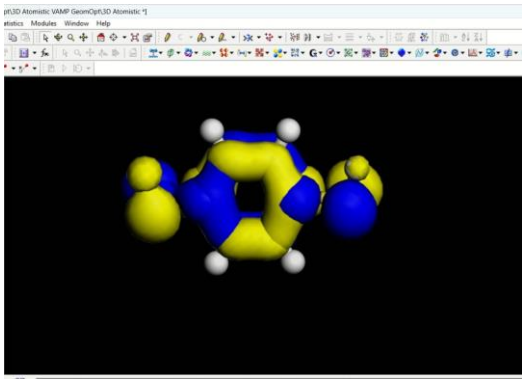	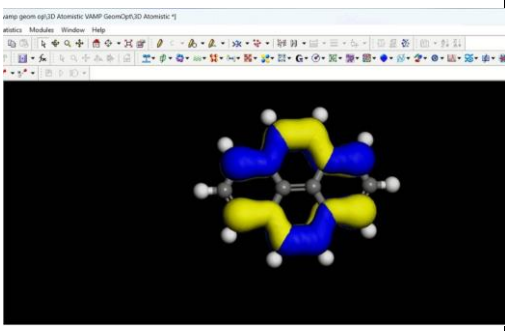

Electrostatic Potential	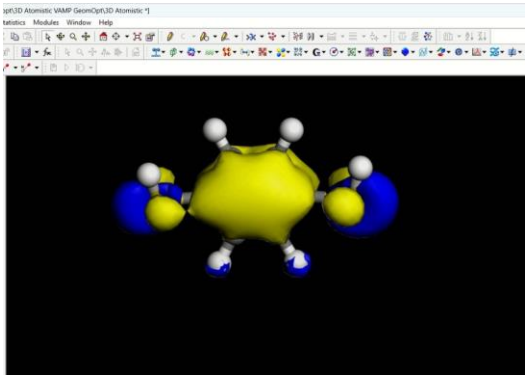	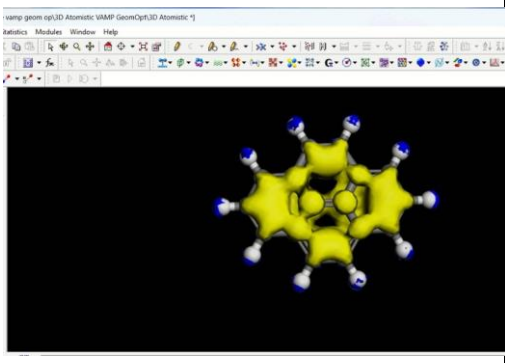

In Table 3.1 above, we can compare some of the main properties of BDT and graphene nanosheet that can be gained by VAMP analysis. We can get information about various electronic properties.

VAMP analysis also gives us information about the bond length and electron density. We got to know about potential electrostatic and orbitals with eigenvalues from this analysis. Orbitals with minimal values showing HOMO and LUMO can be observed from here. The HOMO of BDT is -8.268eV and LUMO is -0.308eV whereas the HOMO of Graphene is -8.117eV and LUMO is -0.903. Two different types of population analysis can be done by assigning either Coulson charges or Mayer charges to the structure.

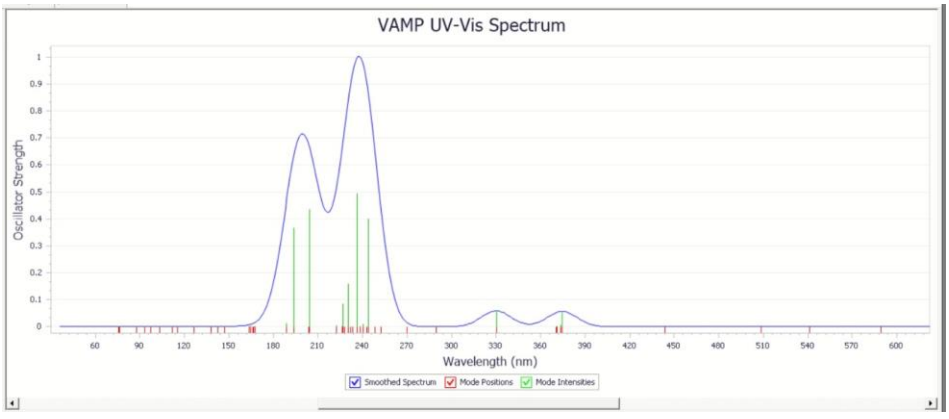

(a)

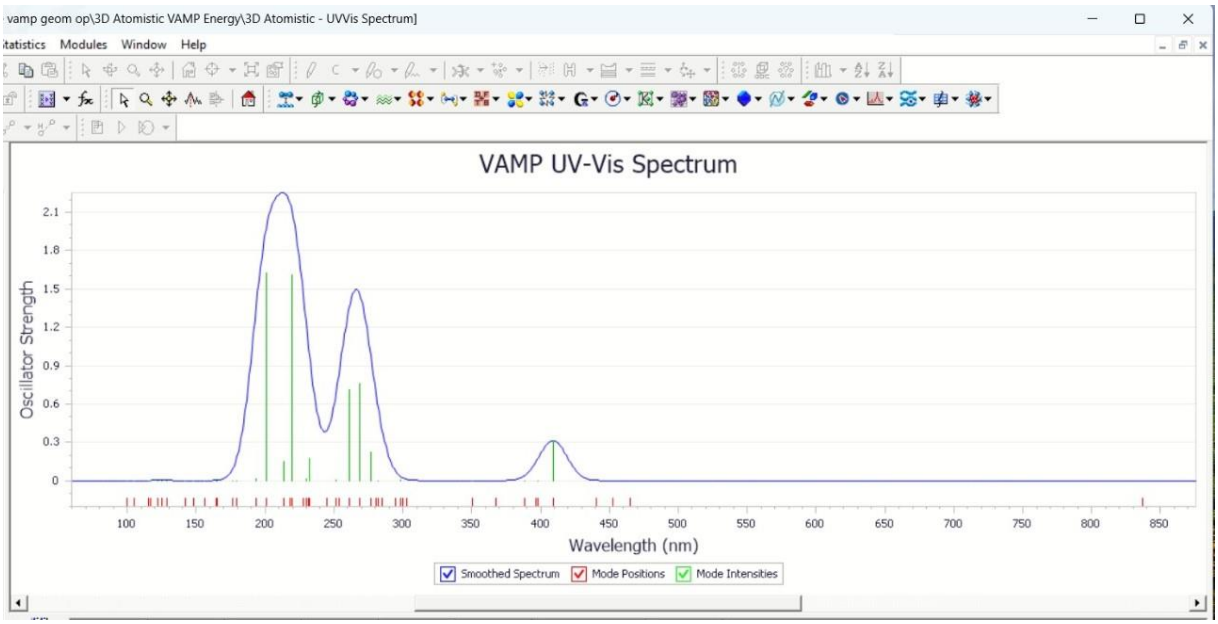

(b)

Figure 3.20: Experimental result of VAMP Energy Analysis of (a) BDT molecule and (b) Graphene Nanosheet

Figure 3.20 also shows some more property such as UV-Vis Spectrum. The positions and non-zero intensities of the absorption frequencies calculated by VAMP are depicte by the green lines on the graph. All computed transitions, including forbidden ones, are indicated by the short red lines. It is worth noting that there are quite a few forbidden transitions. A simulated spectrum, based on the computed frequencies and intensities, is represented by the smooth blue line. This is accomplished by using a Gaussian or Lorentzian function to broaden the computed results [155].

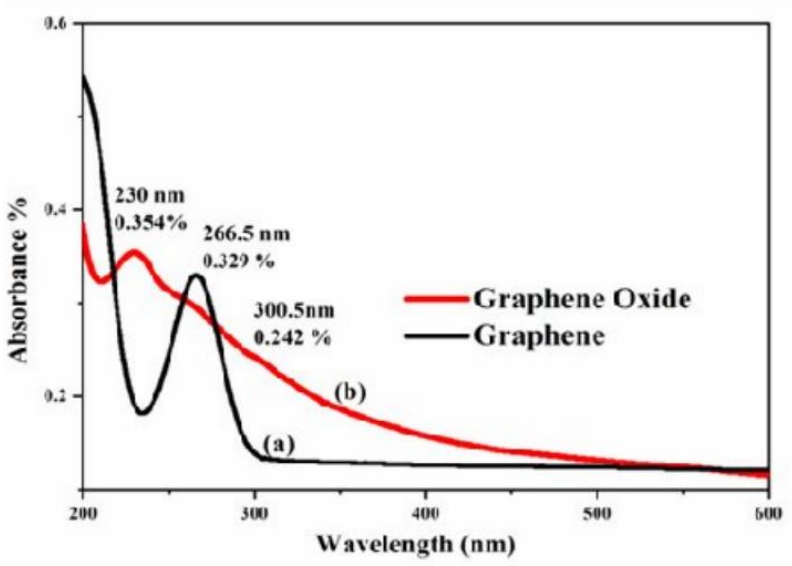

Figure 3.21: UV-Vis absorption spectra of graphene and graphene oxide (adapted from [174])

Figure 3.21 represents UV-Vis absorption spectra of graphene and graphene oxide from a previous study. Obtained UV-Vis spectra of graphene nanosheet is similar to previous study mentioned in Figure 3.21[174].

Values for the energy (in eV), the excitation wavelength (in nm), the multiplicity (spin arrangement), and the oscillator strength (transition dipole moment) of each electronic state are listed in a table provided after the completion of the simulation. This data can be used to plot energy graph to analyze the optical spectrum for a better understanding of the electrical and optical properties of the molecules.

3.4 Conclusion

Several nanoscale hybrid molecular structures consisting of geometry-optimized benzene dithiol molecules and graphene clusters, including linear molecular networks, were investigated through DFT-NEGF studies in this study. The combination of benzene dithiol (BDT) and graphene

nanosheet in a self-assembled metal molecular network shows great promise for advanced material applications. This framework exhibits improved electronic properties such as reduced HOMO-LUMO gaps and enhanced charge transport due to the unique mix of metal atoms, BDT ligands, and graphene nanosheet. The molecular orbitals and transport spectrums of benzene dithiol-graphene nanosheet networks were thoroughly analyzed, revealing delocalized frontier orbitals. An increase in the chain length led to a reduction in the HOMO-LUMO gap, suggesting improved transmission. The interaction between the metal centers and the BDT ligands promotes efficient electron transport by creating delocalized electron channels. Moreover, the inclusion of graphene nanosheet further boosts the conductivity and stability of the system, making it suitable for applications in molecular electronics, sensors, and energy storage devices. The network's properties can be customized by selecting different metals and arranging BDT and graphene nanosheet, providing opportunities for tailored functionalities. Overall, this self-assembled metal molecular network is a significant advancement in the development of hybrid materials with potential for various technological applications.

Chapter 4 - Conclusion and Future Perspective

4.1. Conclusion

This work presents the analysis of different molecules to work on Material Studio. This study also presents the findings on electronic transport through self-assembled networks composed of graphene nanoparticles with thiolated alkane molecules.

4.1.1 Self-Assembled Metal Molecular Network and Modeling

To discuss self-assembled metal molecular networks, unit molecules such as BDT and Graphene nanosheet were analyzed first. Geometry Optimization and Energy Density have been discussed here. Graphene-BDT molecular networks have been structured to observe the electronic and transport properties. Density functional theory non-equilibrium Green's function analyses were conducted on various nanoscale metal-molecular structures, constructed using $Dmol^3$ geometry-optimized benzenedithiol molecules and Graphene nanosheet structures including linear molecular networks. DFT-based calculations have been performed on 1-unit, 2-unit, and 3-unit graphene-BDT linear chains. At the very end, a comparative VAMP analysis has been presented among benzene dithiol and graphene nanosheet.

From DOS and PDOS of BDT, Graphene nanosheet, and 1-unit linear chain, we observed that the peaks can be seen between ~-0.6Ha and 0.3Ha. The HOMO-LUMO difference in BDT, Graphene, and 1-Unit linear chains are 2.8eV, 2.6eV, and 2.35eV respectively. The HOMO-LUMO difference in 2-unit and 3-unit linear chains are 0.211eV and 0.213eV respectively. This shows promising results in the research of graphene-based self-assembled metal molecular networks.

Using VAMP analysis, we got the chance to know electrical properties, bond length and electron density, electrostatic potential, orbitals with eigenvalue showing HOMO and LUMO, and population analysis of benzene dithiol and graphene.

4.2. Future Work

The last fifty years have witnessed a considerable increase in the field of molecular electronics due to advancements in theoretical computation skills and nanofabrication technologies. The pursuit of the ultimate nanoscale electronic devices has drawn substantial attention to the initial goal of implementing a wide variety of electronic functionalities generated from molecular structures. Molecular electronic components also have significant development potential since molecular building blocks have an infinite degree of molecular structure freedom. The field of self-assembled metal molecular networks has a lot more uncharted territory.

4.2.1. Potential Improvements and Challenges

Despite being a superb conductor, high-quality graphene lacks a bandgap, necessitating the incorporation of one for electronic microdevice fabrication. This results in electron mobility levels similar to those of strained silicon sheets. Hence, more research is needed before graphene can replace silicon in electrical systems. Synthesizing and manufacturing graphene poses another major challenge [174].

Before being utilized in biomedical applications, graphene nanomaterials should be thoroughly investigated and confirmed through the provision of extensive information regarding their synthesis, purification, and characterization techniques. It is essential to enhance their in vivo long-term toxicity to bolster their utilization in biomedical fields. Producing consistent graphene nanomaterials with stable and controlled size, morphology, thickness, chemical structure, and

purity is difficult. Composites of graphene nanomaterials can serve as promising smart biomaterials for 4D bioprinting. The primary challenging stage in 4D bioprinting is the selection of the appropriate bioink [175].

4.2.2. Emerging Research Directions and Modeling

The study of mixed metal-molecular networks or networks formed with combinations of different thiolate molecules and gold nanoparticles could be quite intriguing. For instance, metal-molecular networks could be created by using gold nanoparticles, nonanedithiol, and hexanedithiol molecules. In such instances, the networks would probably exhibit hybrid properties, such as different conductance at various locations, resulting from the diverse interactions between gold nanoparticles and the molecules involved. Investigating the metal-molecular networks' behavior at cryogenic temperatures is also valuable. Investigating multi-terminal networks, such as the Y-shaped and diamond-shaped networks, composed of benzene dithiol molecules and graphene nanoflakes, is worthwhile. The electronic and transport properties of these molecular networks may hold potential for future applications in carbon-based nanoelectronics.

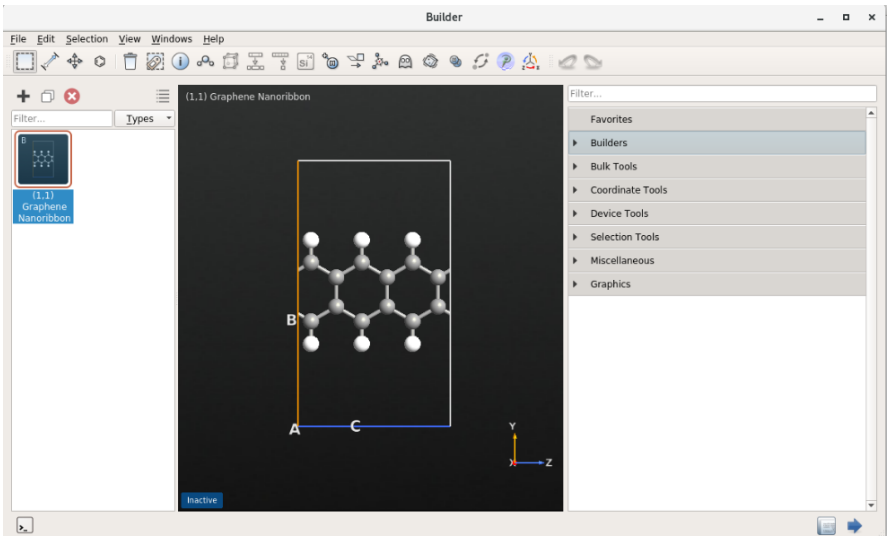

(a)

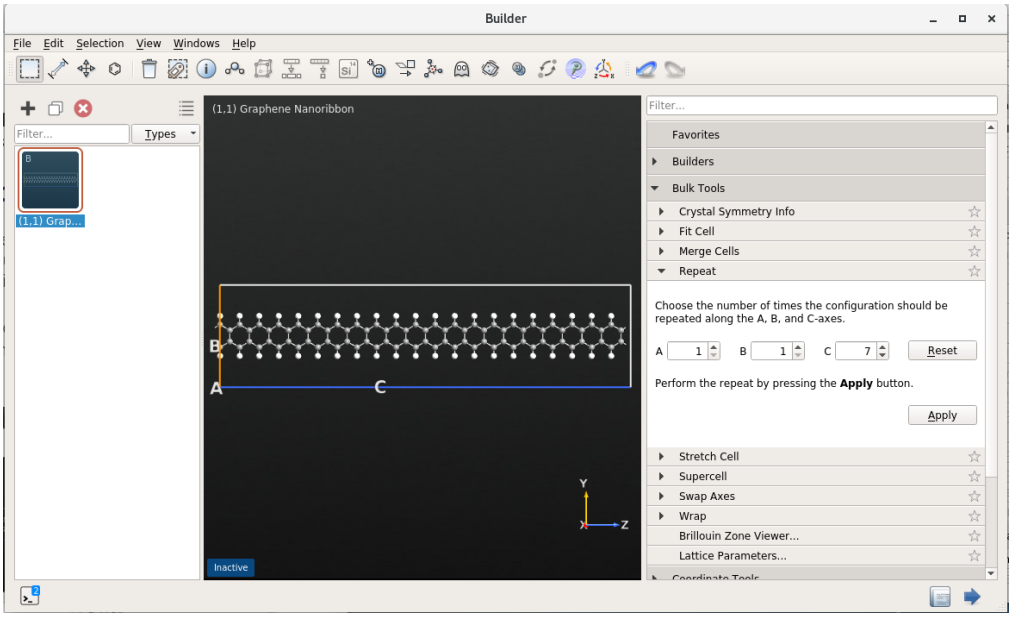
Builder
File Edit Selection View Windows Help
(1,1) Graphene Nanoribbon
Filter...
Types
(1,1) Grap...
Favorites
Builders
Bulk Tools
Crystal Symmetry Info
Fit Cell
Merge Cells
Repeat
Choose the number of times the configuration should be repeated along the A, B, and C-axes.
A 1 B 1 C 7 Reset
Perform the repeat by pressing the Apply button.
Apply
Stretch Cell
Supercell
Swap Axes
Wrap
Brillouin Zone Viewer...
Lattice Parameters...
Inactive

(b)

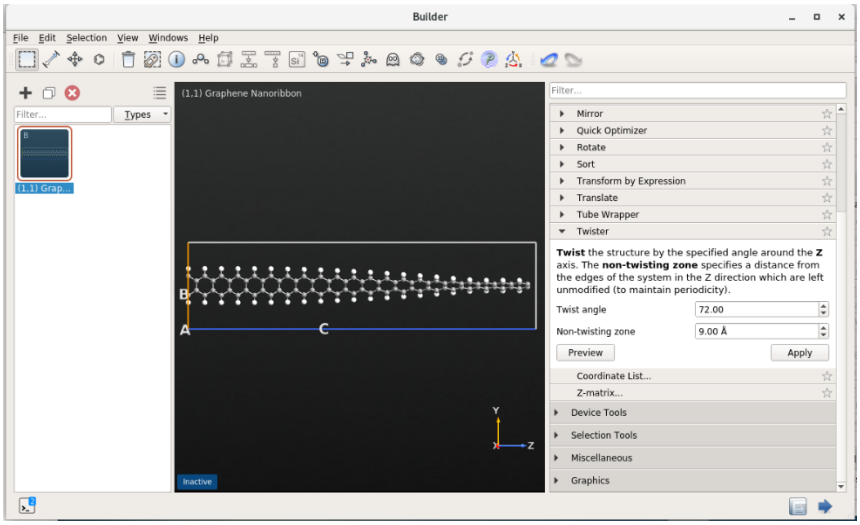
Builder
File Edit Selection View Windows Help
(1,1) Graphene Nanoribbon
Filter...
Types
(1,1) Grap...
Mirror
Quick Optimizer
Rotate
Sort
Transform by Expression
Translate
Tube Wrapper
Twister
Twist the structure by the specified angle around the Z axis. The non-twisting zone specifies a distance from the edges of the system in the Z direction which are left unmodified (to maintain periodicity).
Twist angle 72.00
Non-twisting zone 9.00 Å
Preview Apply
Coordinate List...
Z-matrix...
Device Tools
Selection Tools
Miscellaneous
Graphics
Inactive

(c)

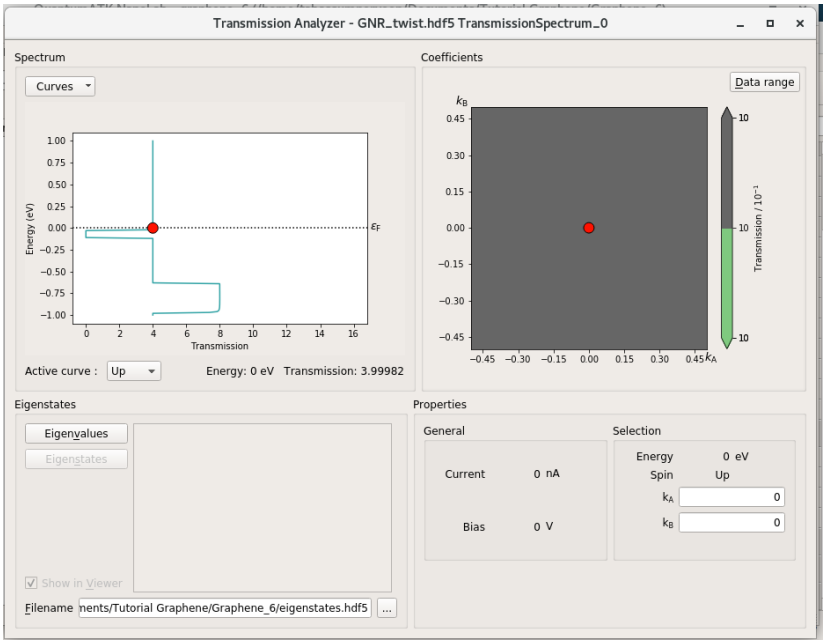

(d)

Figure 4.1: Graphene and its derivatives (a) Graphene (b) Graphene Nanoribbon (c) Twisted Graphene Nanoribbon (d) Transmission Analyzer of twisted graphene nanoribbon by QATK

Figure 4.1 shows the future prospects of graphene. Graphene can be used to form different structures such as rope, ribbon, nanotubes, etc. All of them can be subjected to experiments as graphene itself is a promising element. In this case, different simulation software such as QATK can be used for more detailed analysis.

4.3. Future Applications

One approach that has been found to be promising is nanoscale self-assembly. One-dimensional (1D) carbon nanotubes (CNTs) and two-dimensional (2D) graphene have been used in many other applications such as energy storage systems, portable electronic gadgets, miniature electrical items, sensors, solar cells, transistors, microelectronics, and biomedical applications for drug delivery.

4.3.1. Nanoelectronics and Device Applications

The lithographic and financial constraints of silicon-based electronics may be solved by using single-walled carbon nanotubes (SWNTs) in electronic circuits. In recent times, the production of high-performing field-effect transistors (FETs), light-emitting devices, logic gates, and pure and concentrated solutions of s-SWNT has been made possible. Devices made with SWNTs and polymer without thiol functionalization (not chemically self-assembled) displayed three orders of magnitude lower on-current and ambipolar characteristics than the chemically self-assembled network transistors. The significant number of SWNTs that resist sonication in organic solvents demonstrates the attachment's durability. Additionally, the self-assembly used to create single SWNT devices demonstrates the process's 100% dependability and enables the creation of functional devices from all manufactured samples. Thiol functionalization can facilitate effective contact creation with the gold electrodes and is a viable technique for creating homogenous SWNT networks [176].

The field-effect transistor (FET) made of carbon nanotubes (CNTs) is one alternative to silicon MOSFETs. Ballistic transport, simple integrated circuits, great performance at low voltages down to sub-10 nm channel lengths, and simple integrated circuits have already been provided by these [177].

Graphene derivatives including graphene oxide (GO) and reduced graphene oxide (RGO), as well as carbon nanotubes (CNTs), provide the basis for self-assembled hybrid materials that are particularly significant. These composite materials can be processed using a solution, typically display improved mechanical, electrical, and chemical characteristics, and have uses in optoelectronics, sensors, light harvesting, energy storage, and other related fields [178]. The

continuous 1D architectures of single-walled carbon nanotubes (SWNTs) show electrical characteristics that make them perfect for optoelectronic uses [179].

4.3.2. Sensor and Actuator Technology

An optical, electrical, or mechanical output signal is what a sensor transforms from an input signal—a physical quantity—into the intended output signal for processing. An active component in sensors known as a transducer is responsible for converting energy. Common phenomena that can be detected with sensors include mechanical motion (displacement, velocity, acceleration), biological, electrical, chemical, electromagnetic, heat or temperature, magnetic, optical, and radioactive. Various characteristics, including sensitivity, selectivity, detection limit, reaction time, and recovery time, determine how well these sensors perform [180].

For instance, the addition of metal or metal oxide nanoparticles to graphene-based gas sensors could greatly increase their performance. Graphene oxide (GO) is responsive to reduction and doping whereas gold nanoparticles show excellent electrical conductivity with great controllability in size, shape, and surface-volume ratio. The synergistic effect of the two nanomaterials is expected to increase device performance when Au NPs and GO are properly combined [181].

The electrochemical behavior of carbon-based nanoparticles is inherited in a way that makes them suitable for actuation. CNT actuators are among the most widely used carbon-based actuators. By altering the applied voltage, charge injection in CNTs causes mechanical deformations that result in actuation. Because of van der Waals interactions, the SWCNTs have sheet-like structures as well as a rope-like arrangement. In such a structure, the dimensional shift in the covalent bond orientation establishes the electrostatic and quantum chemical interactions. However, MWCNTs

have a lot of promise because of their multifunctional corroboration, which makes them perfect for raising elastic stiffness. Furthermore, the MWCNTs have a larger interfacial area and a greater aspect ratio, which makes them useful in mechanical, electrical, and thermal processes like impact resistance, vibration damping, and toughness [180].

4.3.3. Potential in Energy Storage

Leading materials for electrode application in electrochemical energy storage and conversion systems include carbon nanostructures like carbon nanotubes (CNTs).

As a popular portable gadget, Lithium-Ion battery is exclusively used where the electrode material has a significant role in recharging the battery. The ideal electrode would have a high surface area, high conductivity, minimal interfacial resistance between the electrode material and the current collector, temperature stability, fast ionic kinetics (low ionic diffusion resistance), ease of processing, compatibility with other components, and relatively low cost of production [182]. Due to the low specific capacity of the commonly utilized graphite, many researchers are now looking into other anode materials. It has been discovered that disordered carbon has a higher capacitance than ordered graphitic carbons. Given how easy it is to thermally enhance the properties of oxygen-containing structural features in the precursor to graphene oxide, it follows that arbitrarily organized graphene nanofibers should have a large specific surface area because of their ability to store lithium.

It has been revealed recently that graphene-metal oxide hybrids, which are employed as active materials in lithium-ion batteries, exhibit great cycle performance and a high specific capacity. Among the metal oxides, "Co_3O_4, NiO, Mn_3O_4, CuO, TiO_2, SnO_2, and Co $(OH)_2$" are the most often occurring [26].

Inexpensive hydrogen storage medium and high-capacity supercapacitor electrodes can be made by controlling the self-assembly interaction of graphene oxide sheet to fabricate graphene-based composite with carbon nanotube (CNTs), and metal [183].

Materials based on carbon nanotubes (CNTs) can be used to create lightweight, flexible gadgets. ZnO-based flexible piezoelectric nanogenerators (NGs) were introduced by Zhang et al [184]. The ZnO film structure can be used to create flexible sensors and energy-harvesting devices. ZnO along with carbon makes complex composite films that increase the efficiency of solar cells [180].

In this study, the findings from nanostructure simulations by DFT modeling matched well with the previous experimental results and produced similar results. These self-organized electronic networks at the nanoscale offer a pathway for designing electronic systems at the molecular level by utilizing various superstructures of organic molecules and topologies. The metal-molecular networks studied in this work could be used in many future applications and it offers a new perspective towards a more advanced research field.

References

[1] Kaehler T. Nanotechnology: basic concepts and definitions. Clin Chem 1994;40(9):1797–9.
[2] Daniel MC, Astruc D. Gold nanoparticles: assembly, supramolecular chemistry, quantumsize-related properties, and applications toward biology, catalysis, and nanotechnology. Chem Rev 2004;104(1):293–346.
[3] Rao CNR, Cheetham AK. Science and technology of nanomaterials: current status and future prospects. J Mater Chem 2001;11(12):2887–94.
[4] National nanotechnology initiative: leading to the next industrial revolution. Washington, DC: National Science and Technology Council; 2000.
[5] Mansoori GA, Soelaiman TAF. Nanotechnology-an introduction for the standards community. J ASTM Int 2005;2(6):17–38.
[6] Ghorbanpour M, Hatami M, Hatami M. Activating antioxidant enzymes, hyoscyamine and scopolamine biosynthesis of Hyoscyamus niger L. plants with nano-sized titanium dioxide and bulk application. Acta Agric Slov 2015;105:23–32.
[7] Ghorbanpour M, Hatami M. Changes in growth, antioxidant defense system and major essential oils constituents of Pelargonium graveolens plant exposed to nano-scale silver and thidiazuron. Indian J Plant Physiol 2015;20(2):116–23.
[8] Mirsasaani SS, Hematia M, Tavasolid T, Dehkorda ES, Yazdia GT, Poshtiri DA. Nanotechnology and nanobiomaterials in dentistry. In: Nanobiomaterials in clinical dentistry. Elsevier Inc.; 2013.
[9] Mahmoud Nasrollahzadeh, S. Mohammad Sajadi, Mohaddeseh Sajjadi, Zahra Issaabadi, Chapter 1 - An Introduction to Nanotechnology, Interface Science and Technology, Elsevier, Volume 28, 2019, Pages 1-27, ISSN 1573-4285, ISBN 9780128135860 ,https://doi.org/10.1016/B978-0-12-813586-0.00001-8.
[10] Panneerselvam, S.; Choi, S. Nanoinformatics: Emerging Databases and Available Tools. *Int. J. Mol. Sci.* **2014**, *15*, 7158-7182. https://doi.org/10.3390/ijms15057158
[11] Feynman RP. There's plenty of room at the bottom. In: Handbook of nanoscience, engineering, and technology. 3rd ed. vol. 23. CRC Press; 1960. p. 22–36.
[12] C. P. Poole and F. J. Owens, Introduction to nanotechnology, Hoboken, NJ: J. Wiley, 2003.
[13] W. F. Brinkman, D. E. Haggan and W. W. Troutman, "A history of the invention of the transistor and where it will lead us," IEEE journal of solid-state circuits, vol. 32, pp. 1858-1865, 1997.
[14] C.-T. Sah, "Evolution of the MOS transistor-from conception to VLSI," Proceedings of the IEEE, vol. 76, pp. 1280-1326, 1988
[15] M. G.E., "Cramming more components onto integrated circuits," Electronics, vol. 38, pp. 114–117, 1965.
[16] A. F. Smith, P. Patton, and S. E. Skrabalak, "Plasmonic Nanoparticles as a Physically Unclonable Function for Responsive Anti-Counterfeit Nanofingerprints," Advanced Functional Materials, vol. 26, no. 9, pp. 1315–1321, 2016.
[17] H. Tanaka, M. Akai-Kasaya, A. TermehYousefi, L. Hong, L. Fu, H. Tamukoh, D. Tanaka, T. Asai, and T. Ogawa, "A molecular neuromorphic network device consisting of single-walled carbon nanotubes complexed with polyoxometalate," Nature Communications, vol. 9, no. 1, pp. 2693–7, 2018.161
[18] J. Dong, J. Liu, G. Kang, J. Xie, and Y. Wang, "Pushing the resolution of photolithography down to 15nm by surface plasmon interference," Scientific reports, vol. 4, no. 1, pp. 5618–5618, 2014.
[19] G. Binnig and H. Rohrer, Scanning tunnelingmicroscopy—from birth to adolescence, Rev. Mod.Phys. 59, 615 (1987).
[20] Iijima, S. (1991). Helical microtubules of graphitic carbon. *Nature, 354*, 56-58.
[21] Festus-Ikhuoria, Igberaese & Nwankwo, Constance & Adebayo, Riliwan & Olajiga, Oladiran. (2023). Nanotechnology in consumer products: A review of applications and safety considerations. World Journal of Advanced Research and Reviews. 21. 2050-2059. 10.30574/wjarr.2024.21.3.0923.
[22] Duan, X., Huang, Y., Cui, Y., Wang, J., & Lieber, C. M. (2001). Indium phosphide nanowires as building blocks for nanoscale electronic and optoelectronic devices. Nature, 409(6816), 66-69.
[23] Li, J., Lu, W., & Lieber, C. M. (2004). Nanoelectronics from the bottom up. Nature Materials, 3(2), 88-90.
[24] Avouris, P. (2007). Carbon nanotube electronics and optoelectronics. MRS Bulletin, 32(11), 829-833.
[25] Y. Wu, D. B. Farmer, F. Xia and P. Avouris, "Graphene Electronics: Materials, Devices, and Circuits," in *Proceedings of the IEEE*, vol. 101, no. 7, pp. 1620-1637, July 2013, doi: 10.1109/JPROC.2013.2260311.
[26] Cheng, H.; Zhao, Y.; Fan, Y.; Xie, X.; Qu, L.; Shi, G. Graphenequantum-dot assembled nanotubes: a new platform for efficient Raman enhancement. ACS Nano 2012, 6, 2237−2244
[27] Chen Y, Hc L, Yc C, Ch C, Yj C. Wireless portable graphene-FET biosensor for detecting H1N1 virus, p. 2017; 2017.
[28] Su, T., Li, H., Steigerwald, M. L., Venkataraman, L., & Nuckolls, C. (2020). Molecular-scale electrical studies on conjugated molecules: from molecular wires to molecular transistors. Chemical Reviews, 120(1), 1008-1061.
[29] Rakshe, Dhananjay & William, P. & Jawale, M. & Pawar, A. & Korde, Sachin & Deshpande, Neeta. (2023). Synthesis and Characterization of Graphene Based Nanomaterials for Energy Applications. Journal of Nano- and Electronic Physics. 15. 03020-1. 10.21272/jnep.15(3).03020.
[30] Hirsch, A. The era of carbon allotropes. Nat. Mater. 2010, 9, 868–871.
[31] Skoda, M.; Dudek, I.; Jarosz, A.; Szukiewicz, D. Graphene: One Material, Many Possibilities-Application Difficulties in Biological Systems. J. Nanomater. 2014, 2014, 190.

[32] Harris, P.J.F. New Perspectives on the Structure of Graphitic Carbons. Crit. Rev. Solid 2005, 30, 235–253.
[33] Torres, L.E.F.; Roche, S.; Charlier, J.-C. Introduction to Carbon-Based Nanostructures, 2nd ed.; Cambridge University Press: Cambridge, UK, 2020; pp. 1–10.
[34] Khalaj, Z.; Monajjemi, M.; Diudea, M.V. Main Allotropes of Carbon: A Brief Review. In Sustainable Nanosystems Development, Properties, and Applications; Putz, M.V., Mirica, M.C., Eds.; IGI Global: Hershey, PA, USA, 2017; pp. 185–213.
[35] Slepicka, P.; Slepickova Kasalkova, N.; Siegel, J.; Kolska, Z.; Bacakova, L.; Svorcik, V. Nano-structured and functionalized surfaces for cytocompatibility improvement and bactericidal action. Biotechnol. Adv. 2015, 33, 1120–1129.
[36] Yang, N.; Jiang, X.; Pang, D.-W. Carbon Nanostructures. In Carbon Nanoparticles and Nanostructures; Yang, N., Jiang, X., Pang, D.-W., Eds.; Springer International Publishing: Cham, Switzerland, 2016; ISBN 978-3-319-28780-5.
[37] Notarianni, M.; Liu, J.; Vernon, K.; Motta, N. Synthesis and applications of carbon nanomaterials for energy generation and storage. Beilstein J. Nanotechnol. 2016, 7, 149–196.
[38] Knupfer, M. Electronic properties of carbon nanostructures. Surf. Sci. Rep. 2001, 42, 1–74.
[39] Saba, N.; Jawaid, M.; Fouad, H.; Alothman, O.Y. Nanocarbon: Preparation, properties, and applications. In Nanocarbon and its Composites; Elsevier: Duxford, UK, 2019; pp. 327–354.
[40] Hemocompatibility of Carbon Nanostructures - by Mariangela Fedel, Center for Health & Bioresources, Biomedical Systems, AIT Austrian Institute of Technology GmbH, 2700 Wiener Neustadt, Austria C 2020, 6(1), 12; https://doi.org/10.3390/c6010012
[41] Pisarciuc, C. Structure, Material Properties and Applications of Diamond-Like Materials. Nonconv. Technol. Rev. 2012, XVI, 13–18.
[42] Perez, G.; Maréchal, A.; Chicot, G.; Lefranc, P.; Jeannin, P.O.; Eon, D.; Rouger, N. Diamond semiconductor performances in power electronics applications. Diamond Rel. Mater. 2020, 110, 108154.
[43] Narayan, J.; Bhaumik, A. Research Update: Direct conversion of amorphous carbon into diamond at ambient pressures and temperatures in air. APL Mater. 2015, 3, 100702-1–100702-11. Nanomaterials 2021, 11, 2368 19 of 23
[44] Bhaumik, A.; Sachan, R.; Narayan, J. High-Temperature Superconductivity in Boron-Doped Q-Carbon. ACS Nano 2017, 11, 5351–5357.
[45] Kopova, I.; Rezek, B.; Stehlik, S.; Ukraintsev, E.; Slepickova Kasalkova, N.; Slepicka, P.; Potocky, S.; Bacakova, L. Growth of Primary Human Osteoblasts on Plasma-Treated and Nanodiamond-Coated PTFE Polymer Foils. Phys. Status Solidi B 2018, 255, 1700595.
[46] Krueger, A. Carbon Materials and Nanotechnology, 1st ed.; WILEY-VCH Verlag GmbH & Co. KGaA: Weinheim, Germany, 2010; pp. 1–32
[47] Stoller, M.D.; Park, S.; Zhu, Y.; An, J.; Ruoff, R.S. Graphene-Based Ultracapacitors. Nano Lett. 2008, 8, 3498–3502.
[48] Gómez-Navarro, C.; Weitz, T.R.; Bittner, A.M.; Scolari, M.; Mews, A.; Burghard, M.; Kern, K. Electronic Transport Properties of Individual Chemically Reduced Graphene Oxide Sheets. Nano Lett. 2007, 7, 3499–3503.
[49] Allen, M.J.; Tung, V.C.; Kaner, R.B. Honeycomb Carbon: A Review of Graphene. Chem. Rev. 2010, 110, 132–145.
[50] Kiew, S.F.; Kiew, L.F.; Lee, H.B.; Imae, T.; Chung, L.Y. Assessing biocompatibility of graphene oxide-based nanocarriers: A review. J. Control. Release 2016, 226, 217–228.
[51] Akinwande, D.; Brennan, C.J.; Bunch, J.S.; Egberts, P.; Felts, J.R.; Gao, H.; Huang, R.; Kim, J.S.; Li, T.; Li, X.; et al. A review on mechanics and mechanical properties of 2D materials-Graphene and beyond. Extrem Mech. Lett. 2017, 13, 42–77.
[52] Mohammad, N.S. Understanding quantum confinement in nanowires: Basics, applications and possible laws. J. Phys. Condens. Matter 2014, 26, 1–28.
[53] Li, H.; Zhang, H. The isolated-pentagon rule and nice substructures in fullerens. Ars Math. Contemp. 2018, 15, 487–497.
[54] Mojica, M.; Alonso, J.A.; Méndez, F. Synthesis of fullerenes. J. Phys. Org. Chem. 2013, 26, 526–539.
[55] Savi, P.; Giorcelli, M.; Quaranta, S. Multi-Walled Carbon Nanotubes Composites for Microwave Absorbing Applications. Appl. Sci. 2019, 9, 851.
[56] Scarselli, M.; Castrucci, P.; De Crescenzi, M. Electronic and optoelectronic nano-devices based on carbon nanotubes. J. Phys. Condens. Matter 2012, 24, 313202.
[57] Rudakiya, Darshan & Patel, Yogesh & Chhaya, Urvish & Gupte, Akshaya. (2019). Carbon Nanotubes in Agriculture: Production, Potential, and Prospects. 10.1007/978-981-32-9370-0_8.
[58] Gately, R.D. Filling of carbon nanotubes and nanofibres. Beilstein J. Nanotechnol. 2015, 6, 508–516.
[59] Tran, P.A.; Zhang, L.; Webster, T.J. Carbon nanofibers and carbon nanotubes in regenerative medicine. Adv. Drug Deliv. Rev. 2009, 61, 1097–1114.
[60] Asaro, L.; Villanueva, S.; Alvarez, V.; Manfredi, L.B.; Rodríguez, E.S. Fire performance of composites made from carbon/ phenolic prepregs with nanoclays. J. Compos. Mater. 2017, 51, 3515–3524.
[61] Maa, P.-C.; Siddiqui, N.A.; Marom, G.; Kim, J.-K. Dispersion and functionalization of carbon nanotubes for polymer-based nanocomposites: A review. Compos. Part A 2010, 41, 1345–1367.
[62] Chen, X.; Xia, J.; Peng, J.; Li, W.; Xie, S. Carbon-nanotube metal-matrix composites prepared by electroless plating. Compos. Sci. Technol. 2000, 60, 301–306.
[63] Narayan, J.; Bhaumik, A.; Gupta, S.; Haque, A.; Sachan, R. Progress in Q-carbon and related materials with extraordinary properties. Mater. Res. Lett. 2018, 6, 353–364.

[64] Haque, A.; Narayan, J. Electron field emission from Q-carbon. Diam. Relat. Mater. 2018, 86, 71–78.
[65] Yoshinaka, H.; Inubushi, S.; Wakita, T.; Yokoya, T.; Muraoka, Y. Formation of Q-carbon by adjusting sp3 content in diamond-like carbon films and laser energy density of pulsed laser annealing. Carbon 2020, 167, 504–511.
[66] Narayan, J.; Bhaumik, A. Q-carbon discovery and formation of single-crystal diamond nano- and microneedles and thin films. Mater. Res. Lett. 2016, 4, 118–126.
[67] Sachan, R.; Bhaumik, A.; Pant, P.; Prater, J.; Narayan, J. Diamond film growth by HFCVD on Q-carbon seeded substrate. Carbon 2019, 141, 182–189.
[68] Narayan, J.; Gupta, S.; Bhaumik, A.; Sachan, R.; Cellini, F.; Riedo, E. Q-carbon harder than diamond. MRS Commun. 2018, 8, 428–436.
[69] Lee, Y.J.; Jung, J.C.; Park, S.; Seo, J.G.; Baeck, S.-H.; Yoon, J.R.; Yi, J.; Song, I.K. Effect of preparation method on electrochemical property of Mn-doped carbon aerogel for supercapacitor. Curr. Appl. Phys. 2011, 11, 1–5. Nanomaterials 2021, 11, 2368 23 of 23
[70] Alex, A.S.; Lekshmi, M.S.A.; Sekkar, V.; John, B.; Gouri, C.; Ilangovan, S.A. Microporous carbon aerogel prepared through ambient pressure drying route as anode material for lithium ion cells. Polym. Adv. Technol. 2017, 28, 1945–1950.
[71] Hanzawa, Y.; Hatori, H.; Yoshizawa, N.; Yamada, Y. Structural changes in carbon aerogels with high temperature treatment. Carbon 2002, 40, 575–581.
[72] Lai, F.; Huang, Y.; Zuo, L.; Gu, H.; Miao, Y.-E.; Liu, T. Electrospun nanofiber-supported carbon aerogel as a versatile platform toward asymmetric supercapacitors. J. Mater. Chem. A 2016, 4, 15861–15869.
[73] Zhang, S.Q.; Wang, J.; Shen, J.; Deng, Z.S.; Lai, Z.Q.; Zhou, B.; Attia, S.M.; Chen, L.Y. The investigation of the adsorption character. Nanostruct. Mater. 1999, 11, 375–381.
[74] Schrand, A.M.; Hens, S.A.C.; Shenderova, O.A. Nanodiamond Particles: Properties and Perspectives for Bioapplications. Crit. Rev. Solid State Mater. Sci. 2009, 34, 18–74.
[75] Hanada, K. Detonation nanodiamond: Perspective and Applications. Surf. Eng. 2009, 25, 487–489.
[76] Vaijayanthimala, V.; Lee, D.K.; Kim, S.V.; Yen, A.; Tsai, N.; Ho, D.; Chang, H.-C.; Shenderova, O. Nanodiamond-mediated drug delivery and imaging: Challenges and opportunities. Expert Opin. Drug Deliv. 2015, 12, 735–749.
[77] Zhang, X.-Q.; Lam, R.; Xu, X.; Chow, E.K.; Kim, H.-J.; Ho, D. Multimodal Nanodiamond Drug Delivery Carriers for Selective Targeting, Imaging, and Enhanced Chemotherapeutic Efficacy. Adv. Mater. 2011, 23, 4770–4775.
[78] Chen, M.; Pierstorff, E.D.; Lam, R.; Li, S.-Y.; Huang, H.; Osawa, E.; Ho, D. Nanodiamond-Mediated Delivery of Water-Insoluble Therapeutics. ACS Nano 2009, 3, 2016–2022.
[79] Xing, Z.; Pedersen, T.O.; Wu, X.; Xue, Y.; Sun, Y.; Finne-Wistrand, A.; Kloss, F.R.; Waag, T.; Krueger, A.; Steinmüller-Nethl, D.; et al. Biological Effects of Functionalizing Copolymer Scaffolds with Nanodiamond Particles. Tissue Eng. Part A 2013, 19, 1783–1791.
[80] Hopper, A.P.; Dugan, J.M.; Gill, A.A.; Fox, O.J.L.; May, P.W.; Haycock, J.W.; Claeyssens, F. Amine functionalized nanodiamond promotes cellular adhesion, proliferation and neurite outgrowth. Biomed. Mater. 2014, 9, 045009.
[81] Whitlow, J.; Pacelli, S.; Paul, A. Multifunctional nanodiamonds in regenerative medicine: Recent advances and future directions. J. Control. Release 2017, 261, 62–86.
[82] Aviram, A., & Ratner, M. A. (1974). Molecular rectifiers. Chemical Physics Letters, 29(2), 277-283.
[83] Metzger, R. M. (1999). Unimolecular rectification in donor− acceptor chains. Journal of the American Chemical Society, 121(29), 5614-5615.
[84] Reed, M. A., Zhou, C., Muller, C. J., Burgin, T. P., & Tour, J. M. (1997). Conductance of a molecular junction. Science, 278(5336), 252-254.
[85] Xu, B., & Tao, N. (2003). Measurement of single-molecule resistance by repeated formation of molecular junctions. Science, 301(5637), 1221-1223.
[86] Nitzan, A., & Ratner, M. A. (2003). Electron transport in molecular wire junctions. Science, 300(5624), 1384-1389.
[87] J. Love, L. Estroff, J. Kriebel, R. Nuzzo, and G. Whitesides, “Self-assembled monolayers of thiolates on metals as a form of nanotechnology,” Chemical Reviews, vol. 105, no. 4, pp. 1103–1169, 2005.
[88] M. Singh, N. Kaur and E. Comini, "The role of self-assembled monolayers in electronic devices," Journal of materials chemistry. C, Materials for optical and electronic devices, vol. 8, pp. 3938-3955, 2020
[89] L. Wang, L. Wang, L. Zhang, and D. Xiang, “Advance of Mechanically Controllable Break Junction for Molecular Electronics,” Topics in Current Chemistry, vol. 375, no. 3, 2017.
[90] D. Xiang, H. Jeong, T. Lee, and D. Mayer, “Mechanically Controllable Break Junctions for Molecular Electronics,” Advanced materials (Weinheim), vol. 25, no. 35, pp. 4845–4867, 2013
[91] M. A. Reed, C. Zhou, C. J. Muller, T. P. Burgin, and J. M. Tour, “Conductance of a Molecular Junction,” Science, vol. 278, no. 5336, pp. 252–254, 1997
[92] Lambert, C. J. (2011). Molecular electronics. In Introduction to Molecular Electronics (pp. 1-29). OUP Oxford.
[93] Ratner, M. A. (2013). Challenges and opportunities for molecular electronics. Nature Nanotechnology, 8(6), 378-381.
[94] M. A. N. N. B. and K. U. H. N. H., "TUNNELING THROUGH FATTY ACID SALT MONOLAYERS," Journal of applied physics, vol. 42, pp. 4398-4405, 1971
[95] T. W. Kelley, E. Granstrom and C. D. Frisbie, "Conducting Probe Atomic Force Microscopy: A Characterization Tool for Molecular Electronics," Advanced materials (Weinheim), vol. 11, pp. 261-264, 1999.

[96] C. Kergueris, J. P. Bourgoin, S. Palacin, D. Esteve, C. Urbina, M. Magoga and C. Joachim, "Electron transport through a metal-molecule-metal junction," Physical review. B, Condensed matter and materials physics, vol. 59, pp. 12505-12513, 1999.
[97] S. Piccinin, "Theoretical modeling of electronic transport in molecular devices," 2006.
[98] S. Rahmanian Koshkaki, "An overview of Density-Functional-Theory (DFT) for students," December 2015.
[99] M. Smeu, R. A. Wolkow and G. A. DiLabio, "Theoretical investigation of electron transport modulation through benzenedithiol by substituent groups," The Journal of chemical physics, vol. 129, pp. 034707-034707-8, 2008.
[100] Y. Komoto, S. Fujii, H. Nakamura, T. Tada, T. Nishino and M. Kiguchi, "Resolving metal-molecule interfaces at single-molecule junctions," Scientific reports, vol. 6, pp. 26606-26606, 2016.136
[101] D. Q. Andrews, R. Cohen, R. P. Van Duyne and M. A. Ratner, "Single molecule electron transport junctions: Charging and geometric effects on conductance," The Journal of chemical physics, vol. 125, pp. 174718-174718, 2006.
[102] M. D. Ganji and F. Nourozi, "Density functional non-equilibrium Green's function (DFT-NEGF) study of the smallest nano-molecular switch," Physica. E, Lowdimensional systems & nanostructures, vol. 40, pp. 2606-2613, 2008.
[103] R.-W. Yan, X. Jin, S.-Y. Guan, X.-G. Zhang, R. Pang, Z.-Q. Tian, D.-Y. Wu and B.-W. Mao, "Theoretical Study of Quantum Conductance of Conjugated and Nonconjugated Molecular Wire Junctions," Journal of physical chemistry. C, vol. 120, pp. 11820-11830, 2016.
[104] W. Y. Wang, T. Lee and M. A. Reed, "Mechanism of electron conduction in self assembled alkanethiol monolayer devices," Physical review. B, vol. 68, 2003.
[105] D. P. Wang, D. E. Feldman, B. R. Perkins, A. J. Yin, G. H. Wang, J. M. Xu and A. Zaslavsky, "Hopping conduction in disordered carbon nanotubes," Solid state communications, vol. 142, pp. 287-291, 2007;2006;.
[106] X. Zhang, L. Yang and H. Liu, "High-temperature conduction behavior of carbon nanotube fiber from 25 °C to 1100 °C," Applied physics letters, vol. 112, p. 164103, 2018.
[107] S. H. M. Jafri, H. Lofas, T. Blom, A. Wallner, A. Grigoriev, R. Ahuja, H. Ottosson and K. Leifer, "Nano-fabrication of molecular electronic junctions by targeted modification of metal-molecule bonds," Scientific reports, vol. 5, pp. 14431-14431, 2015.
[108] W.-T. Hwang, Y. Jang, M. Song, D. Xiang and T. Lee, "Large-area molecular monolayer-based electronic junctions with transferred top electrodes," Japanese Journal of Applied Physics, vol. 59, p. SD0803, 2020.
[109] T.-W. Kim, G. Wang, H. Song, N.-J. Choi, H. Lee and T. Lee, "Charge Transport of Alkanethiol Self-Assembled Monolayers in Micro-Via Hole Devices," Journal of Nanoscience and Nanotechnology, vol. 6, pp. 3487-3490, November 2006
[110] Reed, M. A., Zhou, C., Muller, C. J., Burgin, T. P., & Tour, J. M. (1997). Conductance of a molecular junction. Science, 278(5336), 252-254.
[111] Tour, J. M. (2000). Molecular electronics: Commercial insights, chemistry, devices, architecture and future. Pure and Applied Chemistry, 72(7), 1223-1238.
[112] Tuccitto, N., Papagni, A., Foti, G., Licciardello, A., & Purrello, R. (2006). Functionalization of gold nanoparticles by dipole self-assembly. The Journal of Physical Chemistry B, 110(17), 8754-8758.
[113] Hahm, J. I., Lieber, C. M., & Gao, R. (2003). Rational growth of branched and hyperbranched nanowire structures. Nano Letters, 4(1), 51-54.
[114] Zhong, Z., Fang, X., Baek, M. H., Hahm, J. I., & Lieber, C. M. (2008). Single crystal metallic nanowires and metal/semiconductor nanowire heterostructures. Journal of the American Chemical Society, 130(3), 890-891.
[115] S. H. M. Jafri, H. Lofas, T. Blom, A. Wallner, A. Grigoriev, R. Ahuja, H. Ottosson and K. Leifer, "Nano-fabrication of molecular electronic junctions by targeted modification of metal-molecule bonds," Scientific reports, vol. 5, pp. 14431-14431, 2015.
[116] C. Kergueris, J. P. Bourgoin, S. Palacin, D. Esteve, C. Urbina, M. Magoga and C. Joachim, "Electron transport through a metal-molecule-metal junction," Physical review. B, Condensed matter and materials physics, vol. 59, pp. 12505-12513, 1999
[117] Advances of Various Heterogeneous Structure Types in Molecular Junction Systems and Their Charge Transport Properties Jaeho Shin, Jung Sun Eo, Takgyeong Jeon, Takhee Lee,* and Gunuk Wang Adv. Sci. 2022, 9, 2202399 DOI: 10.1002/advs.202202399
[118] J. H. Chen, C. Jang, S. Xiao, M. Ishigami, and M. S. Fuhrer, Intrinsic and extrinsic performance limits of graphene devices on SiO2, Nature Nanotech, 3, 206 (2008).
[119] A. K. Geim and P. Kim, Carbon wonderland, Scientific American, 298, 90 (2008)
[120] Yang, G., Li, L., Lee, W. B., & Ng, M. C. (2018). Structure of graphene and its disorders: a review. Science and Technology of Advanced Materials, 19(1), 613–648. https://doi.org/10.1080/14686996.2018.1494493
[121] Cooper, Daniel R.; D'Anjou, Benjamin; Ghattamaneni, Nageswara; Harack, Benjamin; Hilke, Michael; Horth, Alexandre; Majlis, Norberto; Massicotte, Mathieu; Vandsburger, Leron; Whiteway, Eric; Yu, Victor (26 April 2012). "Experimental Review of Graphene". *ISRN Condensed Matter Physics*. **2012**: 1–56.
[122] Lee JH, Park SJ, Choi JW. Electrical Property of Graphene and Its Application to Electrochemical Biosensing. Nanomaterials (Basel). 2019 Feb 20;9(2):297. doi: 10.3390/nano9020297. PMID: 30791566; PMCID: PMC6409852.

[123] Sang M, Shin J, Kim K, Yu KJ. Electronic and Thermal Properties of Graphene and Recent Advances in Graphene Based Electronics Applications. Nanomaterials (Basel). 2019 Mar 5;9(3):374. doi: 10.3390/nano9030374. PMID: 30841599; PMCID: PMC6474003.
[124] P. C. Guha; M. N. Chakladar (1925). "Dithiocatechol". *J. Indian Chem. Soc*. **2**: 318.
[125] https://www.chembk.com/en/chem/benzene-1,4-dithiol
[126] https://www.sigmaaldrich.com/CA/en/product/aldrich/763969?utm_source=google&utm_medium=cpc&utm_campaign=20674735406&utm_content=157607443431&gclid=CjwKCAjw88yxBhBWEiwA7cm6pQoPyEP-txvFgYGcdZa38owzRvckqqHm-sWd8-8yJYX9_tzcdFdJRxoCElgQAvD_BwE
[127] Schwingenschlögl, U & Schuster, C. (2007). Electronic structure of the Au/benzene-1, 4-dithiol/Au transport interface: Effects of chemical bonding. Chemical Physics Letters. 202063. 10.1016/j.cplett.2006.12.049.
[128] Measurement of Single Molecule Conductance: Benzenedithiol and Benzenedimethanethiol, Xiaoyin ,Bingqian, and, and Nongjian J. Tao, Nano Letters 2004 4 (2), 267-271, DOI: 10.1021/nl035000m
[129] Cian Hughes, Ronán M. McCann, Brian Freeland, Dermot Brabazon, Electrochemical and chronoamperometry assessment of nano-gold sensor surfaces produced via novel laser fabrication methods, Journal of Electroanalytical Chemistry, Volume 880, 2021, 114813, ISSN 1572-6657, https://doi.org/10.1016/j.jelechem.2020.114813.
[130] H. Simchi, M. Esmaeilzadeh, and M. Heydarisaani, Phys. Status Solidi B 249, 1735 (2012), Electronic and spin transport properties of a benzene molecule connected to graphene leads
[131] Y. Kim, T. Pietsch, A. Erbe, W. Belzig, E. Scheer, Nano Lett. 2011, 11, 3734.
[132] Y. Jang, S. J. Kwon, J. Shin, H. Jeong, W. T. Hwang, J. Kim, J. Koo, T. Y. Ko, S. Ryu, G. Wang, T. W. Lee, T. Lee, ACS Appl. Mater. Interfaces 2017, 9, 42043.
[133] X. Zhao, M. Chen, RSC Adv. 2014, 4, 63596.
[134] T.-T. You, N. Yang, Y.-Q. Shu, P.-G. Yin, A DFT study on graphene-based surface enhanced Raman spectroscopy of Benzenedithiol adsorbed on gold/graphene, Journal of Raman Spectroscopy, 50 (2019) 1510-1518.
[135] Friesner, Richard A. (May 10, 2005). "Ab initio quantum chemistry: Methodology and applications". Proceedings of the National Academy of Sciences of the United States of America. **102** (19): 6648–6653.
[136] Hall, George G. (1991). "The Lennard-Jones paper of 1929 and the foundations of Molecular Orbital Theory". *Advances in Quantum Chemistry*. **22**: 1–6.
[137] Rimola, A.; Ferrero, S.; Germain, A.; Corno, M.; Ugliengo, P. Computational Surface Modelling of Ices and Minerals of Interstellar Interest—Insights and Perspectives. *Minerals* **2021**, *11*, 26. https://doi.org/10.3390/min11010026
[138] Paulsson, Magnus. (2002). Non Equilibrium Green's Functions for Dummies: Introduction to the One Particle NEGF equations.
[139] Licker, Mark, J. (2004). McGraw-Hill Concise Encyclopedia of Chemistry. New York: McGraw-Hill. *ISBN 978-0-07-143953-4*.
[140] Miessler, Gary L.; Fischer, Paul J.; Tarr, Donald A. (2013-04-08). Inorganic Chemistry. *Pearson Education*. ISBN 978-0-321-91779-9.
[141] Miessler and Tarr (2013), Inorganic Chemistry, 5th ed, 117-165, 475-534
[142] Cramer, Christopher J. (2002). Essentials of Computational Chemistry. Chichester: John Wiley & Sons, Ltd. pp. 153–189. *ISBN 978-0-471-48552-0*
[143] Møller, C.; Plesset, M.S. Note on an Approximation Treatment for Many-Electron Systems. Phys. Rev. **1934**, 46, 618–622.
[144] Siegbahn, P.E.M. The Configuration Interaction Method. In Lecture Notes in Quantum Chemistry: European Summer School in Quantum Chemistry; Roos, B.O., Ed.; Springer: Berlin/Heidelberg, Germany, 1992; pp. 255–293.
[145] Vignale, G.; Rasolt, Mark (1987). "Density-functional theory in strong magnetic fields". *Physical Review Letters*. **59** (20): 2360–2363.
[146] Hohenberg, Pierre; Walter, Kohn (1964). *"Inhomogeneous electron gas"*. Physical Review. **136** (3B): B864–B871.
[147] *Kohn, Walter; Sham, Lu Jeu (1965).* "Self-Consistent Equations Including Exchange and Correlation Effects". Physical Review. ***140*** *(4A): A1133–A1138.* doi:10.1103/PhysRev.140.A1133.
[148] The Nonequilibrium Green Function (NEGF) Method, Springer Handbook of Semiconductor Devices, 2023, ISBN: 978-3-030-79826-0, Kerem Y. Camsari, Shuvro Chowdhury, Supriyo Datta
[149] S. Datta, Electronic transport in mesoscopic systems. 3, (Cambridge University Press: Cambridge, UK;New Yor, 1954.
[150] M. Smeu, R. A. Wolkow and G. A. DiLabio, "Theoretical investigation of electron transport modulation through benzenedithiol by substituent groups," The Journal of chemical physics, vol. 129, pp. 034707-034707-8, 2008.
[151] Y. Kim, T. Pietsch, A. Erbe, W. Belzig and E. Scheer, "Benzenedithiol: A BroadRange Single-Channel Molecular Conductor," Nano letters, vol. 11, pp. 3734- 3738, 2011
[152] M. D. Ganji and F. Nourozi, "Density functional non-equilibrium Green's function (DFT-NEGF) study of the smallest nano-molecular switch," Physica. E, Lowdimensional systems & nanostructures, vol. 40, pp. 2606-2613, 2008.
[153] Xiao, Xu and N. J. Tao, "Measurement of Single Molecule Conductance: Benzenedithiol and Benzenedimethanethiol," Nano Letters, vol. 4, pp. 267-271, 2004.

[154] B. Delley, "From molecules to solids with the DMol3 approach," The Journal of chemical physics, vol. 113, pp. 7756-7764, 2000.
[155] Material Studio 2017 Online help.pdf
[156] U. Schwingenschlögl, C. Schuster, Electronic structure of the Au/benzene-1,4-dithiol/Au transport interface: Effects of chemical bonding, Chemical Physics Letters, Volume 435, Issues 1–3, 2007, Pages 100-103, ISSN 0009-2614, https://doi.org/10.1016/j.cplett.2006.12.049.
[157] Yu, Cuiju & Miao, Yuanyuan & Qiu, Shuai & Cui, Yangjun & He, Guangmeng & Zhang, Guang-Ping & Wang, Chuankui & Hu, Gui-chao. (2018). Modulating spin-dependent electron transport in benzene-dithiolate magnetic junctions by hybrid interface states. Journal of Physics D Applied Physics. 51. 345302. 10.1088/1361-6463/aad350.
[158] K. Arulaabaranam, S. Muthu, G. Mani, A.S. Ben Geoffrey, Speculative assessment, molecular composition, PDOS, topology exploration (ELF, LOL, RDG), ligand-protein interactions, on 5-bromo-3-nitropyridine-2-carbonitrile, Heliyon, Volume 7, Issue 5, 2021, e07061, ISSN 2405 8440, https://doi.org/10.1016/j.heliyon.2021.e07061.
[159] A.M. Scheer, G.A. Gallup, P.D. Burrow, Unoccupied orbital energies of 1,4-benzenedithiol and the HOMO–LUMO gap, Chemical Physics Letters, Volume 466, Issues 4–6, 2008, Pages 131-135, ISSN 0009-2614, https://doi.org/10.1016/j.cplett.2008.10.057.
[160] Tran, Thoa & Tuan, Vu & Hoan, Pham & Hoang, Hung & Nguyen, Hue. (2022). Study of structural and electronic properties of graphene and some graphene derivatives based on orthorhombic unit cell by density functional theory. Vietnam Journal of Science and Technology. 60. 794-802. 10.15625/2525-2518/16542.
[161] Lin, He & Fratesi, Guido & Brivio, G.. (2014). Graphene magnetism induced by covalent adsorption of aromatic radicals. Physical chemistry chemical physics : PCCP. 17. 10.1039/c4cp04476b.
[162] D. Q. Andrews, R. Cohen, R. P. Van Duyne and M. A. Ratner, "Single molecule electron transport junctions: Charging and geometric effects on conductance," The Journal of chemical physics, vol. 125, pp. 174718-174718, 2006
[163] Chouk, Rihab & Manel, Bergaoui & Khalfaoui, Mohamed. (2018). On the optoelectronic properties of non-covalently functionalized graphene for solar cell application. Journal of Computational Electronics. 17. 10.1007/s10825-018-1149-1.
[164] P. Tian, L. Tang, K.S. Teng, S.P. Lau, Graphene quantum dots from chemistry to applications, Mater. Today Chem. 10 (2018) 221–258.
[165] N. Troullier and J. Martins, "Efficient pseudopotentials for plane-wave calculations," Physical review. B, Condensed matter, vol. 43, no. 3, p. 1993— 2006, Jan. 1991
[166] Horiguchi, K & Tsutsui, Makusu & Kurokawa, Shu & Sakai, A. (2009). Electron transmission characteristics of Au/1,4-benzenedithiol/Au junctions. Nanotechnology. 20. 025204. 10.1088/0957-4484/20/2/025204.
[167] Jin-Kyu Choi, Hien Thu Pham, Hyun-Dam Jeong, A comparative study of electron transport in benzene molecule covalently bonded to gold and silicon electrodes for pioneering the electron transport properties of silicon quantum dot-molecule hybrid polymers, Current Applied Physics, Volume 15, Issue 8, 2015, Pages 877-884, ISSN 1567-1739, https://doi.org/10.1016/j.cap.2015.03.021.
[168] Wu, Kunlin & Bai, Meilin & Sanvito, Stefano & Hou, Shimin. (2013). Quantitative interpretation of the transition voltages in gold-poly(phenylene) thiol-gold molecular junctions. The Journal of chemical physics. 139. 194703. 10.1063/1.4830399.
[169] Horiguchi K, Tsutsui M, Kurokawa S, Sakai A. Electron transmission characteristics of Au/1,4-benzenedithiol/Au junctions. Nanotechnology. 2009 Jan 14;20(2):025204. doi: 10.1088/0957-4484/20/2/025204. Epub 2008 Dec 9. PMID: 19417266.
[170] H. Cheraghchi and K. Esfarjani, "Negative differential resistance in molecular junctions: Application to graphene ribbon junctions," Physical Review B, vol. 78, no. 8, p. 085123, Aug. 2008
[171] Seenithurai, Sonai & Pandyan, Kodi & Kumar, Shanmugam & Mahendran, Manickam. (2013). Electronic Properties of Boron and Nitrogen Doped Graphene. Nano Hybrids. 5. 65-83. 10.4028/www.scientific.net/NH.5.65.
[172] Kwon, Hyuk & Kwon, Yongju & Kim, Taeyoon & Jung, Youngsuk & Lee, Seunggeol & Cho, Min & Kwon, Soonchul. (2017). Enhanced competitive adsorption of CO 2 and H 2 on graphyne: A density functional theory study. AIP Advances. 7. 125013. 10.1063/1.5006839.
[173] Wazir, Arshad & Kundi, I.W.. (2016). Synthesis of graphene nano sheets by the rapid reduction of electrochemically exfoliated graphene oxide induced by microwaves. 38. 11-16.
[174] Y. Veera Manohara Reddy, Jae Hwan Shin, Venkata Narayana Palakollu, Bathinapatla Sravani, Chang-Hyung Choi, Kyeongsoon Park, Sun-Ki Kim, G. Madhavi, Jong Pil Park, Nagaraj P. Shetti,, Strategies, advances, and challenges associated with the use of graphene-based nanocomposites for electrochemical biosensors, Advances in Colloid and Interface Science, Volume 304, 2022, 102664, ISSN 0001-8686, https://doi.org/10.1016/j.cis.2022.102664.
[175] Kaur H, Garg R, Singh S, Jana A, Bathula C, Kim HS, Kumbar SG, Mittal M. Progress and challenges of graphene and its congeners for biomedical applications. J Mol Liq. 2022 Dec 15;368(A):120703. doi: 10.1016/j.molliq.2022.120703. Epub 2022 Nov 1. PMID: 38130892; PMCID: PMC10735213.

[176] Derenskyi V, Gomulya W, Talsma W, Salazar-Rios J M, Fritsch M, Nirmalraj P, Riel H, Allard S, Scherf U and Loi M A 2017 On-chip chemical self-assembly of semiconducting single-walled carbon nanotubes (SWNTs): toward robust and scale invariant SWNTs transistors Adv. Mater.
[177] Aaron D. Franklin, Siyuranga O. Koswatta, Damon B. Farmer, Joshua T. Smith, Lynne Gignac, Chris M. Breslin, Shu-Jen Han, George S. Tulevski, Hiroyuki Miyazoe, Wilfried Haensch, and Jerry Tersoff; Carbon Nanotube Complementary Wrap-Gate Transistors, Nano Letters 2013 13 (6), 2490-2495 DOI: 10.1021/nl400544q
[178] Vedhanarayanan B, Praveen V K, Das G and Ajayaghosh A 2018 Hybrid materials of 1D and 2D carbon allotropes and synthetic π-systems NPG Asia Mater. 10 107-26.
[179] Ji M, Mason M L, Modarelli D A and Parquette J R 2019 Threading carbon nanotubes through a self-assembled nanotube Chem. Sci. 10 7868–77
[180] Ponnamma, D., Parangusan, H., Deshmukh, K., Kar, P., Muzaffar, A., Pasha, S. K. K.,Al-Maadeed, M. A. A. (2019). Green synthesized materials for sensor, actuator, energy storage and energy generation: a review. *Polymer-Plastics Technology and Materials*, *59*(1), 1–62. https://doi.org/10.1080/25740881.2019.1614327
[181] Tan Nhiem Ly, Sangkwon Park, Highly sensitive gas sensor using hierarchically self-assembled thin films of graphene oxide and gold nanoparticles, Journal of Industrial and Engineering Chemistry, Volume 67, 2018, Pages 417-428, ISSN 1226-086X. https://doi.org/10.1016/j.jiec.2018.07.016.
[182] Adu, K., Rajagopalan, R., Kaschalk, C., & Randall, C. (2019). CNT flexible membranes for energy storage and conversion systems. *MRS Communications*, *9*(2), 670 674. https://doi.org/10.1557/mrc.2019.45
[183] Islam M M, Aboutalebi S H, Cardillo D, Liu H K, Konstantinov K and Dou S X 2015 Self-assembled multifunctional hybrids: toward developing high- performance graphene-based architectures for energy storage devices ACS Cent. Sci. 1 206-16
[184] Zhang, Y.; Liu, C.; Liu, J.; Xiong, J.; Liu, J.; Zhang, K.; Liu, Y.; Peng, M.; Yu, A.; Zhang, A.; et al. Lattice Strain Induced Remarkable Enhancement In Piezoelectric Performance Of ZnO-based Flexible Nanogene